Rheinische Friedrich-Wilhelms-Universität Bonn
- Institut für Molekulare Physiologie und Biotechnologie der Pflanzen -

The Role of Phytol Degradation in Chlorophyll and Tocopherol (Vitamin E) Metabolism

Dissertation

zur
Erlangung des Doktorgrades (Dr. rer. nat.)
der
Mathematisch-Naturwissenschaftlichen Fakultät
der
Rheinischen Friedrich-Wilhelms-Universität Bonn

vorgelegt von

Wentao Yang 杨文韬
aus Qingdao, China
Bonn 2021

Angefertigt mit Genehmigung der Mathematisch-Naturwissenschaftlichen Fakultät der Rheinischen Friedrich-Wilhelms-Universität Bonn

1. Gutachter: Prof. Dr. Peter Dörmann
2. Gutachterin: Prof. Dr. Dorothea Bartels
Tag der Promotion: 08.10.2021
Erscheinungsjahr: 2021

TABLE OF CONTENTS

LIST OF FIGURES

Figure. X. Y: X is the section number in the thesis. Y is the figure number in the section.

LIST OF TABLES

ABBREVIATIONS

APS	ammonium persulfate
BSA	bovine serum albumin
cDNA	complementary DNA
CTAB	cetyltrimethylammonium bromide
ddH_2O	double deionized water
CoA	Coenzyme A
DMSO	dimethyl sulfoxide
DMAPP	dimethylallyl-pyrophosphate
DNA	deoxyribonucleic acid
dNTPs	deoxyribonucleotide triphosphates
DUF	domain of unknown function
EDTA	ethylenediaminetetraacetic acid
ER	endoplasmic reticulum
ESI	electrospray ionization
EtBr	ethidium bromide
FAME	fatty acid methyl ester
fw	fresh weight
g	standard gravity (9.81 m s^{-2})
GC	gas chromatography
eGFP	enchanted green fluorescent protein
GGR	geranylgeranyl reductase
GUS	β-glucuronidase
HPLC	high pressure liquid chromatography
HRP	horseradish peroxidase
HPT	homogentisate phytyltransferase
IPP	isopentenyl-pyrophosphate
IPTG	Isopropyl β-D-1-thiogalactopyranoside
LB medium	Luria-Bertani medium
LC	liquid chromatography
kb	kilo base pair

kDa	kilo Dalton
MES	2-(N-morpholino) ethanesulfonic acid
MOI	multiplicity of infection
MRM	multiple reaction monitoring
MS medium	Murashige and Skoog medium
MS	mass spectrometry
MSTFA	N-methyl-N- (trimethylsilyl) trifluoroacetamide
m/z	mass to charge ratio
NASC	Nottingham *Arabidopsis* stock center
Ni-NTA	nickel-nitrilotriacetic acid
OD	optical density
ORF	open reading frame
P3	passage three
PBS	phosphate buffered saline
PC	phosphatidylcholine
PCR	polymerase chain reaction
PES	phytyl ester synthase
PPH	pheophytin pheophorbide hydrolase
pfu	plaque forming unit
Q-TOF	quadrupole time-of-flight
Q-Trap	quadrupole-linear ion trap
RNA	ribonucleic acid
rpm	revolutions per minute
RT	room temperature
RT-PCR	reverse transcription-PCR
SD	standard deviation
SDS-PAGE	sodium dodecyl sulfate-polyacrylamide gel electrophoresis
SOB medium	super optimal broth
SPE	solid phase extraction
TAE	Tris-acetate-EDTA
T-DNA	transfer DNA

TEMED	tetramethylethylenediamine
TM	transmembrane
Tris	tris (hydroxymethyl)aminomethane
v/v	volume per volume
VTE	vitamin E deficient
WT	wild type
w/v	weight per volume
X-Gal	5-bromo-4-chloro-3-indolyl-β-D-galactopyranoside
YEP	yeast extract peptone

1. INTRODUCTION

Photosynthesis plays a vital role in the biosphere: it results in the fixation of carbon dioxide from the atmosphere and energy from the sun which are stored in the form of carbohydrates, and it produces oxygen. Both of these products are essential for all organisms. Photosynthesis is localized to chloroplasts. According to the endosymbiont theory, chloroplasts are derived from the endosymbiosis of a photosynthetic bacterium by a protoeukaryotic cell (Kutschera & Niklas, 2005). Chloroplasts are commonly hemispherical or lens-shaped in vascular plants but vary considerably in shape in mosses and algae. Chloroplasts are surrounded by a double-membrane system consisting of an outer and inner envelope and also contain a complex internal membrane system (Fig. 1.1). The internal membrane system, also known as thylakoids, contains distinct regions. Some thylakoids (granal thylakoids) are organized into grana, stacks of appressed membranes, whereas others (stromal thylakoids) are unstacked and are thus exposed to the surrounding fluid medium, the chloroplast stroma. The thylakoid membranes are interconnected and enclose an internal space known as the lumen. As the most abundant photosynthetic pigment, chlorophyll binds to proteins to form the antenna complexes, which transfers the energy to the photosystems (Nelson et al., 2004). Chlorophyll is composed of a porphyrin ring and a hydrophobic side chain, namely phytol. The phytol chain is connected to the porphyrin ring via an ester bond. The biosynthetic pathway for chlorophyll has been elucidated in depth. Glutamic acid is the precursor of porphyrin head synthesis (Tanaka et al., 2011). Phytol belongs to the group of terpenoids (also known as isoprenoids or terpenes), which is the largest class of small molecular natural products in plants. Although the phytol degradation pathway has been elucidated in depth in humans, the degradation of phytol in plants still remains elusive. This research aims to investigate the phytol degradation pathway in the model plant *Arabidopsis thaliana*.

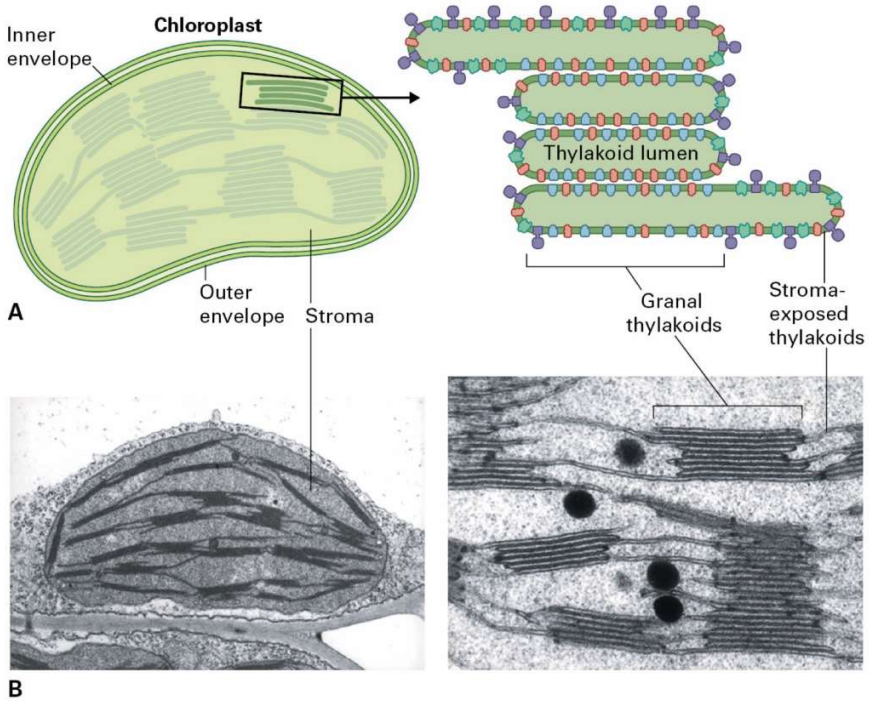

Figure. 1.1 Plant chloroplast structure

A. Schematic diagram showing the compartmentalization of plant chloroplasts.

B. Transmembrane electron scanning micrograph of plant chloroplast.

Source: Biochemistry and Molecular Biology of Plants, 2nd edition. Chapter 12, p510.

1.1 Synthesis of Isoprenoids

The biosynthesis of isoprenoids can be conveniently divided into 4 stages: 1) the synthesis of the biological C_5 isoprene unit; 2) repetitive condensations of the C_5 unit to form a series of larger prenyl diphosphate; 3) conversion of prenyl diphosphate to the basic terpenoid skeletons; 4) further modifications to the basic skeletons. The C_5 isoprene unit is represented by isopentenyl-diphosphate (IPP) and dimethylallyl-diphosphate (DMAPP). These two precursors can be synthesized in two different pathways in plants, namely the mevalonate pathway and the methylerythritol 4-phosphate (MEP) pathway.

1.1.1 Mevalonate Pathway

The mevalonate pathway is operating in most eukaryotes, archaea, and some eubacteria (Miziorko, 2011) (Fig. 1.2). The mevalonate pathway accounts for the conversion of acetyl-CoA to isopentenyl 5-diphosphate. This well-elucidated pathway starts with condensations of 3 molecules of acetyl-CoA in two steps to form the C_6 intermediate, 3-hydroxy-3-methylglutaryl-CoA (HMG-CoA) (Carrie et al., 2007). HMG-CoA is reduced by HMG-CoA reductase to form mevalonic acid (Learned & Fink, 1989). Mevalonic acid undergoes 2 sequential phosphorylation reactions, forming mevalonic acid-5-diphosphate (Simkin et al., 2011). Finally, a decarboxylase converts mevalonic acid-5-diphosphate into isopentenyl-diphosphate (Simkin et al., 2011). Isopentenyl-diphosphate can be isomerized to dimethylallyl-diphosphate by isopentenyl-diphosphate isomerase, an enzyme which also catalyzes the reverse reaction (Phillips et al., 2008).

HMG-CoA reductase is of interest, because the reduction of HMG-CoA is the committed step in the mevalonate pathway. Because the mevalonate pathway is essential for sterol synthesis, HMG-CoA reductase catalyzes the rate-limiting step in the biosynthesis of sterols, such as cholesterol (Gil et al., 1985). Many studies have reported a strong correlation between changes in the HMG-CoA reductase activity and alternations in the biosynthesis rate of isoprenoids (Giorgi et al., 2020; Schumacher et al., 2018).

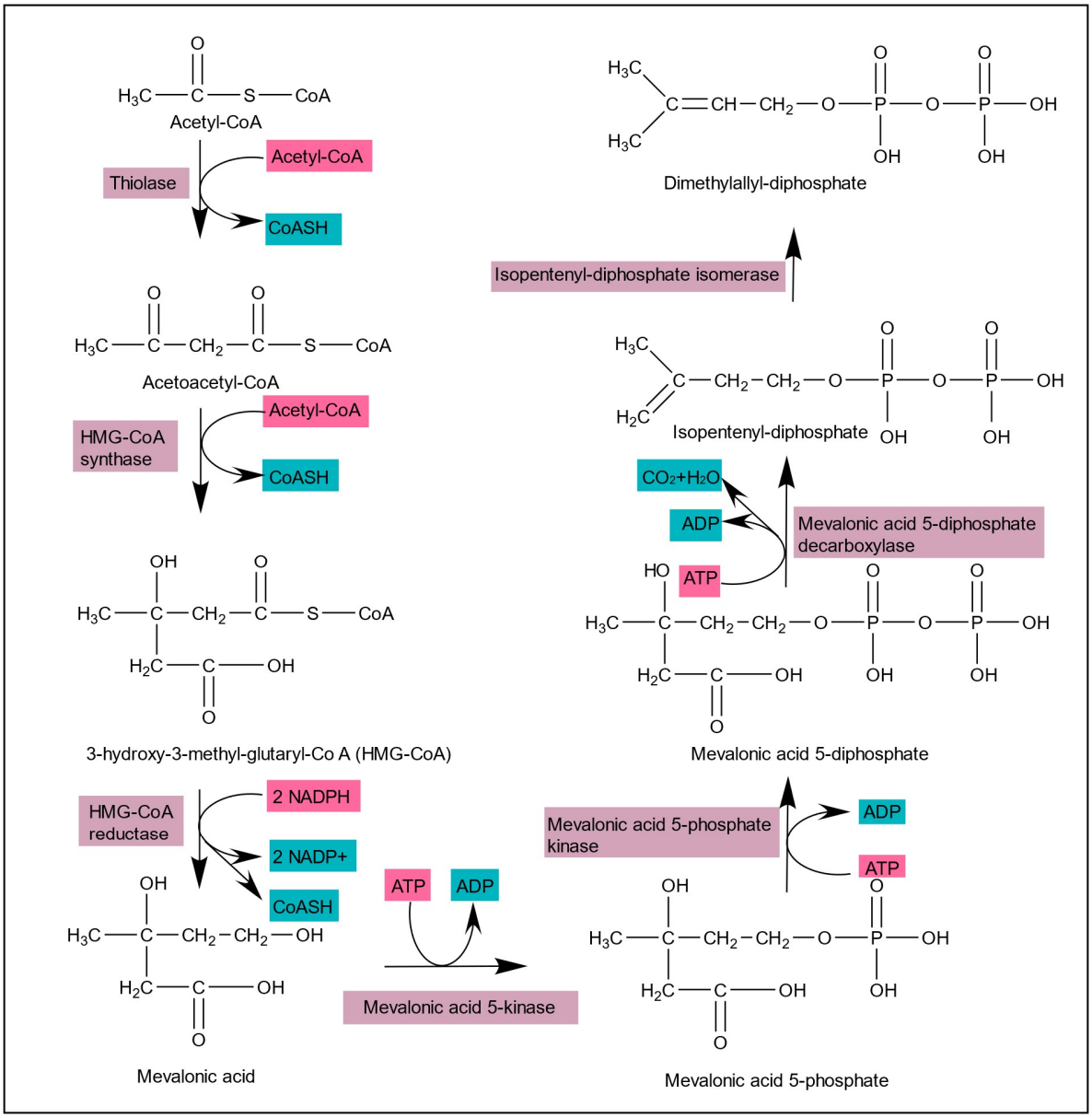

Figure. 1.2 Mevalonate pathway

Enzymes, substrates and side-products are in purple, pink and blue background, respectively. Modified from Biochemistry and Molecular Biology of Plants, 2nd edition. Chapter 24, p1137.

1.1.2 MEP Pathway

The methylerythritol 4-phosphate pathway (MEP pathway) functions in plastids and bacteria and is completely different from mevalonate pathway (Fig. 1.3). The MEP pathway starts with the attachment of one molecule of glyceraldehyde to one molecule of pyruvate by 1-deoxy-D-xylulose 5-phosphate synthase (DXS), forming 1-deoxy-D-xylulose 5-phosphate (DXP) (Estevez et al., 2000). DXP is rearranged and reduced by 1-deoxy-D-xylulose 5-phosphate reductoisomerase (DXR) to 2C-methyl-D-erythritol 4-phosphate (MEP) (Schwender et al., 1999). Next, cytidine 4-phosphate is transferred followed by an additional phosphate group from ATP to give 4-diphosphocytidyl-2C-methyl-D-erythritol 2-phosphate (Rohdich et al., 2000). The phosphate group at the second carbon of erythritol forms a cyclic diphosphate structure with the phosphate moiety of the nucleotide. This cyclic-forming reaction is catalyzed by MEP-2,4-cyclodiphosphate synthase, releasing a cytidyl-phosphate (Hsieh & Goodman, 2006). The product, 2C-methyl-D-erythritol 2,4-cyclophosphate, is reduced to give isopentyl diphosphate and its allylic isomer, dimethylallyl-diphosphate, in a 5:1 ratio (Adam et al., 2002; Querol et al., 2002)

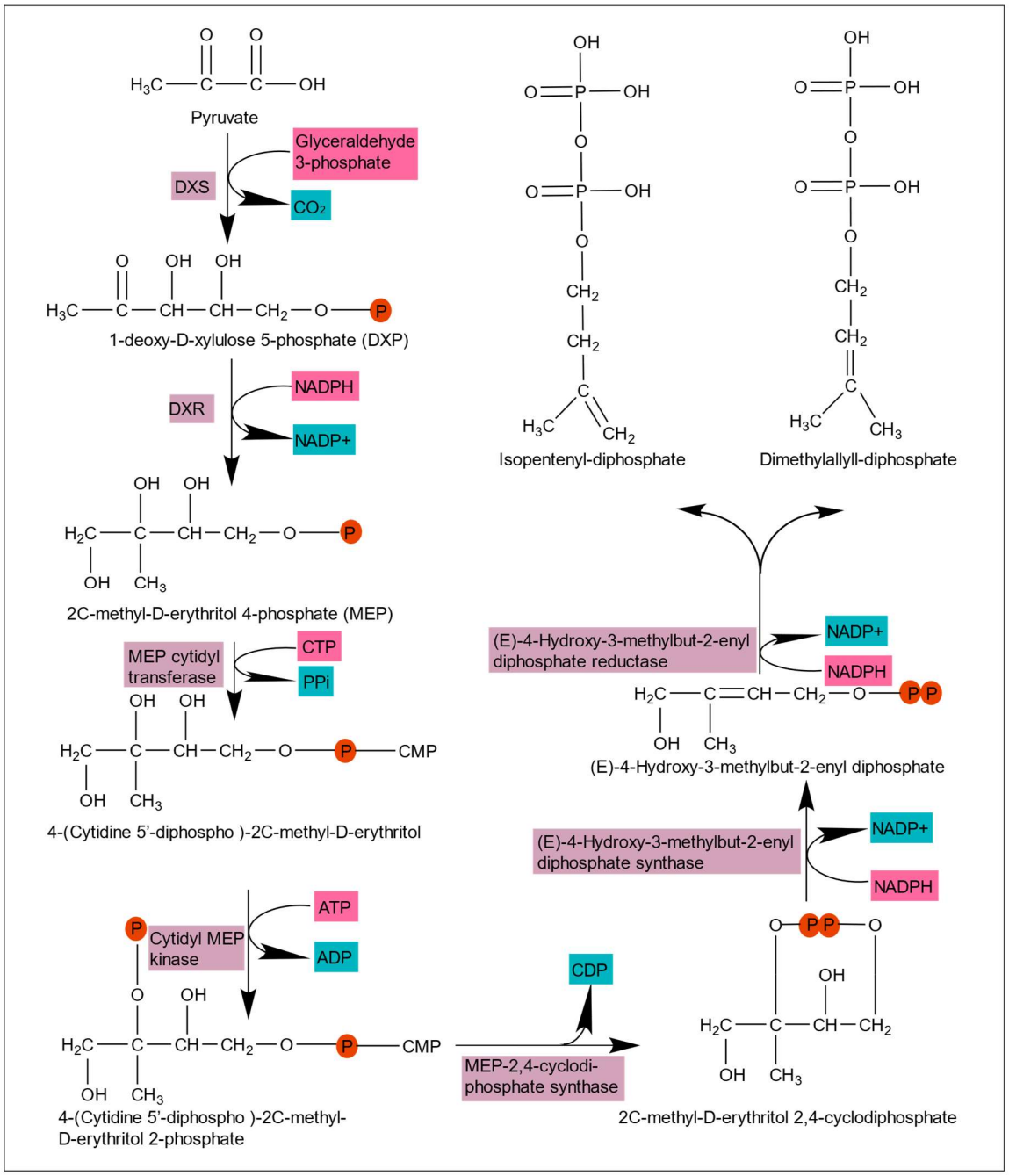

Figure. 1.3 Non-Mevalonate Pathway

Enzymes, substrates and side-products are in purple, pink and blue background, respectively. DXS, 1-deoxy-D-xylulose 5-phosphate synthase; DXR, 1-deoxy-D-xylulose 5-phosphate reductoisomerase. Modified from Biochemistry and Molecular Biology of Plants, 2nd edition. Chapter 24, p1139.

1.1.3 Repetitive Additions of C_5 Units

The second stage of isoprenoid synthesis involves condensation reactions of different numbers of C_5 units into larger products. The smallest prenyl-diphosphate molecule with an allylic double bond is dimethylallyl diphosphate, which serves as the “primer” to which varying numbers of isopentenyl-diphosphate units can be added in sequential steps (Fig1.4). In the beginning, one isopentenyl-diphosphate and one dimethylallyl-diphosphate condense to form geranyl-diphosphate (G-PP, C_{10} compound) (G. Wang & Dixon, 2009). The enzyme responsible for this step is a heterodimeric protein which contains 2 subunits, namely GGPPS LSU and GGPPS SSU type I, respectively. The GGPPS LSU produces mostly geranylgeranyl-diphosphate (GG-PP), its specificity is shifted to the production of geranyl-PP after binding to SSU type I. Another molecule of isopentenyl-diphosphate can be attached to the geranyl-diphosphate by FPS1 or FPS2 (Closa et al., 2010; Manzano et al., 2016), forming farnesyl-diphosphate (C_{15} compound). Addition of a further isopentenyl-diphosphate results in geranylgeranyl-diphosphate production (C_{20} compound), the unsaturated form of phytol.

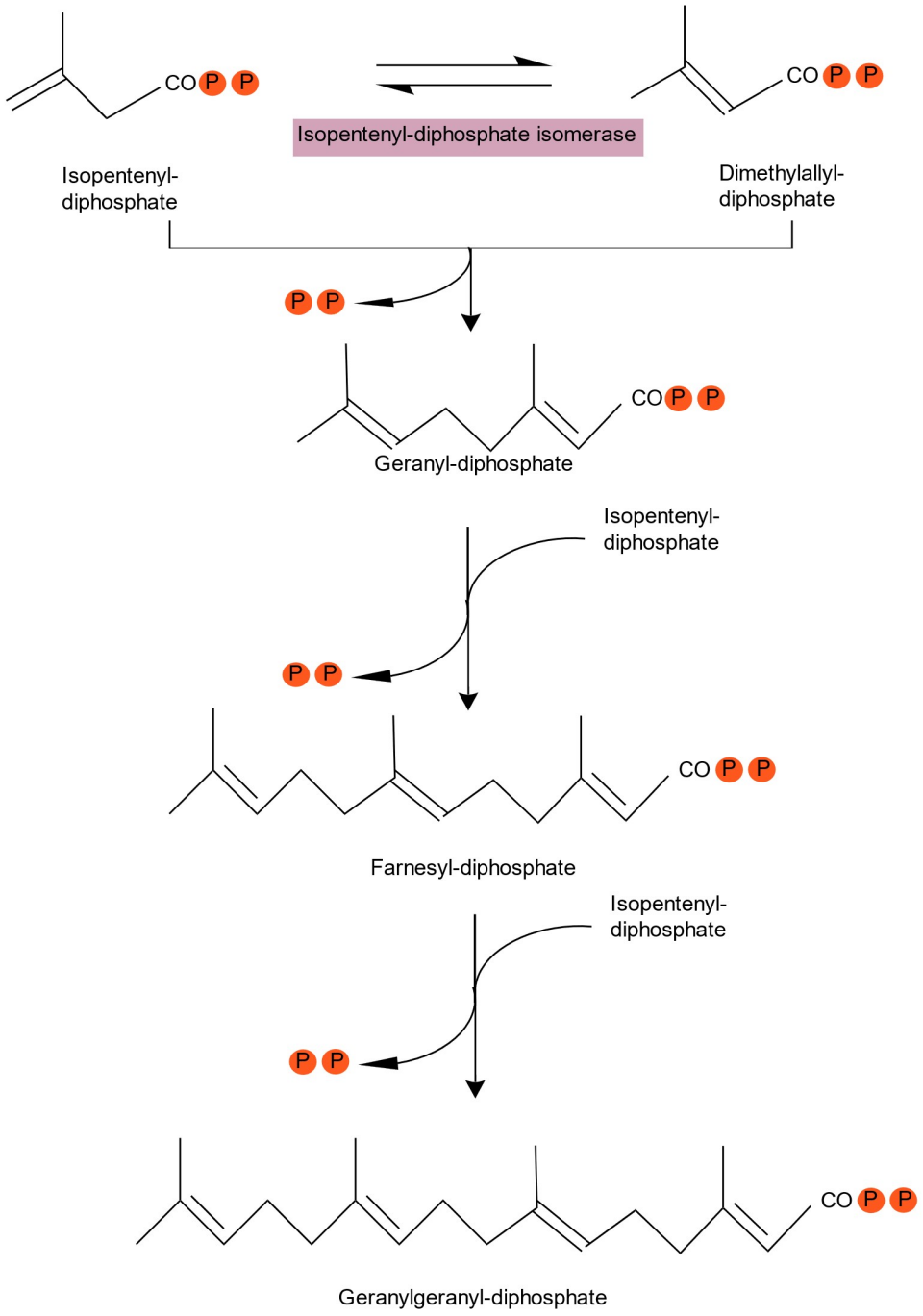

Figure. 1.4 Synthesis of geranylgeranyl-diphosphate.

Geranylgeranyl-diphosphate (GG-PP) contains 3 more double bonds than phytyl-diphosphate (Phytyl-PP). Both of GG-PP and phytyl-PP can be the prenyl side chain donor in chlorophyll synthesis. P in red circle indicates phosphoric acid. Modified from Biochemistry and Molecular Biology of Plants, 2nd edition. Chapter

24, p1140.

1.2 Chlorophyll Synthesis

Chlorophyll can be synthesized via esterification of chlorophyllide, the side-chain free form of chlorophyll. The prenyl side chain donor can be phytyl-diphosphate or geranylgeranyl-diphosphate (Fig. 1.5). The enzyme responsible for this reaction is chlorophyll synthase (CHLG) (Lin et al., 2014; Oster et al., 1997). When the prenyl side donor is geranylgeranyl-diphosphate, the product is chlorophyll-GG, which has three more unsaturated carbon-carbon double bonds in the side chain. Chlorophyll-GG undergoes three sequential reduction reactions catalyzed by GGR, producing chlorophyll (Keller et al., 1998). GGR can also convert geranylgeranyl-diphosphate to phytyl-diphosphate.

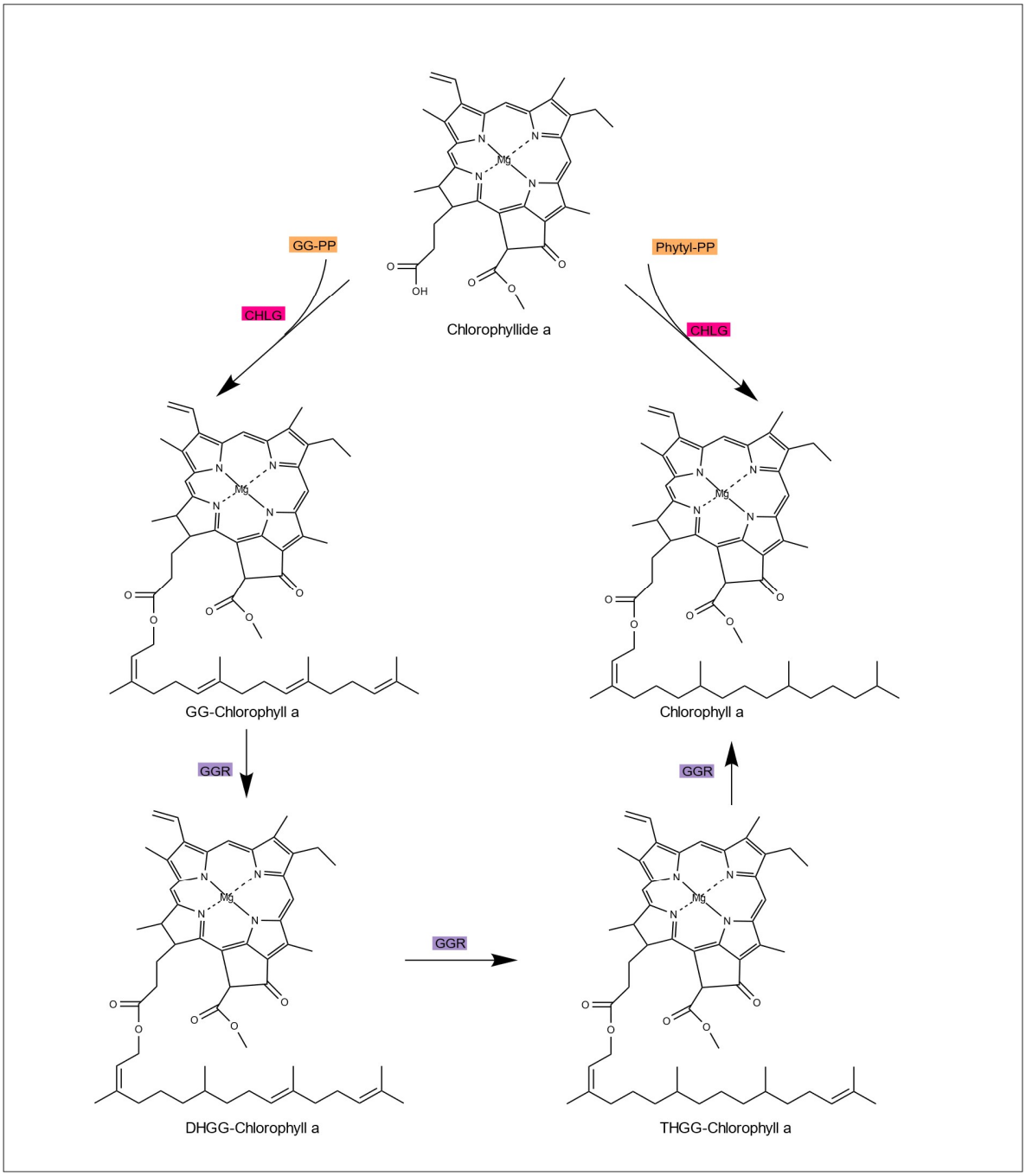

Figure. 1.5 Synthesis of chlorophyll.

Chlorophyll is synthesized via the attachment of geranylgeranyl-diphosphate (GG-PP) to the chlorophyllide a by chlorophyll synthase (CHLG). The product GG-chlorophyll a needs to be reduced by geranylgeranyl reductase (GGR) giving rise to chlorophyll a. GGR can also convert geranylgeranyl-diphosphate to phytyl-diphosphate, which could also serve as the prenyl side chain donor. Modified from

Katharina Gutbrod (Gutbrod et al., 2019).

1.2.1 Chlorophyll Turnover and Degradation

Chlorophyll is continuously synthesized and degraded during turnover (Beisel et al., 2010). During biotic or abiotic stress or during leaf senescence, metabolism shifts from anabolism to catabolism, and chlorophyll degradation is strongly increased (Guo et al., 2004). Chlorophyll is converted to chlorophyllide by highly active chlorophyllases, which was considered to be involved in chlorophyll degradation. However, the *Arabidopsis* chlorophyllases CLH1 and CLH2 do not localize to the plastid but rather to the ER and tonoplast, and the *clh1 clh2* double mutant is still capable of chlorophyll breakdown (Schenk et al., 2007). Moreover, chlorophyllide a can act as anti-microbial and anti-herbivory compound. Therefore, the chlorophyllase CLH1 and CLH2 may play some roles in plant protection, because after cell disruption during plant pathogen interactions, chlorophyll from the chloroplast get in contact with the extraplastidic CLH proteins.

Chlorophyll b needs to be converted to chlorophyll a prior to degradation (Kusaba et al., 2007). The initial step of chlorophyll a degradation is the removal of the Mg ion in the center of the porphyrin ring. The enzyme responsible for this reaction is SGR (Shimoda et al., 2016). The removal of the Mg ion produces pheophytin, which is structurally identical with chlorophyll but lacks the Mg ion. The ester bond connecting the phytyl side chain and the porphyrin ring is hydrolyzed by pheophytin pheophorbide hydrolase or pheophytinase (PPH), releasing pheophorbide a and free phytol (Schelbert et al., 2009). Pheophorbide a is oxidized by pheophorbide a oxidase (PAO) and the ring structure is opened, producing the red metabolite, the first non-green breakdown product of chlorophyll (Pružinská et al., 2003).

CLD1 and CHLG are two enzymes which are involved in chlorophyll turnover and harbor reverse functions (Lin et al., 2016; Oster et al., 1997). CLD1 shows sequence similarities with PPH and is localized to plastids. CLD1 can dephytylate chlorophyll a, chlorophyll b and pheophytin a *in vitro*. Chlorophyllide a can be used as substrate for chlorophyll synthase CHLG during the chlorophyll turnover cycle.

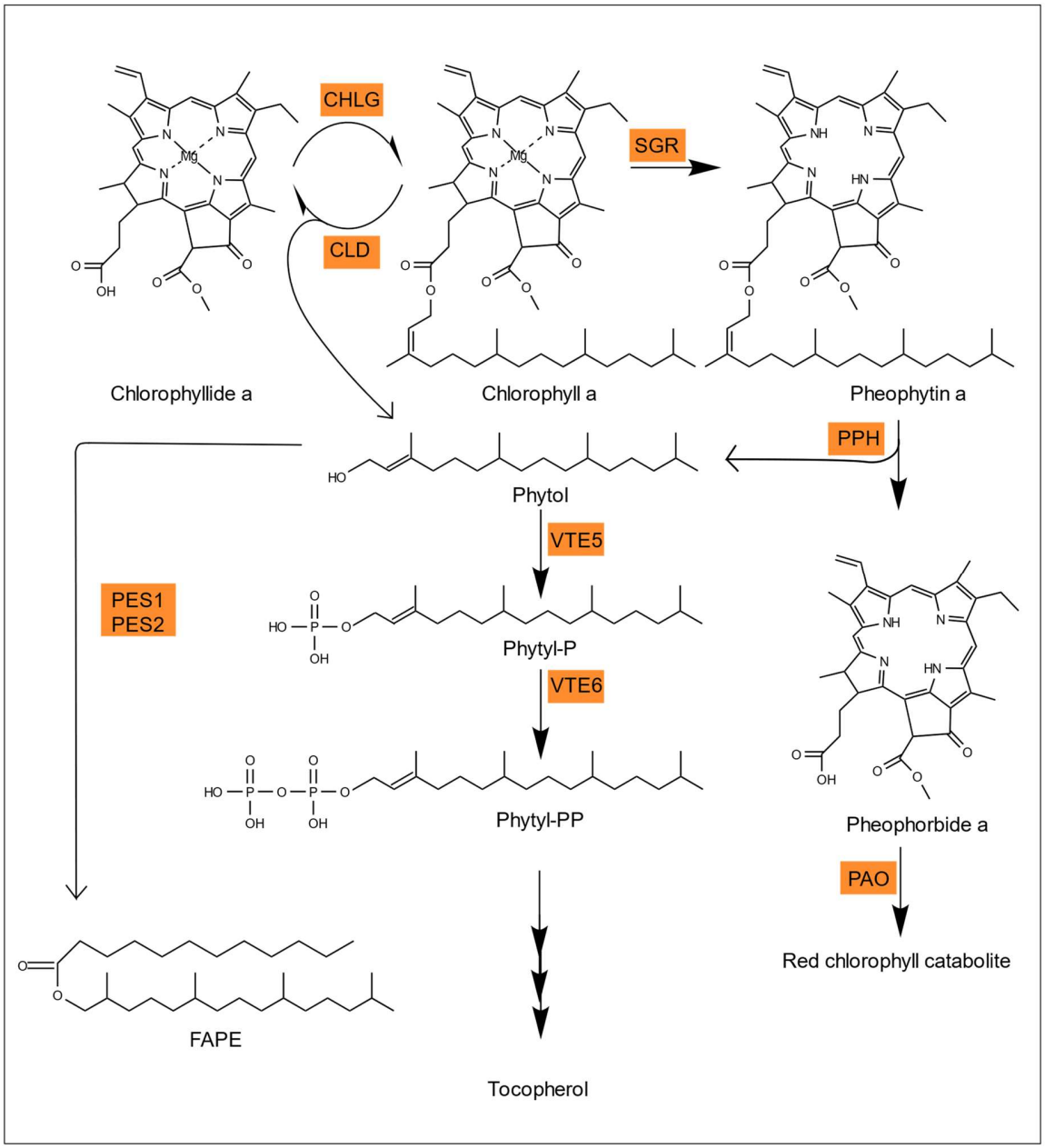

Figure. 1.6 Chlorophyll turnover and degradation

CHLG, chlorophyll synthase; CLD, chlorophyll dephytylase; SGR, stay green protein; PES, phytyl ester synthase; PPH, pheophytin pheophorbide hydrolase; PAO, pheophorbide a Oxygenase; VTE, vitamin E deficient. Modified from (Gutbrod et al., 2019).

1.2.2 Metabolism of phytol

Degradation of chlorophyll results in the release of pheophorbide a and free phytol. Free phytol is then esterified or phosphorylated to be stored as fatty acid phytyl ester (FAPE) or vitamin E, which usually accumulates in the plastoglobules to avoid accumulations of phytol in the chloroplast.

1.2.2.1 Fatty acid phytyl esters (FAPE)

Fatty acid phytyl ester were first detected in chlorotic leaves of Norway maple (*Acer platanoides*) (Grob & Csupor, 1967). Marine bacteria synthesize fatty acid phytyl esters as alternative carbon and energy reservoir (Rontani et al., 1999). FAPE is at very low concentrations in green tissue (Lippold et al., 2012). When plants are under nitrogen limitation condition or cold stress or experience aging, large amounts of FAPE are produced. Different from the fatty acid composition of leaves, most of the fatty acid moieties of FAPE are medium-chain fatty acids (10:0, 12:0, 14:0) and 16:3. Medium-chain fatty acids are the intermediates of fatty acid *de novo* synthesis, while 16:3 fatty acid almost exclusively occurs in the sn-2 position of monogalactosyldiacylglycerol (MGDG) in plants like *Arabidopsis* (Gaude et al., 2007; Lippold et al., 2012). The phenomenon that 1) FAPE exists at very low concentration in green tissues; 2) FAPE accumulates under stress; 3) FAPE decreases when stress is removed, implies that FAPE acts as a temporary storage sink for free phytol, which is detrimental to membrane stability.

The enzymes catalyzing the esterification of free phytol, phytyl ester synthases 1 and 2 (PES1, PES2) belong to the family of esterase/lipase/ thioesterase (ELT) proteins. Both of PES1 and PES2 localize to the plastoglobules, the site of fatty acid phytyl ester accumulation. FAPE contents strongly decrease in the double mutant *pes1 pes2* (Lippold et al., 2012; vom Dorp, 2015).

1.2.2.2 Vitamin E

Vitamin E (tocochromanol) is a class of lipids synthesized in cyanobacteria and in chloroplasts of eukaryotic algae and plants. Tocochromanol is a very important

natural anti-oxidant, which can neutralize toxic reactive oxygen species and free radicals. Tocochromanol is a vitamin which humans must take up from the food (Rizvi et al., 2014). Tocochromanol is composed of a chromanol ring to which a nonpolar prenyl side chain is attached. Depending on the nature of the prenyl side chain, four forms of tocochromanols can be distinguished, i.e. tocopherols, tocotrienols, plastochromanol-8 and tocomonoenols. Depending on the number and position of the methyl groups on the chromanol ring, tocopherol, tocotrienol and tocomonoenol have different sub-types: α, β, γ and δ. *Arabidopsis* can synthesize tocopherol and plastochromanol-8. Two enzymes, phytol kinase (VTE5) and phytyl-phosphate kinase (VTE6) convert free phytol into phytyl-diphosphate (Valentin et al., 2006; vom Dorp, 2015). The chromanol head group of tocochromanol is derived from the shikimate pathway (Tzin & Galili, 2010). The product of the shikimate pathway, chorismate, undergoes a series of reactions to form homogentisate (HGA) (Mène-Saffrané, 2018). Phytyl-diphosphate is attached to HGA by VTE2, forming 2-methyl-6-phytyl-benzoquinol (MPBQ) (Sattler et al., 2004). When the prenyl side chain donor is geranylgeranyl-diphosphate (GG-PP) during tocotrienol synthesis, homogentisate geranylgeranyltransferase (HGGT), a VTE2-related enzyme, catalyzes the condensation of HGA and GG-PP (Cahoon et al., 2003; Yang et al., 2011). Closure of the second ring of the tocochromanol head group is conducted by tocopherol cyclase (VTE1), producing δ-tocopherol (Vidi et al., 2006). Methylation of MPBQ is catalyzed by VTE3, producing 2,3-dimethyl-5-phytyl-1,4-benzoquinone (DMPBQ) (Cheng et al., 2003). VTE1 also catalyzes the ring-closure of DMPBQ, producing γ-tocopherol. δ-Tocopherol and γ-tocopherol can be methylated by VTE4, producing β- and α- tocopherol, respectively (Bergmüller et al., 2003; Zbierzak et al., 2010).

Plastoquinol-9 (PQ-9) is the lipid electron carrier of photosystem II and is derived from condensation of HGA with solanesyl-PP, catalyzed by HGA solanesyl transferase (HST) (Sadre et al., 2006), and methylated by VTE3. Plastochromanol-8 (PC-8) is synthesized from PQ-9 by VTE1. Thus, PC-8 harbors the same head group as γ-tocopherol which carries two methyl groups, but a much longer side chain of 40 carbon atoms.

1.2.2.3 Vitamin K

Phylloquinol (vitamin K1) is the lipid electron carrier in photosystem I. Like tocopherol, phylloquinol is found in the thylakoid membranes and in plastoglobules. The head group of phylloquinol is also derived from the shikimate pathway (Tzin & Galili, 2010). Prior to synthesis of phylloquinol, chorismate needs to be converted to isochorismate by isochorismate synthase (Wildermuth et al., 2002). Isochorismate is transformed into 1,4-dihydroxy-2-naphthoate. Demethylphylloquione is synthesized by attachment of phytyl-diphosphate to 1,4-dihydroxy-2-naphthoate by phytyl transferase ABC4 (Shimada et al., 2005). Demethylphylloquione is reduced to demethylphylloquinol by NAD(P)H quinone oxidoreductase (NDC1) (Fatihi et al., 2015; Piller et al., 2011). Finally, demethylphylloquinol is methylated by MenG, giving rise to phylloquinol (Lohmann et al., 2006).

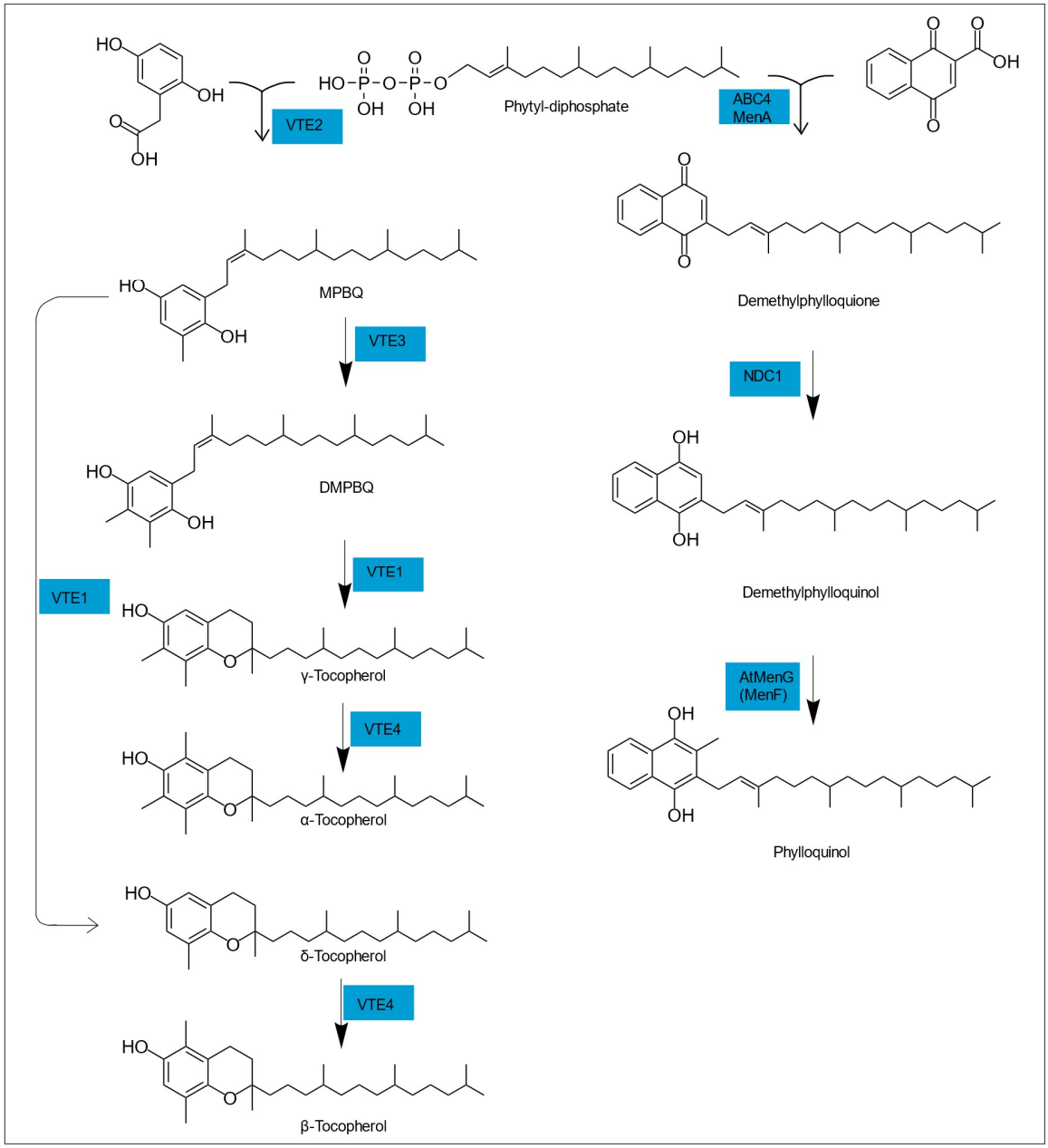

Figure. 1.7 Tocopherol and phylloquinol synthesis

VTE, vitamin E deficient; ABC4/MenA, 1,4-dihydroxy-2- naphthoate phytyltransferase; NDC1, NAD(P)H quinone oxidoreductase; AtMenG/MenG: demethylphylloquinol methyltransferase. Modified from Gutbrod (Gutbrod et al., 2019).

1.3 Branch Chain Fatty Acid Degradation

1.3.1 β-Oxidation

In plants, fatty acid oxidation localizes primarily to the peroxisome. The β oxidation enzymes of peroxisomes form a protein complex. The β oxidation of fatty acids can be conveniently divided into 4 stages: 1) dehydrogenation to a Δ^2-*trans*-unsaturated molecule; 2) addition of a molecule of water to the double bond; 3) oxidation of the β-hydroxyacyl-CoA to a ketone; 4) thiolytic cleavage. The final degradation products of normal fatty acids are (n/2) acetyl-CoA units, n=number of the C atoms.

1.3.2 α-Oxidation

Phytol ([2E,7R,11R]-3,7,11,15-tetramethyl-2-hexadecen-1-ol) harbors a methyl group at the γ position, which inhibits the β oxidation. Therefore, the degradation of phytol has some differences compared to conventional β oxidation.

Humans take up a large amount of phytol from food, as phytol is a component of chlorophyll. The pathway of phytol degradation in humans has been studied in detail, because mutations in genes involved in phytol catabolism result in inheritable genetic diseases. Free phytol is first oxidized to phytenal by an unknown alcohol dehydrogenase (fatty alcohol oxidase). Phytenal is subsequently oxidized by an aldehyde dehydrogenase (ALDH) yielding phytenic acid. The human ALDH3A (P51648, FALDH) was implicated in phytenal oxidation (van den Brink et al., 2004; Nanda M. Verhoeven et al., 1998). Mutations in the *ALDH3A* gene result in the Sjögren-Larsson syndrome, a neurocutaneous disorder. Phytenic acid is converted into its coenzyme A (CoA) ester form by an unknown acyl-CoA synthetase. In animals, these initial steps of phytol degradation are localized to the ER, while phytenoyl-CoA is transported to the peroxisome for α-oxidation. Phytenoyl-CoA is reduced by phytenoyl-CoA reductase (PECR, Q9BY49) yielding phytanoyl-CoA (Gloerich et al., 2006; van den Brink et al., 2005). Phytanoyl-CoA is hydroxylated by phytanoyl hydroxylase (phytanoyl-CoA 2-hydroxylase, PHYH or PAHX; O14832) (Mihalik et al., 1997). Mutations in the human *PHYH/PAHX* locus cause Refsum disease, accompanied with strong

increases of phytanic acid in the blood. 2-Hydroxy-phytanoyl-CoA is then cleaved by hydroxy-acyl-CoA lyase (HPCL or HACL1; Q9UJ83), yielding pristanal, a C19 isoprenoid aldehyde (Casteels et al., 2007; Jansen et al., 1999; Verhoeven et al., 1997). Formyl-CoA is released during this reaction. Pristanal is further oxidized to pristanic acid by an aldehyde dehydrogenase (ALDH), presumably one of three enzymes in humans: ALDH2(P05091), ALDH3A2 (P51648, FALDH) or ALDH9A1 (P49189) (van den Brink et al., 2004). Pristanic acid is converted into pristanoyl-CoA by the very long chain acyl-CoA synthetase (VLCS, O14975) (Steinberg et al., 1999). The C2 atom of pristanoyl-CoA is isomerized from the 2R into the 2S configuration prior to further degradation by β-oxidation. The human α-methylacyl-CoA racemase (AMACR, AF158378) which catalyzes this reaction shows dual localization to the peroxisome and mitochondrion (Ferdinandusse et al., 2000). Patients with inherited AMACR deficiency accumulate pristanic acid in their blood. 2S-Pristanoyl-CoA is then broken down by branched chain fatty acid β-oxidation accompanied with the release of acetyl-CoA and propionyl-CoA in the mitochondria.
In contrast to humans, the phytol degradation pathway in plants is mostly elusive. During senescence or stress, large amounts of phytol are cleaved from chlorophyll in the chloroplast. Plants use alternative pathways to recycle a certain proportion of phytol for the synthesis of chlorophyll, tocochromanol (vitamin E), phylloquinol (vitamin K) or fatty acid phytyl esters in the chloroplast. It has been suggested that plant phytol degradation follows a similar route as described for humans.
Two genes, *PHYH/PAHX (At2g01490)* and *HPCL (At5g17380)* with sequence similarities to the human *PAHX* and *HPCL* genes, respectively, were identified in *Arabidopsis*. *Arabidopsis pahx* mutants (At2g01490) accumulate phytanoyl-CoA (Araújo et al., 2011), but the *Arabidopsis HPCL* gene (At5g17380) has not been studied. While PHAX activity was measured in *Arabidopsis* wild type and *pahx* mutant plants, no enzymatic data are available for HPCL (Araújo et al., 2011).

1.3.3 α-Dioxygenase

An alternative α-oxidation pathway is based on the introduction of a 2-hydroperoxy group into a fatty acid by α-dioxygenases. Two enzymes, α-DOX1 (pathogen-

induced oxygenase, PIOX, At3g01420) and α-DOX2 (At1g73680) were described. Both of α-DOX1 and α-DOX2 can convert free fatty acids into their 2-hydroperoxy derivatives in *Arabidopsis* and other plants (Bannenberg et al., 2009; Sanz et al., 1998). Single and double mutants of the two *Arabidopsis α-dox* genes were produced, but they show no obvious growth phenotype. Interestingly, 2-hydroxy-octadecatrienoic acid (2-hydroxy-18:3) accumulates in senescent leaves of the *α-dox1*, but not in the *α-dox2* mutant. Expression of the two genes is upregulated during senescence. α-DOX1 was localized to the oil bodies, while α-DOX2 was found in the ER. 2-Hydroperoxy-fatty acids can be reduced to the corresponding 2-hydroxy-fatty acids by an unknown peroxidase. Alternatively, spontaneous decarboxylation of the 2-hydroperoxy-fatty acid results in an aldehyde shortened by one carbon atom. In this way, 2-hydroperoxy-phytanic acid could be converted into pristanal. So far, it remains unclear whether phytanic acid is a substrate for α-DOX1 and α-DOX2 and whether α-DOX1 and α-DOX2 are involved in phytol degradation in plants.

1.4 Objective

In the course of this project, I will study the role of the candidate genes for phytol catabolism by characterizing the enzymatic functions of the proteins and the metabolites in insertional mutants. *Arabidopsis* mutants for most of the candidate genes have already been isolated in other groups with whom we collaborate. I will not only measure the amounts of phytol and other metabolites including aldehydes (phytenal, pristinal), isoprenoid acids (phytenic acid, phytanic acid, pristanic acid), but also phytol-containing compounds derived from alternative pathways (tocopherol, fatty acid phytyl esters). I will study the enzymatic activity of the *Arabidopsis* HPCL protein to prove its involvement in phytol degradation. I will study the subcellular localization of *Arabidopsis* HPCL protein to further confirm its function.

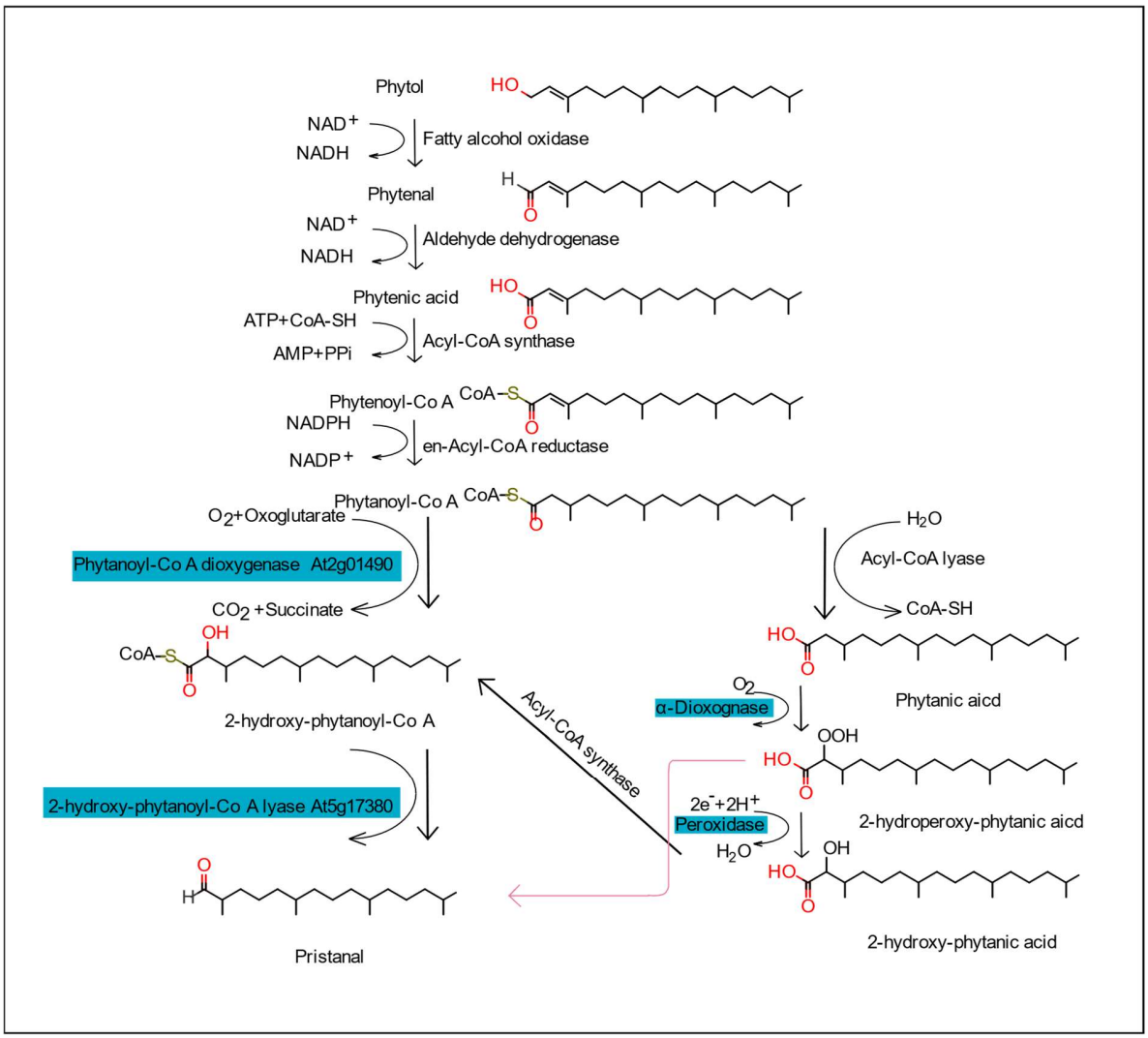

Figure. 1.8 Hypothetical phytol degradation pathway in plants

Genes potentially involved in phytol degradation are highlighted in blue background. The pink arrow indicates a putative non-enzymatic reaction.

2. MATERIALS AND METHODS

2.1 Equipment

6530 Accurate-mass quadrupole time-of-flight (Q-TOF) LC/MS	Agilent, Böblingen (DE)
7890 gas chromatography with mass spectrometry (GC-MS)	Agilent, Böblingen (DE)
6500 LC-MS/MS Q-Trap	Agilent, Böblingen (DE)
Autoclave	Systec, Linden (DE)
Balance 770	Kern, Balingen-Frommern (DE)
Balance PG503-S Delta Range	Mettler Toledo, Gießen (DE)
Block heater SBH130D/3	Bioer, Hangzhow (CHN)
Centrifuge 5417 R	Eppendorf, Hamburg (DE)
Centrifuge 5810 R	Eppendorf, Hamburg (DE)
Centrifuge 5430	Eppendorf, Hamburg (DE)
Centrifuge Sorvall RC 5C PLUS	Thermo Fisher Scientific, Braunschweig (DE)
Chemiluminescence documentation system	Bio-Rad, California (USA)
Gel caster, Mighty small II	GE Healthcare Europe, Freiburg (DE)
High-performance-liquid-chromatography (HPLC) 1200 series	Agilent, Böblingen (DE)
Homogeniser Precellys 24	PeQlab, Erlangen (DE)
Horizontal electrophoresis chamber	Cti, Idstein (DE)
Incubator with light supply	Snijiders Scientific b.v., Tilburg (NL)
Magnetic stirrer MR30001	Heidolph Instruments, Schwabach (DE)
pH meter inoLab pH Level 1	WTW, Weilheim (DE)
Photometer LI-185B	LI-COR, inc. (USA)
Photometer, Specord 205	Analytik Jena, Jena (DE)
Phytochamber	SIMATiC OP17, York International, York (USA)
PowerPac Basic electrophoresis power Supply	Bio-Rad Laboratories, München (DE)
Sample concentrator	Techne (Bibby Scientific), Stone (GB)
Semi-dry transfer cell Trans-BLOT SD	Bio-Rad Laboratories, München (DE)
Shaking Incubator with light supply	INFORS, Einsbach (DE)
Spectrophotometer Nanodrop 1000	PeQlab, Erlangen (DE)
Sterile bench model 1.8	Holten Lamin Air, Allerød (DK)
Synergy Water Purification System	Merck Millipore, Darmstadt (DE)
Thermocycler TPersonel 48	Biometra, Göttingen (DE)
Ultracentrifuge Optima L 90K equipped with Ti60 Rotor	Beckman Coulter, Krefeld (DE)

VortexGenie2	Scientific Industries, Bohemia (USA)
Water bath TW20	Julabo, Seelbach (DE)
Zeiss LSM780 Confocal laser scanning microscope	Carl Zeiss, Zaventem (BEL)

2.2 Materials

2.2.1 Consumables

Auto sampler vials with inlets and screw caps with PTEF septa	VWR, Darmstadt (DE)
Centrifuge tubes (15 and 50 mL)	Greiner Bio-One, Frickenhausen (DE)
Ceramic beads different sizes	Mühlmeier Mahltechnik, Bärnau (DE)
Culture glass tubes (15.5 x 160 mm)	Schott, Mainz (DE)
Electroporation cuvettes	PeQlab, Erlangen (DE)
Glass Pasteur pipettes (150 and 225 mm)	Brand, Wertheim (DE)
Glass vials with and without screw up 8 mL	VWR, Darmstadt (DE)
Glass vials with screw up 40 mL	Schmidlin, Neuheim (CH)
Microcentrifuge tubes (1.5 and 2 mL)	Greiner Bio-One, Frickenhausen (DE)
PCR tubes	Brand, Wertheim (DE)
Petri dishes (round, 94 x 16 and 145 x 20 mm)	Greiner Bio-One, Frickenhausen (DE)
Petri dishes (square, 100 x 100 mm)	Greiner Bio-One, Frickenhausen (DE)
Pipette tips	Axygen, Corning, Karlsruhe (DE) or Greiner Bio-One, Frickenhausen (DE)
Pots for plant cultivation	Pöppelmann, Lohne (DE)
PTFE screw caps for 8 mL glass vials	Schott, Mainz (DE)
PTFE septa for screw caps for 8 mL glass vials	Schmidlin, Neuheim (CH)
Soil (type Topf 1.5)	Gebrüder Patzer, Sinntal-Jossa (DE)
SPE silica column (Strata Si-1 silica, 55µm, 100 mg)	Macherey-Nagel, Düren (DE)
Sterile filter for syringes 0.2 µm pore size	Schleicher and Schuell, Dassal (DE)
SuperSignal® West Pico Chemiluminescent Substrate	Thermo Fisher Scientific, Braunschweig (DE)
Syringes 30 and 5 mL	Labomedic, Bonn (DE)
Teflon septa for screw caps	Schmidlin, Neuheim (DE)
Trays for plants cultivation	Pöppelmann, Lohne (DE)
Vermiculite	Klemens Rolfs, Siegburg (DE)

2.2.2 Chemicals

Acetic acid	AppliChem, Darmstadt (DE)
Acetone	Prolabo VWR, Darmstadt (DE)
Acetonitrile	Roth, Karlsruhe (DE)
Acetosyringone	Sigma-Aldrich, Taufkirchen (DE)
Acetyl coenzyme A lithium salt	Sigma-Aldrich, Taufkirchen (DE)
Acrylamide/Bis-acrylamide	Roth, Karlsruhe (DE)
Agarose	PeQlab, Erlangen (DE)
ε-Aminocaproic acid	Sigma-Aldrich, Taufkirchen (DE)
Ammonia solution 25%	Merck, Darmstadt (DE)
Ammonium acetate	Sigma-Aldrich, Taufkirchen (DE)
Ammonium nitrate	AppliChem, Darmstadt (DE)
Ammonium persulfate	AppliChem, Darmstadt (DE)
Bacto agar	Duchefa Biochemie, Haarlem (NL)
Bacto peptone Benzene	Duchefa Biochemie, Haarlem (NL)
Benzamidine	Sigma-Aldrich, Taufkirchen (DE)
Boric acid	AppliChem, Darmstadt (DE)
Bovine serum albumin (BSA)	Sigma-Aldrich, Taufkirchen (DE)
Bromophenol blue	Serva, Heidelberg (DE)
Calcium chloride	Merck, Darmstadt (DE)
Calcium nitrate	Sigma-Aldrich, Taufkirchen (DE)
Cellfectin II	Thermo Fisher Scientific, Braunschweig (DE)
Cetyltrimethylammonium bromide (CTAB)	Roth, Karlsruhe (DE)
CHAPS	AppliChem, Darmstadt (DE)
Chloroform	Merck, Darmstadt (DE)
Citric acid	Sigma-Aldrich, Taufkirchen (DE)
Cobalt (II)-chloride-hexahydrate	Merck Millipore, Darmstadt (DE)
Coomassie Brilliant Blue R250	Merck, Darmstadt (DE)
Copper(II) sulfate	Merck, Darmstadt (DE)
Dichloromethane	AppliChem, Darmstadt (DE)
Diethylether	Prolabo VWR, Darmstadt (DE)
Dimethylsulfoxide (DMSO)	AppliChem, Darmstadt (DE)
EDTA	AppliChem, Darmstadt (DE)
Ethanol	Merck, Darmstadt (DE)
Ethidium bromide	Serva, Heidelberg (DE)
Ethyl chloroformate	Sigma-Aldrich, Taufkirchen (DE)
Fe-EDTA	Sigma-Aldrich, Taufkirchen (DE)
Glucose	Duchefa Biochemie, Haarlem (NL)
Glycerol	AppliChem, Darmstadt (DE)
Glycine	Roth, Karlsruhe (DE)
n-Hexane	Merck, Darmstadt (DE)

Hydrochloric acid (HCl)	AppliChem, Darmstadt (DE)
LB Broth (Lennox) low salt	Formedium, Norfolk (UK)
IPL-41 Insect medium	PAN-biotech, Aidenbach (DE)
Isoamyl alcohol	Roth, Karlsruhe (DE)
Isopropyl-β-D-1-thiogalactopyranoside (IPTG)	Formedium, Swaffham (UK)
Isopropanol	AppliChem, Darmstadt (DE)
Leupeptin	Sigma-Aldrich, Taufkirchen (DE)
Lipid mix (1000x)	Sigma-Aldrich, Taufkirchen (DE)
Lithium aluminum hydride	Sigma-Aldrich, München (DE)
Magnesium chloride	AppliChem, Darmstadt (DE)
Magnesium sulfate	Duchefa Biochemie, Haarlem (NL)
Manganese (II) chloride	AppliChem, Darmstadt (DE)
β-Mercaptoethanol	Sigma-Aldrich, Taufkirchen (DE)
Methanol	Fisher Chemicals, Braunschweig (DE)
Methanolic hydrochloric acid (3N)	Sigma-Aldrich, München (DE)
Methoxylamine HCl	Sigma-Aldrich, Mu (DE)
Mono potassium phosphate	Roth, Karlsruhe (DE)
MS salt with vitamins	Duchefa Biochemie, Haarlem (NL)
N-Methyl-N-(trimethylsilyl)-trifluoroacetamide (MSTFA)	AppliChem, Darmstadt (DE)
2-(N-Morpholino) ethanesulfonic acid mono hydrate (MES H_2O)	Duchefa Biochemie, Haarlem (NL)
Oxalyl chloride	AppliChem, Darmstadt (DE)
Pepstatin	AppliChem, Darmstadt (DE)
Peptone	Formedium, Swaffham (UK)
Phenol	Roth, Karlsruhe (DE)
Phenylmethylsulfonyl fluoride (PMSF)	Sigma-Aldrich, Taufkirchen (DE)
Phosphoric acid	AppliChem, Darmstadt (DE)
Phytoagar	Duchefa Biochemie, Haarlem (NL)
4-Piperazinediethanesulfonic acid (PIPES)	AppliChem, Darmstadt (DE)
Potassium bicarbonate	Sigma-Aldrich, Taufkirchen (DE)
Potassium chloride	Merck, Darmstadt (DE)
Potassium dihydrogenphosphate	Merck, Darmstadt (DE)
Potassium hydroxide	Merck, Darmstadt (DE)
Potassium nitrate	Grüssing, Filsum (DE)
Pyridine	AppliChem, Darmstadt (DE)
Pyridinium chlorochromate	Sigma-Aldrich Taufkirchen (DE)
Sodium chloride	Duchefa Biochemie, Haarlem (NL)
Sodium dodecyl sulfate (SDS)	AppliChem, Darmstadt (DE)

Sodium hydroxide	Prolabo VWR, Darmstadt (DE)
Sodium hydrogen carbonate	Merck, Darmstadt (DE)
Sodium hypochlorite	Roth, Karlsruhe (DE)
Sodium molybdate	Merck Millipore, Darmstadt (DE)
Sorbitol	Duchefa Biochemie, Haarlem (NL)
Sucrose	Duchefa Biochemie, Haarlem (NL)
Tetramethylethylenediamine (TEMED)	Roth, Karlsruhe (DE)
Tetrahydrofuran	Fisher Scientific, Schwerte (DE)
Thiomersal	Sigma-Aldrich, Taufkirchen (DE)
Toluene	Prolabo VWR, Darmstadt (DE)
Toluidine blue	Sigma-Aldrich, Taufkirchen (DE)
Trasylol	Sigma-Aldrich, Taufkirchen (DE)
Triethylamine	Acros, Geel (BE)
Tris-(hydroxymethyl)-aminomethane	Duchefa Biochemie, Haarlem (NL)
Trypan blue	Sigma-Aldrich, Taufkirchen (DE)
Tryptone	AppliChem, Darmstadt (DE)
Tween-20	Sigma-Aldrich, Taufkirchen (DE)
Yeast extract	Duchefa Biochemie, Haarlem (NL)
Yeast nitrogen base	BD, Heidelberg, (DE)
Xylene cyanol FF	Sigma-Aldrich, Taufkirchen (DE)
Zinc sulfate	Merck Millipore, Darmstadt (DE)

2.2.3 Kits and Enzymes

Ambion TURBO DNA-free™ Kit	Thermo Fisher Scientific Karlsruhe, (DE)
CloneJET PCR Cloning Kit	Thermo Fisher Scientific, Karlsruhe (DE)
Color Prestained Protein Standard, Broad Range (11–245 kDa)	New England Biolabs, Frankfurt a. M. (DE)
DCS DNA Polymerase	DNA Cloning Service (DCS), Hamburg (DE)
dNTPs	DNA Cloning Service (DCS), Hamburg (DE)
ECL prime western blot detection kit	Thermo Fisher Scientific, Braunschweig (DE)
First Strand cDNA Synthesis Kit	Fermentas, St. Leon-Rot, (DE)
GeneRuler 1kb DNA ladder	Thermo Fisher Scientific, Braunschweig (DE)
High speed plasmid mini kit	DNA Cloning Service (DCS),

	Hamburg (DE)
Lysozyme	Sigma-Aldrich, Taufkirchen (DE)
NucleoSpin Gel and PCR Clean-up Kit	Macherey-Nagel, Düren (DE)
NucleoSpin Plant RNA kit	Macherey-Nagel, Düren (DE)
NucleoSpin Plasmid Kit	Macherey-Nagel, Düren (DE)
Q5® High-Fidelity DNA Polymerase	New England Biolabs, Frankfurt, (DE)
Restriction endonucleases and Buffers	New England Biolabs, Frankfurt, (DE)
RNase A	Boehringer Mannheim, Roche, Grenzach- Wyhlen (DE)
T4 DNA Ligase	New England Biolabs, Frankfurt, (DE)

2.2.4 Lipid Standards

16:0 Aldehyde (Hexadecanal)	Cayman Chemical, Michigan (USA)
15:0 Fatty acid (Pentadecanoic acid)	Sigma-Aldrich, München (DE)
17:0 Fatty acid (Heptadecanoic acid)	Sigma-Aldrich, München (DE)
17:0 Fatty acid phytyl ester	Synthesized in the IMBIO
19:0 Fatty acid (Nonadecanoic acid)	Sigma-Aldrich, München (DE)
20:0 Fatty acid (Eicosanoic acid)	Sigma-Aldrich, München (DE)
18:1 Alcohol (Octadecenol)	Sigma-Aldrich, Taufkirchen (DE)
di-14:0 PC	Avanti, Alabaster (USA)
2-Hydroxy-palmitic acid	TCI, Tokyo, Japan
Phytol (natural isomer)	Chem-Impex International, Wood Dale, Illinois (USA)
Pristanic acid	Larodan, Solna (Sweden)
Phytanic acid	Larodan, Solna (Sweden)
rac-Tocol	Matreya, Pleasant Gap, PA (USA)

2.2.5 Antibiotics

All the antibiotics used in this studied were purchased from Duchefa (Haarlem, Netherlands). Tetracycline, chloramphenicol, G418, penicillin, streptomycin, spectinomycin, kanamycin and gentamicin were dissolved in de-ionized water and filter-sterilized. Rifamycin was dissolved in DMSO. All the antibiotics were prepared as 1000x stock(50mg/mL) and stored at -20°C.

2.2.6 Organisms

Table. 1 *Saccharomyces cerevisiae* (yeast) lines used in this study

Line	Resistance	Genotype	Source
Wild type	-		Euroscarf, Frankfurt (DE)
Δ*pxp1*	G418	MATa;his3D1;leu2D0;met15D0; ura3D0; yel020c::KanMX4	Euroscarf, Frankfurt (DE)
Δ*mpo1*	G418	MATa;his3D1;leu2D0;met15D0;ura3D0; ygl010w::KanMX4	Euroscarf, Frankfurt (DE)

Table. 2 Other microorganisms used in this study

Line	Organism	Resistance	Usage	Reference
Electroshox	*E.coli*	Streptomycin	Cloning	Bioline，DE
BL21pLySs	*E.coli*	Chloramphenicol	Protein expression	Invitrogen, DE
DH10 Bacα	*E.coli*	Kanamycin, tetracycline	Bacmid preparation	Invitrogen, DE
GV3101: pMP90	*A.tumefaciens*	Rifampicin, gentamucin	Protein expression	DNA Cloning service, DE
SF9	*S.frugiperda*	–	Protein expression and activity study	Invitrogen, DE

Table. 3 *Arabidopsis thaliana* lines used in this study

Genotype	Ecotype	Gene	Accession No.	Source	Reference
Wild type	Col-0	–	–	–	–
pahx-1	Col-0	At2g01490	SALK065006	Kimitsune Ishizaki	(Araújo et al., 2011)
pahx-2	Col-0	At2g01490	GK010F09	Kimitsune Ishizaki	(Araújo et al., 2011)
pahx-3	Col-0	At2g01490	GK220D06	Kimitsune Ishizaki	(Araújo et al., 2011)
αdox1	Col-0	At3g01420	SALK_005633	Carmen Castresana	(Sanz et al., 1998)
αdox2	Col-0	At1g73680	SALK_029547	Carmen Castresana	(Bannenberg et al., 2009)
αdox1αdox2	Col-0	At3g01420-At1g73680		Carmen Castresana	(Bannenberg et al., 2009)

Genotype	Ecotype	Gene	Accession No.	Source	Reference
hpcl-1	Col-0	At5g17380	SALK_142717	NASC	-
hpcl-2	Col-0	At5g17380	SAIL_343D06/ CS816002	Kimitsune Ishizaki	-
hpcl-3	Col-0	At5g17380	SALK_001425 C	NASC	-
pes1 pes2	Col-0	At1g54570-At3g28640		Katharina Gutbrod	(Lippold et al., 2012)
vte5-2	DS-11	At5g04490	pst12490	RIKEN, Japan	(Valentin et al., 2006)
wsd1-2	Col-0	At5g37300	SALK_118165	NASC	(Patwari, 2019)
wsd6-1	Col-0	At3g49210	SALK_130459	NASC	(Patwari, 2019)
wsd6-2	Col-0	At3g49210	SAIL_1257_G 12	NASC	(Patwari, 2019)
wsd7-2	Col-0	At5g12420	SALK_028121	NASC	(Patwari, 2019)

2.2.7 Vectors and Recombinant Plasmids

Table. 4 Vectors

Vector	Target organism	Resistance	Usage	Reference
pJet1.2	*E.coli*	Penicillin	Cloning	Thermo Fisher Scientific
pQE81L	*E.coli*	Penicillin	Protein expression	Qiagen
pET43b	*E.coli*	Penicillin	Protein expression	Novagen
pDR196	*S.cerevisiae*	Penicillin/uracil defective	Protein expression	(Rentsch et al., 1995)
pL9000-35s-GFP	*A.tumefaciens*	Streptomycin, spectinomycin	Protein expression	Dr. Georg Hölzl, IMBIO,
pFastBac1	*E.coli*	Penicillin, gentamycin	Bacmid preparation	Invitrogen
pIVEX1.3	–	Penicillin	Protein expression	Biotechrabbit
pIVEX1.4	–	Penicillin	Protein expression	Biotechrabbit

Table. 5 Recombinant plasmids

Plasmid	Usage
pJet-AtHPCL	Cloning
pQE81L-6xHis-AtHPCL	Protein expression
pET43b-Nus-AtHPCL-6xHis	Protein expression
pDR196-AtHPCL	Protein expression
pL9000-35s-eGFP-AtHPCL	Protein expression
pFastBac1-6XHis-AtHPCL	Bacmid preparation
pIVEX1.3-AtHPCL-6xHis	Protein expression
pIVEX1.4-6xHis-AtHPCL-	Protein expression

2.3 Methods

2.3.1 Cultivation and Transformation of Organisms

2.3.1.1 *Arabidopsis thaliana*

2.3.1.1.1 *Arabidopsis thaliana* Germination on Murashige-Skoog Medium

Arabidopsis lines were surface-sterilized and germinated on MS medium (Murashige & Skoog, 1962) containing 0.7% agar and 2% sucrose. 1 week old plants were transferred onto fresh MS medium with forceps. For surface-sterilization, ~100 seeds were put in a 1.5 mL Eppendorf tube and washed with 1 mL 99% ethanol. Subsequently, 1 mL of sterilization solution (0.1% Tween, 5-6% sodium hypochlorite) was added and mixed for 12 min. Then 1 mL of sterile water was added. Afterwards the sterilization solution was discarded and the seeds were washed with sterile water 5 times to completely remove the remaining sterilization solution. Finally, the seeds were plated onto MS medium and vernalized at 4 °C for 24 h and transferred to a Percival growth chamber. Parameters: light intensity, 120 µmol m^{-2} s^{-1}; 16 h light and 8 h dark; 21 °C and 60% relative humidity.

2.3.1.1.2 *Arabidopsis thaliana* Growth on Soil

Arabidopsis plants were germinated on MS medium containing sucrose as described above. After about 7 days, the seedlings were transferred to 10 cm pots containing soil/vermiculite (2:1, v/v). Plants were grown in phytochambers with a light intensity of 150 µmol m^{-2} s^{-1}. Parameters: 16 h light per day, 20 °C and 55% relative humidity.

2.3.1.1.3 *Arabidopsis thaliana* Growth under Nitrogen Deprivation

Plants were first grown on MS medium containing sucrose for 3 weeks and then transferred to synthetic *Arabidopsis* nutrient medium (+N) or nutrient medium depleted of nitrogen sources (-N) under sterile condition. Afterwards, the growth conditions were the same as in chapter 2.3.1.1.1.

Table. 6 Synthetic *Arabidopsis* nutrient medium

Ingredient	－N	＋N
Agarose	0.8 % (w/v)	0.8 % (w/v)
Sucrose	1 % (w/v)	1 % (w/v)
$MgSO_4$	1 mmol/L	1 mmol/L
KH_2PO_4	1 mmol/L	1 mmol/L
Fe-EDTA	25 µmol/L	25 µmol/L
Boric acid	35 µmol/L	35 µmol/L
$MnCl_2$	7 µmol/L	7 µmol/L
$CuSO_4$	0.25 µmol/L	0.25 µmol/L
$ZnSO_4$	0.5 µmol/L	0.5 µmol/L
Na_2MoO_4	0.1 µmol/L	0.1 µmol/L
NaCl	5 µmol/L	5 µmol/L
$CoCl_2$	5 nmol/L	5 nmol/L
KNO_3	0	2.5 mmol/L
$CaNO_3$	0	1 mmol/L
NH_4NO_3	0	1 mmol/L
KCl	2.5 mmol/L	0
$CaCl_2$	1 mmol/L	0

2.3.1.1.4 *Arabidopsis thaliana* Phytol Supplementation

Plants were grown on MS medium with 1 % sucrose. After 3 weeks, plants were transferred to flasks containing MES-KOH buffer, pH= 6.5. Phytol was added to a final concentration of 0.1 %. Flasks were incubated for 12 h in the phytochambers with a light intensity of 150 µmol m^{-2} s^{-1}. Parameters: 16 h light per day, 20 °C and 55% relative humidity.

2.3.1.2 *Nicotiana benthamiana*

2.3.1.2.1 *Nicotiana benthamiana* Growth on Soil

To study the subcellular location, AtHPCL was transiently expressed in *Nicotiana benthamiana* leaves. *Nicotiana benthamiana* seeds were germinated on a mixture of soil and vermiculite (2:1; v/v) and grown in phytochambers. Parameters: light intensity, 160 µmol m^{-2} s^{-1}; 16 h light and 8 h dark; 25 °C and 60% relative humidity. The seedlings were transferred to single pots after two weeks with forceps and grown for another 3 weeks. Young fully expanded leaves of 5-week-old plants were used for infiltration.

2.3.1.2.2 *Nicotiana benthamiana* Transformation

Transient expression of AtHPCL in leaves was done according to previous work (Patwari, 2019). *A.tumefaciens* strains harboring the different vectors were grown in YEP medium supplemented with appropriate antibiotics at 28 °C with shaking at 180 rpm until OD_{600nm} reached 0.4-1.5. Cells were collected by centrifuging and gently resuspended in infiltration buffer (5 mM MES-KOH, pH 5.7, 5 mM $MgSO_4$, 100 µM acetosyringone). Then *A.tumefaciens* cultures harboring different vectors were mixed such that for each construct mixture OD_{600nm} = 0.8. Each *Agrobacterium* mixture consisted of constructs P19 and eGFP-AtHPCL (target gene) or CFP-SKL (peroxisome marker). The final mixture was injected into the lower epidermis (abaxial side) of the leaves by a 5-mL syringe without the needle. Plants were grown for another 2-3 days before imaging by confocal laser scanning microscopy (CLSM).

YEP medium

10 g/L	Bac peptone
10 g/L	Yeast extract
0.5%	NaCl

2.3.1.3 *Escherichia coli*

2.3.1.3.1 *Escherichia coli* Cultivation and Generation of Competent Cells

Escherichia coli (*E.coli*) cells were grown on solid or in liquid Luria-Bertani (LB) medium at 37°C complemented with appropriate antibiotics. Liquid cultures were shaken at 180 rpm. For competent cell generation, all procedures were performed under sterile conditions. A single colony of *E.coli* strain was inoculated in 1 mL of SOB medium and grown at 37 °C overnight (preculture). Subsequently, 200 mL SOB medium was inoculated with the preculture containing antibiotics and the cells were grown until the OD_{600nm} reached 0.5. The following steps took place on ice. The culture was cooled on ice for 30 min. Afterwards cells were harvested by centrifugation (4000 x *g*, 10 min, 4°C) and resuspended in 80 mL cold TB buffer. The centrifugation step was repeated once. *E.coli* cells were resuspended in 8 mL ice-cold TB buffer (+7% DMSO) and aliquoted into 80 µl portions in sterile 1.5 mL Eppendorf tubes.

LB medium:

20 g/L	LB broth salt
(For solid) 15g/L	Bacto-Agar
pH=7.2 with NaOH	

TB buffer:

10 mmol/L	PIPES
55 mmol/L	$MnCl_2$
15 mmol/L	$CaCl_2$
250 mmol/L	KCl
pH=7.0 with KOH	
Filter-sterilize	

SOB medium:

20 g/L	Tryptone
5 g/L	Yeast extract
0.5 g/L	NaCl
25 mmol/L	KCl
pH=7.2 with NaOH	
Autoclave 121°C, 20 min	
10 mmol/L	$MgCl_2$
10 mmol/L	$MgSO_4$

2.3.1.3.2 *Escherichia coli* Transformation

For electroporation and transformation of *E.coli*, 80 µL of competent cells were thawed on ice, mixed with 5 µL of plasmid DNA and incubated for 5 min on ice. The cell/DNA mixture was transferred to a pre-cooled electroporation cuvette and a pulse of 1800 V was applied. 1 mL of ice-cold LB medium without antibiotics was added immediately and the cells were incubated for 1 h at 37°C with shaking at 180rpm. Finally, the cells were plated on LB medium with appropriate antibiotics and grown overnight.

2.3.1.4 *Saccharomyces cerevisiae*

2.3.1.4.1 *S.cerevisiae* Cultivation and Generation of Competent Cells

S.cerevisiae cells were grown on solid or in liquid YPD or minimal medium at 28 °C complemented with appropriate antibiotics. Liquid cultures were shaken at 180 rpm. For competent cell generation, all procedures were performed under sterile conditions. A single colony of *S.cerevisiae* strain was inoculated in 10 mL of YPD medium and grown at 28 °C overnight (preculture). Subsequently, 500 mL YPD medium was inoculated with the preculture containing antibiotics and was grown until the OD_{600nm} reached 1.3-1.5. The following steps took place on ice. Cells were harvested by centrifugation (4000 x *g*, 10 min, 4°C) and resuspended in 500 mL of ice cold sterile de-ionized water. The centrifugation step was repeated once. Cells were washed with 250 mL ice-cold sterile de-ionized water again. Then, cells were

washed with 20 mL cold 1 M sterile sorbitol and collected via centrifugation. Finally, cells were resuspended in 0.5 mL ice cold 1 M sterile sorbitol (+10% glycerol) and aliquoted into 80 µL portions in sterile 1.5 mL Eppendorf tube.

YPD medium:

10 g/L	Yeast extract
20 g/L	Peptone
(For solid) 20 g/L	Bacto agar
121°C 20 min	
2%	Glucose

Minimal medium:

1.16 g/L	Dropout powder
20 g/L	Bacto agar
121°C 20 min	
0.67%	Yeast nitrogen base
2%	Glucose
1 g/L	L-histidine
3 g/L	L-Leucine
2 g/L	L-tryptophan

Dropout powder: 2.5 g of adenine (hemisulfate), 1.2 g of L-arginine, 6.0 g of L-aspartic acid, 6.0 g of L-glutamic acid (sodium salt), 1.8 g of L-lysine (hydrochloric acid), 1.2 g L-methionine, 3.0 g L-phenylalanine, 22.5 g L-serine, 12.0 g L-threonine, 1.8 g L-tyrosine, 9.0 g L-valine. Mixed properly in a mortar.

2.3.1.4.2 *S.cerevisiae* transformation

For electroporation and transformation of *S.cerevisiae*, 80 µL of competent cells were thawed on ice, mixed with 5 µL of plasmid DNA and incubated for 5 min on ice. The cell/DNA mixture was transferred to a pre-cooled electroporation cuvette and a pulse of 1800 V was applied. 1 mL of ice-cold 1 M sterile sorbitol without antibiotics was added immediately and the cells were incubated for 2 min on ice. Cells were collected via centrifugation (3000 rpm, 4°C, 10 min), resuspended in 100 µl 1 M sorbitol (+10% glycerol) and plated on minimal medium.

2.3.1.4.3 *S.cerevisiae* Growth Curve and Growth Assay

3 x 2-mL precultures in minimal medium were inoculated from single colonies of *S.cerevisiae* and grown at 28 °C overnight. Then precultures were added into 100 mL fresh minimal medium and continued growing until OD_{600nm} reached 4.0. Cells were harvested via centrifugation (4000 rpm, 10 min) and resuspended in fresh minimal medium and OD_{600nm} was measured. Afterwards the cultures were diluted to OD_{600nm}=0.01 and 1.0, respectively.

The former one (OD_{600nm}=0.01) was the initial measurement of the growth curve. OD_{600nm} was measured regularly by a spectrophotometer with fresh minimal medium as the blank. 3 replicates were adopted. For growth assay, cultures with OD_{600nm}= 1.0 were diluted to OD_{600nm}= 0.1 and 0.01. All three cultures with different OD_{600nm} (1.0, 0.1, 0.01) were spotted on minimal medium and incubated at 28°C for 36 hours.

2.3.1.4.4 Supplementation of *S.cerevisiae* Cultures with 2-Hydroxy-Palmitic Acid

Yeast cells were grown in minimal medium lacking uracil at 28°C until they reached an OD_{600nm} of about 4.0. The cells were harvested and resuspended in fresh medium to an OD_{600nm} of 4.0. Then 2-hydroxy-palmitic acid, thiamine-pyrophosphate (TPP) and $MgCl_2$ were added at final concentrations of 10 µM, 1 µM and 1 µM, respectively. Yeast cultures continued growing for another 3 h at 28°C. Finally, lipids were extracted for analysis.

2.3.1.5 *Agrobacterium tumefaciens*

2.3.1.5.1 *A.tumefaciens* Cultivation and Generation of Competent Cells

A.tumefaciens cells were grown on solid or in liquid YEP medium at 28°C. Liquid cultures were shaken at 180 rpm. For competent cell generation, all procedures took place under sterile conditions. A single colony of *A.tumefaciens* strain was inoculated in 10 mL of YEP medium and grown at 28 °C for 28 h (preculture). Subsequently, 400 mL YEP medium was inoculated with the preculture containing antibiotics and was grown until the OD_{600nm} reached 0.6. The following steps took

place on ice. Cells were cooled on ice for 10 min and harvested by centrifugation (4000 x *g*, 10 min, 4°C) and resuspended in 400 mL ice cold sterile de-ionized water. This step (cooling and washing) was repeated once to wash away residual medium. Finally, cells were resuspended in 1 mL ice cold 10% glycerol and aliquoted into 80 µl portions in sterile 1.5 mL Eppendorf tubes.

2.3.1.5.2 *A.tumefaciens* transformation

For electroporation and transformation of *A.tumefaciens*, 80 µL of competent cells were thawed on ice, mixed with 5 µl of plasmid DNA and incubated for 5 min on ice. The cell/DNA mixture was transferred to a pre-cooled electroporation cuvette and a pulse of 1800 V was applied. 1 mL of YEP medium without antibiotics was added immediately and the cells were regenerated for 4h at 28°C. Afterwards cells were plated on YEP medium containing appropriate antibiotics.

2.3.1.6 *Spodoptera frugiperda*

2.3.1.6.1 *Spodoptera frugiperda* Cultivation

Spodoptera frugiperda cells (Sf9) were grown in serum free IPL-41 medium by routine sub-cultivation at 27°C with shaking at 120rpm in Erlenmeyer flasks.

IPL-41 insect medium:

2.463% (w/v)	IPL-41 powder medium
0.035% (w/v)	$NaHCO_3$
0.09938% (w/v)	L-Glutamine
0.4% (w/v)	Yeast extract
0.1% (w/v)	Lipidmix (1000x)
1% (w/v)	Pluronic-F68 (10%)
0.26% (w/v)	NaCl
0.28% (w/v)	KOH
1% (v/v)	Penicillin/Streptomycin for suspension cultures

2.3.1.6.2 *Spodoptera frugiperda* Cell Viability Test

The insect cell viability was determined by the Trypan-staining method. The Trypan

blue dye stains the non-viable and dead cells and does not penetrate the living cells. Under the optical microscope, non-viable and dead cells were bright blue, while living cells were not stained and remained transparent. 50 µl of insect cells culture was mixed with 50 µl of Trypan blue solution and incubated for 15 min at room temperature and loaded on a hemacytometer, and cells were counted immediately under an optical microscope. Cell viability was calculated as the number of living cells divided by the total number of cells within the grids of the hemacytometer. The cell viability should be at least 95% for healthy suspension cultures.

2.3.1.6.3 *Spodoptera frugiperda* Transfection

Sf9 cells were transfected to introduce recombinant baculovirus particles containing the desired gene into the cells for heterologous expression of proteins. The Bac-to-Bac® Baculovirus Expression system was employed for the generation of desired recombinant baculoviruses. Aliquots of 100 µL insect cell medium without antibiotics were mixed with 8 µl Cellfectin II reagent and recombinant bacmid DNA or control bacmid DNA containing the GUS gene. The aliquots were combined and incubated for 30 min at room temperature. ~ 0.8 million cells in the log phase with a cell density of 1.5-2.5 million cells/mL were seeded in 6-well plates without antibiotics and incubated for 15 min for the cells to adhere to the bottom of the plate. The medium was removed gently with a sterile glass Pasteur pipet. Then, fresh medium for transfection and the DNA-lipid transfection mixture were added dropwise onto the cells and incubated for 6 h at 27 °C. Afterwards the transfection mixture was removed and replaced with 2 mL fresh medium containing antibiotics and incubated at 27 °C for 72 h. The cells were inspected daily for the infection efficiency using an optical microscope. The characteristic signs of infection such as increased cell size, granular appearance, cell rupture and lysis were observed after more than 72 h of infection. After 5-6 days of transfection, the budded virus was harvested in 15 mL falcon tubes by centrifugation at 1000 x *g* for 5 min to remove the cell debris. The harvested P1 viral stock was kept sterile and stored at 4 °C.

2.3.1.6.4 Amplification of Baculovirus Stock

The P1 viral stock has a low titer and was used to infect cells to generate viral stocks with higher titer. The cells were infected with a multiplicity of infection (MOI) of 1, which is defined as the number of virus particles per cell. The formula used to calculate the volume of viral stock needed is:

$$\text{Inoculation volumn(mL)} = \frac{\text{MOI} * \text{number of cells}}{\text{Titer of the parent stock}}$$

2.3.2 Methods in Molecular Biology

2.3.2.1 DNA Isolation

2.3.2.1.1 DNA Isolation from *Arabidopsis*

Genomic DNA was extracted from plants with CTAB buffer. A green leaf from plants grown on soil was harvested, frozen in liquid nitrogen and ground to a fine powder using the Precellys homogenizer and small ceramic beads (6500 rpm, 30 s). Immediately, 1 mL of CTAB buffer was added and the sample was incubated for 15 min at 65°C with shaking on a heating block. Afterwards, 0.4 mL of chloroform was added and the sample was centrifuged to achieve phase separation (5000 rpm, 5 min). The upper phase (aqueous phase) was transferred to a fresh tube containing 0.7 mL of isopropanol. The sample was mixed and incubated at -20 °C for at least 2 h for precipitation of genomic DNA. Afterwards the DNA was spun down and washed with pre-cooled 70% (v/v) ethanol twice (14000 rpm, 5 min). Residual ethanol was evaporated under room temperature. The DNA was dissolved in 50 µl de-ionized water.

CTAB buffer:

140 mM	Sorbitol
220 mM	Tris-HCl, pH=8.0
22 mM	EDTA
800 mM	NaCl
0.8%	CTAB
pH=8.0	

2.3.2.1.2 Plasmid DNA Isolation from *E. coli*

Plasmid DNA was isolated from *E. coli* with BF buffer and lysozyme. To do this, 2-mL cultures in LB medium were inoculated from *E. coli* single colonies and grown overnight at 37 °C with shaking at 180 rpm. Cells were harvested by centrifugation (14000 rpm, 5 min) and the pellet was resuspended in 200 µL BF buffer and 10 µL of lysozyme (20 mg/mL in water, stored at -20°C). The suspension was incubated for 1 min at 95°C and then placed on ice for 1 min. The sample was centrifuged (14000 rpm, 5 min) and the supernatant was transferred to a fresh Eppendorf tube containing 480 µl IS mix to precipitate the plasmid DNA. The plasmid DNA was spun down and washed with 70% (v/v) ethanol. The residual ethanol was evaporated at room temperature and the dried DNA was dissolved in 50 µL ddH_2O.

BF buffer:

8% (w/v)	Sucrose
0.5% (w/v)	Triton X-100
50 mM	EDTA
10 mM	Tris-HCl buffer, pH=8

IS mix:

400 µL	Isopropanol
80 µL	5 M Ammonium Acetate

2.3.2.1.3 DNA isolation from *S.cerevisiae*

To extract total DNA (genomic DNA + plasmid DNA) from *S.cerevisiae* cells, 5 mL of cultures in minimal medium were inoculated from single colonies and grown at 28 °C for 36 h. Cells were harvested via centrifugation (5000 rpm, 5 min) and resuspended in 0.2 mL DNA release solution. 0.2 mL of phenol/chloroform/isoamyl alcohol (25:24:1; v/v/v) and some acid-washed glass beads were added. Cells were disrupted by vortexing. Phase separation was achieved via centrifugation (14000 rpm, 5 min) and the upper phase (aqueous) was transferred into a fresh Eppendorf tube containing 0.2 mL isopropanol. Total DNA was precipitated at -20 °C for at least 2 h and collected via centrifugation (14000 rpm, 15 min, 4°C) and washed with 70% ethanol (v/v) twice. Residual ethanol was evaporated at room

temperature and DNA was dissolved in 50 µl de-ionized water.

DNA release solution:

2%	Triton X-100
1%	SDS
100 mmol/L	NaCl
10mmol/L	Tris-HCl buffer, pH=8.0
1 mmol/L	EDTA

2.3.2.2 PCR

PCR was used to genotype *Arabidopsis* insertion lines and *Saccharomyces cerevisiae* lines and clone DNA fragments.

2.3.2.2.1 PCR Analysis to Genotype *Arabidopsis* and *S.cerevisiae*

To genotype *Arabidopsis* insertion lines, genomic DNA was extracted from leaf tissue (section 2.3.2.1.1). The three-primer system was used. The genomic sequence around the insertion site was amplified with the forward primer and the reverse primer. The T-DNA insertions in the mutants were amplified using the border primer and the reverse primer. To genotype *S.cerevisiae*, total DNA was extracted from 5 mL cultures (section 2.3.2.1.3). Primer pairs binding to the ends of genes were used.

Table. 7 PCR components to genotype *Arabidopsis* and *S.cerevisiae*

PCR components	Volume
DNA	1 µL
DCS DNA Polymerase	0.2 µL
10 x Buffer	1.5 µL
25 mmol/L $MgCl_2$	1.5 µL
10 mmol/L dNTPs	0.3 µL
10 µmol/L Forward primer	1.5 µL
10 µmol/L Reverse Primer	1.5 µL
De-ionized water	7.5 µL

Table. 8 PCR Reactions to Genotype *Arabidopsis* and *S.cerevisiae*

PCR stage	Temperature	Duration
Initial denaturation	94 °C	1 min
Denaturation	94 °C	30 s
Annealing	55 °C	30 s
Elongation	72 °C	100 s. Go to denaturation, repeat 34 times
Final elongation	72 °C	100 s
End	15 °C	1 min

2.3.2.2.2 PCR to Clone DNA Fragments

To clone DNA fragments, Q5® High-Fidelity DNA Polymerase was used to replace DCS DNA polymerase. With the highest fidelity amplification available (~280 times higher than *Taq*), Q5 DNA Polymerase results in ultra-low error rates.

Table. 9 PCR Components to Clone DNA Fragments

PCR components	Volume
DNA	1 µL
DCS DNA Polymerase	0.5 µL
5 x Buffer	10 µL
25 mmol/L $MgCl_2$	2 µL
10 mmol/L dNTPs	1 µL
10 µmol/L Forward primer	2.5 µL
10 µmol/L Reverse Primer	2.5 µL
De-ionized water	31.5 µL

Table. 10 PCR Reactions to Clone Fragment DNA

PCR stage	Temperature	Duration
Initial denaturation	94 °C	1 min
Denaturation	94 °C	10 s
Annealing	55 °C	30 s

Elongation	72 °C	100 s. Go to denaturation. Repeat 34 times
Final elongation	72 °C	100 s
End	15 °C	1 min

2.3.2.3 Isolation of RNA

Total RNA was extracted from *Arabidopsis* leaves with NucleoSpin plant RNA kit. Afterwards genomic DNA contamination in RNA samples was digested using the Ambion TURBO DNA-free™ Kit. The total RNA was reverse transcribed using the total RNA as the template with the First Strand cDNA Synthesis kit according to the manufacturer's protocol.

2.3.2.4 Semi-quantitative RT-PCR

To analyze the expression of the *HPCL* gene in *A. thaliana* mutants, semi-quantitative reserve transcription PCR (RT-PCR) was used. The cDNA synthesized from section 2.3.2.3 was diluted and used as the template for amplification of the *ACTIN* gene (ACT2) to normalize the concentrations of the cDNA samples and obtain comparable RT-PCR signals. ACT2 (At3g18780) was used as a constitutive control (housekeeping gene). The RT-PCR products were separated in agarose gels and stained with ethidium bromide.

2.3.2.5 Agarose Gel Electrophoresis

DNA fragments were separated via gel electrophoresis on a 1% (w/v) agarose gel, stained with ethidium bromide and observed under UV light. Agarose gels were prepared in 1x Tris-Acetate-EDTA (TAE) buffer. Ethidium bromide (final concentration 0.01 µg/mL) was added to the liquid agarose in TAE buffer. The DNA was mixed with 6 x loading buffer before loading into the wells.

50 x TAE buffer

2 M	Tris-HCl, pH8.0
1 M	Acetic acid
50 mmol/L	EDTA

6 x loading buffer:

30% (v/v)	Glycerol
0.25% (w/v)	Bromophenol blue
0.25% (w/v)	Xylene cyanol FF

2.3.2.6 SDS-PAGE

Heterologously expressed proteins were separated via gel electrophoresis on 7.2% (v/v) sodium dodecyl sulfate-polyacrylamide gels and stained with Coomassie Brilliant Blue R250. The samples to be separated were incubated at 95 °C for 5 min in 4x sample loading buffer. 5 µL of denatured protein sample was loaded into the well and a current of 25 mA was applied onto the gel to concentrate the protein sample into a sharp band before entering the separating gel after which the current was increased to 35 mA. After the dye reached the bottom of the gel, the electrophoresis was stopped. Then the gel was taken out from the chamber and cleaned with de-ionized water and stained with Coomassie Brilliant Blue R-250. To fix the protein in the gel, the staining solution was added and heated in a microwave oven and gently shaken for 5 min at RT. To remove additional Coomassie blue, the gel was destained in destaining solution by heating in the microwave oven and gently agitated for 5 min at RT. Afterwards, the gel was immersed in de-ionized water and shaking gently at room temperature for at least 45 min. Replace the de-ionized water every 15 min.

5 x Laemmli SDS sample loading buffer:

500 mM	Tris-HCl, pH=6.9
10% (w/v)	SDS
0.03% (w/v)	Bromophenol blue
10% (v/v)	Glycerol
5 mM	EDTA

4 x Laemmli SDS sample loading buffer:

50 µl	β-Mercaptoethanol
50 µl	De-ionized water
400 µl	5 x Laemmli SDS sample loading buffer
Make freshly	

Coomassie Brilliant Blue staining solution:

50% (v/v)	Ethanol
7% (v/v)	Acetic acid
0.252% (w/v)	Coomassie Brilliant Blue R-250

Destaining solution:

10% (v/v)	Glycerol
15% (v/v)	Acetic acid

5 x tank buffer:

125 mmol/L	Tris base
960 mmol/L	Glycine
0.5% (w/v)	SDS

Table. 11 Stacking Gel and Separating Gel:

Stock solution	Concentration gel	Stacking gel
40% Acrylamide/bis-acrylamide 29:1 (v/v) stock solution	4.5 mL	1 mL
1.5 mol/L Tris-HCl, pH 8.8	6.25 mL	—
0.5 mol/L Tris-HCl, pH 6.8	—	2.5 mL
10% SDS	250 µL	100 µL
De-ionized water	13.85 mL	6.3 mL
TEMED	10 µL	5 µL
10% APS (w/v)	150 µL	100 µL
Total volume	25 mL	10 mL

2.3.2.7 Western Blot

Heterologously expressed plant proteins harbored a His6 tag at the N- or C-

terminus of the protein, which can be detected by the His-detector system (Nickel-horseraddish peroxidase (HRP) conjugate) in the Western blot. Proteins were first separated on 7.2% separating gel in the SDS-PAGE and transferred onto a nitrocellulose membrane in a semi-dry transfer apparatus using Towbin buffer at a constant voltage of 15 V and 70 mA for 60 min. The nitrocellulose membrane was blocked with 2% BSA solution in TBSTXSB buffer at 4°C overnight. The membrane was then incubated with Nickel-HRP (Abs) conjugate (1:20000; v/v) in the TBSTXSB buffer with 2% BSA for 60 min at RT on a rotary shaker for 1 h. The membrane was washed 3 times with TBSTXSB buffer. For each time, the membrane was kept on the rotary shaker with gently shaking. The blots were developed with the ECL prime western blot detection kit. The chemical fluorescence signals of protein binding were detected with X-ray film in the dark room or with a Chemiluminescence documentation system.

Towbin Buffer:

25 mM	Tris base
192 mM	Glycine
20% (v/v)	Methanol
0.1% (w/v)	SDS

TBSTXSB buffer:

10 mM	Tris HCl, pH7.4
155 mM	NaCl
0.01% (v/v)	Triton X-100
0.75 mM	SDS
15.5 mM	BSA
250 mM	Thimerosal

2.3.2.8 Plasmid Recombination

The cDNA of AtHPCL was amplified from the plasmid pda08833 ordered from RIKEN BRC Experimental Plant Division (Japan) with Q5 polymerase as described in section 2.3.2.2.2. The blunt ended PCR product had restriction endonuclease sites added to both ends and was re-ligated to the linearized pJet1.2 vector. The

ligated circle pJet1.2 vector containing the insert was introduced into *E.coli* for amplification. Afterwards recombinant pJet1.2 vector was extracted from *E.coli* cells and digested with endonuclease, producing the cDNA of AtHPCL with sticky ends which was re-ligated into expression plasmid (e. g. pFastBac1, pQE81L, etc.). The recombinant expression vectors were sequenced to ensure no nucleotide was mutated during the cloning procedure and introduced into microorganisms (*E.coli*, *S.cerevisiae* or *A.tumefaciens*) via electroporation. To enhance the bacterial transformation efficiency by electroporation, the ligation reaction was desalted for 2-3 h on a cellulose membrane (0.025 µm pore size) floating on de-ionized water in a Petri dish at room temperature.

Ligation mixture:

X µL	DNA insert
Y µL	Linearized vector
1 µL	10x T_4 DNA ligase buffer with ATP
0.5 µL	T_4 DNA ligase

Make up to 10 µL with nuclease-free water

Ligate for 12 min for sticky ends and 4 h for blunt ends at room temperature

For an efficient ligation, a molar ratio of vector/insert 1:3 or 1:5 was used

Digestion mixture:

5-10 µL	Plasmid DNA
0.5 µL	Endonuclease 1 (10 U/µl)
0.5 µL	Endonuclease 2 (10 U/µl)
5 µL	10 x Cut smart buffer

Made up to a final volume of 50 µL with nuclease-free nuclease water.

Incubate at 37 °C for 30 min.

2.3.2.9 Heterologous Protein Expression

2.3.2.9.1 Expression of AtHPCL in *E. coli*

The *E. coli* expression vectors pQE81L and pET43b harbor a His6 tag at the N- and C- termini of the open reading frame, respectively. Besides, pET43b also has a Nus tag at the N-terminus, which increases solubility of proteins in the aqueous

phase. The cDNA of AtHPCL was cloned into the opening reading frame of these two vectors and Sanger sequence was performed to confirm that no nucleotide was mutated during the cloning procedure. The pQE81L-6xHis-AtHPCL and pET43b-Nus-AtHPCL-6xHis constructs were then introduced into *E.coli* strain Bl21pLySs via electroporation. From the single colonies of transformed *E.coli* strains, precultures in 2 mL LB medium with appropriate antibiotics were inoculated and grown at 37 °C and 180 rpm overnight. Cells from the preculture were collected via centrifugation (4000 rpm, 10 min) and washed 2 times with de-ionized water and used to inoculate fresh 50 mL main cultures in LB medium. Main cultures continued to grow until the OD_{600nm} reached 0.6, and IPTG was added (final concentration: 0.1 mM) to induce protein expression. Afterwards, *E.coli* cultures were grown at 16 °C overnight or 28 °C for 2 h. The expression of AtHPCL was confirmed by SDS-PAGE (section 2.3.2.6) and western blot (2.3.2.7). Finally, protein-expressing cultures were used in the 2-hydroxy-16:0 fatty acid feeding experiment or in *in vitro* enzyme.

2.3.2.9.2 Expression of AtHPCL In *in vitro* Cell-Free Wheat Germ System

The *in vitro* wheat germ expression system (biotechrabbit, Germany) allows for rapid (<2.5h) expression of proteins in the cell-free system. Two specialized vectors, pIVEX1.3 and pIVEX1.4 are provided in the kit. The former harbors a His6 tag at the C-terminus of the ORF, while the latter's His6 tag is localized to the N-terminus. The cDNA of AtHPCL was cloned into these two vectors. The reaction solution and the feeding solution were prepared according to the producer's manual.

Reaction solution:

4 µL	Amino acids
1 µL	Methionine
15 µL	Wheat Germ Lysate
15 µL	pIVEX1.3-AtHPCL-6×His or pIVEX1.4-6×His -AtHPCL or pIVEX-GUS

Feeding solution:

900 µL	Feeding Mix

80 µL Amino Acids

20 µL Methionine

To the feeding compartment and the reaction compartment, 1 mL of feeding solution and 50 µL of reaction solution were added, respectively. The compartments were sealed and incubated at 24°C for 2.5 h. Product proteins with His6 tag were checked by western blot.

2.3.2.9.3 Expression of AtHPCL in Sf9 Insect Cells

The pFastBac1 vector harboring the cDNA of AtHPCL was constructed and converted into the respective bacmids by transfer into *E.coli* DH10 Bac cells. The bacmids were transfected into insect cells (Sf9) using a reagent called Cellfectin II. The viral stock was amplified to produce high-titer virus by recurrent infections. The P3 (Passage 3) stock was used to transfect insect cells with a seeding density of $2x10^6$ cells for subsequent protein expression.

2.3.3 Methods in Biochemistry

2.3.3.1 Analysis of Aldehydes

2.3.3.1.1 Synthesis of Aldehydes Standards

Fatty aldehydes (Nonadecanal, Eicosanal, Pristanal, Phytanal) were synthesized from corresponding fatty acids following methods described in the previous study (Gutbrod et al., 2021). About 5 µmol fatty acid was transmethylated in 1 N methanolic HCl at 80 °C for 30 min. After cooling to room temperature, products (fatty acid methyl esters, FAMEs) were extracted with 1 mL n-hexane 2 times after the addition of 1 mL 0.9% NaCl. Solvents were evaporated and FAMEs were dissolved in 0.2 mL anhydrous diethylether. Then 3 mg lithium aluminum hydride ($LiAlH_4$, 3 mg/mL in anhydrous diethylether) was added and the mixture was incubated at 45°C for 2 h while shaking to reduce the FAMEs to the corresponding alcohols. After cooling, the excess hydride was decomposed by addition of 1 mL methanol and the mixture was acidified with 0.5 mL 0.1 N hydrochloric acid, diluted with 1 mL water and extracted with 2 mL diethylether two times. The combined diethylether extracts were washed with 1 mL water and evaporated to an oil under

a stream of nitrogen gas. Aldehydes were prepared by oxidation of corresponding alcohols using pyridinium chlorochromate. A molar ratio of 0.01 mmol alcohol to 0.09 mM of pyridinium chlorochromate in dichloromethane was stirred for 90 minutes at room temperature. The reaction mixture was passed through a silica column (500 mg of silica) equilibrated with dichloromethane. The reaction products were eluted from the silica column using 5 mL dichloromethane. Finally, the synthesized aldehydes were obtained.

2.3.3.1.2 Extraction, Derivatization and Purification of Aldehydes from Tissues

Aldehydes were derivatized with methoxylamine and the products, aldehyde-methyloximes, were quantified with GC-MS or Q-Trap following methods described in the previous study (Gutbrod et al., 2021). Leaves (~100 mg) or cells (~20 mL culture) were frozen in liquid nitrogen and homogenized with ceramic beads in a Precellys homogenizer (6500 rpm, 45 s). To the homogenate, 1 mL of chloroform/methanol (2:1, v/v) and 10 nmol hexadecanal (16:0 aldehyde, internal standard) and 500 µL of 300 mM ammonium acetate were added. Samples were vortexed, centrifuged for 3 min at 5000 x *g* and the organic phase collected. Samples were extracted again with 1 mL of chloroform and the organic phases combined. The solvent was evaporated under a stream of nitrogen gas. The aldehydes were derivatized with 100 µL methoxylamine hydrochloride in pyridine (20 mg/mL) for 1 h at room temperature. To the reaction mixture, 100 µl of toluene was added and pyridine was evaporated under a stream of nitrogen gas. Afterwards, the samples were dissolved in 1 mL of n-hexane and loaded onto a solid phase extraction column (100 mg of silica) equilibrated with n-hexane. The column was washed with 3 volumes of hexane. Long chain aldehyde-methyloximes were eluted with 3 volumes of n-hexane/diethylether (99:1, v/v). The solvent was evaporated under a flow of nitrogen. The samples were dissolved in 100 µl hexane and transferred to autosampler vials.

2.3.3.1.3 Quantification of Aldehydes via Mass Spectrometry (GC-MS or LC-MS)

The aldehyde-methyloximes were analyzed with GC-MS or Q-Trap. Detailed conditions for mass spectrometry are given in the tables below (Gutbrod et al., 2021).

GC-MS conditions

Parameter	Setting
Column	Agilent HP-5MS
Column length	30 m
Carrier gas	Helium
Flow rate	7 mL/min

Stage	Temperature
Initialization	70 °C
5°C/min	to 310 °C
Hold 1 min	310 °C
5°C/min	to 70 °C

Q-Trap conditions

Parameter	Setting
Column	Eurospher II C8, with precolumn, Knauer
Column length	150 mm
Column diameter	3 mm
Particle size	3 µm
Flowrate	0.5 mL/min
Injection volume	10 µL
Solvent A	H_2O: Acetonitrile: Formic acid (63: 37: 0.02, v: v: v)
Solvent B	100% Acetonitrile
Mode	Positive mode
declustering potential	70 V
collision energy	45 V

Table. 12 Q-Trap Gradient Elution Conditions

Collapsed time/min	Solvent A %	Solvent B %
0	20	80
2	20	80
12	0	100

25	0	100
32	20	80

2.3.3.2 Analysis of Non-Polar Lipids

2.3.3.2.1 Extraction of Non-Polar Lipids

Non-polar lipids were extracted from *Arabidopsis* leaves (~100 mg leaf tissue) and used for analysis via HPLC-FLD (tocopherol), GC-MS (phytol) or Q-TOF MS/MS (fatty acid phytyl esters, FAPEs). The tissue was harvested, frozen in liquid nitrogen and ground to a fine powder with Precellys and ceramic beads (6500 rpm, 45 s). Internal standards were spiked (10 nmol octadecenol for phytol，500 ng rac-tocol for tocopherol and 1 nmol 17:0 fatty acid phytyl ester for FAPEs). To the homogenate, 0.5 mL diethylether and 0.5 mL 0.3 M ammonium acetate were added. The samples were centrifuged (5 min, 5000 rpm) to achieve phase separation and the upper phase was harvested. The extraction procedure was repeated twice with 1 mL diethylether and the pooled extracts were dried under a stream of nitrogen gas. FAPEs, tocopherol and phytol were separated via solid phase extraction as described in the next section.

2.3.3.2.2 Purification of Non-Polar Lipids via Solid Phase Extraction

Dried lipids isolated as described above were dissolved in 1 mL n-hexane and loaded on silica columns equilibrated with n-hexane. Undesired impurities were washed away with 3 volumes of hexane. Afterwards lipids of interest were eluted in a gradient elution way (vom Dorp, 2015). Elution reagents were evaporated and samples were re-dissolved in solvents for following quantitative measurement with mass spectrometry.

SPE procedures to separate non-polar lipids

Step	Solvent	Lipids	Analysis
1	3 x n-Hexane: diethylether (99:1,v/v)	FAPE	Q-TOF
2	3 x n-Hexane: diethylether (95:5,v/v)	Tocopherols	HPLC
3	3 x n-Hexane: diethylether (92:8,v/v)	Phytol	GC-MS

2.3.3.2.3 Quantification of FAPEs via Q-TOF

FAPEs should be quantitatively measured via direct infusion on a Q-TOF mass spectrometer with 17:0 fatty acid phytyl ester as the internal standard (vom Dorp et al., 2015). To this end, the elution solvent was evaporated under a stream of nitrogen gas and FAPEs were dissolved in 200 µL chloroform: methanol: 0.3 M ammonium acetate (300: 665: 35, v/v/v). Samples were delivered to the Q-TOF MS using an Agilent Series 1100/1200 nanopump and HPLC-Chip Cube MS interface. Detailed parameters are shown in the table below.

Q-TOF conditions

Parameter	Setting
Drying gas	8 L/min N_2
Fragmentor voltage	200 V
Gas temperature	300 °C
HPLC-Chip V_{cap}	1700 V
Scan rate	1 spectrum/s
Mode	Positive mode
flow rate	1 µL/min

2.3.3.2.4 Quantification of Tocopherol via HPLC

Tocopherols were quantified via HPLC (Zbierzak et al., 2010). Briefly, the elution solvent was evaporated under a stream of nitrogen gas. Then samples were dissolved in 100 µL n-hexane and separated on a LiChrospher diol column (Knauer, 250 x 3 mm, 2.1 µm particle size). The running phase was n-hexane/tertiary butylmethylether (96:4, v/v) at a flow rate of 0.75 mL/min. Chromatography was carried out using an Agilent 1100 series HPLC system with fluorescent light

detector (FLD). The excitation wavelength was 290 nm, and the emission wavelength was 330 nm.

2.3.3.2.5 Quantification of Phytol via GC-MS

Free phytol was quantified via GC-MS after derivatization with MSTFA (vom Dorp et al., 2015). Briefly, the elution solvent was evaporated under a stream of nitrogen gas. 80 µl of MSTFA was added and the sample was incubated at 80 °C for 30 min. Afterwards, MSTFA was completely evaporated under a stream of nitrogen gas. Samples were dissolved in 100 µL of hexane and transferred into autosampler vials for analysis. GC-MS parameters were identical to those presented in section 2.3.3.1.3.

The derivatization product of phytol or octadecenol (18:1 alcohol, internal standard) with MSTFA is a trimethylsilyl (TMS)-derivative. A product ion of the TMS group (m/z 73) was used to determine the amount of octadecenol, while a product ion of the silylated phytol moiety (m/z 143) was used for the quantification of phytol.

Analyte	Formula	Mass	M+TMS	Product ion m/z
Octadecenol	$C_{18}H_{36}O$	268.2766	340	73
Phytol	$C_{20}H_{40}O$	296.3079	368	143

2.3.3.3 Analysis of Phosphatidylcholine from *S.cerevisiae*

Phospholipids were quantified by direct infusion mass spectrometry on a Q-TOF instrument (Gasulla et al., 2013). To this end, cells from 10 mL of yeast culture were harvested by centrifugation (4000 rpm, 10 min). Cells were washed 2 times with de-ionized water, resuspended in 10 mL de-ionized water and incubated in a boiling water bath for 30 minutes. After centrifugation, lipids were extracted from the pellet two times with 1 mL of chloroform/methanol (2:1). The internal standard (1 nmol of dilauroyl-phosphatidylcholine, di12:0-PC) was added to the combined extracts. Phospholipids were dissolved in 200 µL chloroform: methanol: 0.3 M ammonium acetate (300: 665: 35, v/v/v). Afterwards phosphatidylcholines were quantitatively measured with Q-TOF using methods described in section 2.3.3.2.3 and a collision energy of 35 V. Phosphatidylcholines were protonated and a

product ion with m/z=184.0739 was scanned and used for quantification.

2.3.3.4 Analysis of Chlorophyll

Chlorophyll was extracted with 80% acetone and measured with a spectrophotometer (Porra et al., 1989). About 20 mg leaf tissue was collected and ground to fine powder with ceramic beads and Precellys homogenizer (6500 rpm, 45 s). Chlorophyll was extracted with 0.5 mL 80% acetone 2 times. High speed centrifugation (14000 rpm, 1 min, 4°C) was used to precipitate cell debris and supernatants were pooled. The extraction was transferred to a quartz cuvette. The absorbances at the wavelengths of 663.3 nm, 646.6 nm and 750 nm were measured with a spectrophotometer. The following formulas were used to calculate the amount of chlorophyll:

Chlorophyll *a* (µg/mL) = 12.25 x ($A_{663.6nm}$ - A_{750nm}) - 2.55 x ($A_{646.6nm}$ - A_{750nm})
Chlorophyll *b* (µg/mL) = 20.31 x ($A_{646.6nm}$ - A_{750nm}) - 4.91 x ($A_{663.6nm}$ - A_{750nm})

2.3.3.5 2-Hydroxy-Acyl-CoA Lyase Assay with Recombinant AtHPCL or *Arabidopsis* Peroxisomal Proteins

To study the enzymatic function of AtHPCL, *in vitro* 2-hydroxy-acyl-CoA lyase assays were conducted with proteins expressed in *E.coli*, *S.cerevisiae*, SF9 cells or with peroxisomal proteins isolated from *Arabidopsis* leaves.

2.3.3.5.1 Membrane Protein Isolation

Cells were harvested from cultures (*E.coli*, *S.cerevisiae*, Sf9 cells) via centrifugation (4000 rpm, 10 min), washed with phosphate buffered saline (PBS) and homogenized with glass beads in a Precellys homogenizer (6500 rpm, 45 s) in homogenization buffer (Patwari, 2019). The homogenization was repeated 10 times and samples were kept on ice during the intervals. Cell debris was removed by centrifugation at 4000 × *g* for 2 min at 4 °C. The supernatant was subjected to ultracentrifugation (100,000 × *g* for 1 h) to obtain microsomal membrane pellets which were resuspended in homogenization buffer. The protein concentration was measured with the bicinchoninic acid (BCA) reagent using bovine serum albumin

(BSA) as standard as described in the next section.

PBS buffer:

NaCl	8 g/L
KCl	0.2 g/L
Na2HPO4	1.42 g/L
KH2PO4	0.24 g/L
pH=7.4	

Homogenization buffer:

1 mM	EDTA
200 mM	Sucrose
100 mM	Tris-HCl, pH 7.4

2.3.3.5.2 BCA Assay

To quantify the protein concentration in samples, the bicinchoninic acid (BCA) assay was used (Patwari, 2019). In the BCA assay, two molecules of bicinchoninic acid chelate with one Cu^{+} ion, which comes from the reduction of Cu^{2+} by peptide bonds in proteins. The purple Cu^{+} BCA complexes strongly absorb light at a wavelength of 562 nm. Because the amount of Cu^{2+} reduced is proportional to the amount of protein present in the solution, the amount of protein present in a solution can be quantified by measuring the absorbance in comparison with protein solutions of known concentrations. 20 µL of protein was mixed with 200 µl BCA reagent. The mixture was incubated at 60 °C for 15 min. The samples were measured with a Nanodrop photometer at a wavelength of 550 nm. A defined standard curve with bovine serum albumin (BSA) was used for the determination of the protein concentration in the samples.

BCA reagent:

99 %	Bicinchoninic acid (BCA) solution
1 %	4% $CuSO_4$ (w/v)
Make freshly	

2.3.3.5.3 Peroxisome Preparation

Peroxisomes from *Arabidopsis* wild type Col-0 and three mutant lines (*hpcl-1*, *hpcl-2*, *hpcl-3*) were prepared at 4 °C. ~60 g green leaves were harvested after the end of the dark period. 120 mL GB buffer was added and the tissue was ground in a mortar until no solid tissue could be seen. The crude extracts were passed through medical gauze to remove cell debris. The flow-through was collected and loaded onto the first gradient (Percoll gradient) and centrifuged (13000 x *g* for 10 min, then increase to 27000 x *g* for 20 min at 4 °C). Afterwards the supernatant was discarded and the pellet was resuspended in 65 mL of 36% sucrose in TE buffer. Samples suspended in sucrose were loaded onto the second gradient (sucrose gradient) and centrifuged at 80000 x *g* and 4 °C for 2 h. After centrifugation, peroxisomes were localized in the middle-layer between the 50.5% and 55.2% positions of the sucrose gradient. Finally, peroxisomes were suspended in de-ionized water complemented with protease inhibitors (Reumann & Singhal, 2014).

GB buffer:

170 mM	Tris-HCl, pH 7.5
1 M	Sucrose
2 mM	EDTA
1 % (w/v)	BSA
10 mM	KCl
1 mM	$MgCl_2$
0.5 % (w/v)	PVP-40
5 mM	DTT
0.1 mM	PMSF
0.2 mM	Benzamidine
0.2 mM	ε-Aminocaproic acid

TE buffer:

10 mM	Tris-HCl, pH 8.0
1 mM	EDTA

Protease Inhibitor:

1 mM	PMSF
2 mM	Benzamidine
2 mM	ε-Aminocaproic acid
1 µg/mL	Trasylol
1 µg/mL	Pepstatin
1 µg/mL	Leupeptin

2.3.3.5.4 2-Hydroxy-Acyl-CoA Lyase Assay

Recombinant proteins or peroxisomes isolated from *Arabidopsis* were prepared according to the methods described above. Then the assay mixture was combined: 10 µM 2-hydroxy-stearoyl-CoA (substrate); 800 µM $MgCl_2$; 20 µM thiamine pyrophosphate (TPP); 6.6 µM BSA; 200 mM sucrose; 50 mM Tris-HCl, pH=7.4 (Foulon et al., 1999). Reactions were started by adding the protein into the mixture. Reaction mixtures were incubated at 28 °C for 30 min. Afterwards 10 nmol internal standard (hexadecanal, 16:0 aldehyde) was spiked. To the samples, 1 mL of chloroform: methanol (1:1, v/v) was added to stop the reaction and extract aldehydes. Residual mixtures were extracted twice again with 1 mL chloroform. Pooled extracts were evaporated to dryness under a stream of nitrogen gas and derivatized with methoxylamine-HCl and quantitatively measured with GC-MS according to methods described in section 2.3.3.1.2 and 2.3.3.1.3.

2.3.3.6 Analysis of Fatty Acids

To quantify total fatty acid from *S.cerevisiae*, cells from 10 mL cultures were collected by centrifugation (4000 rpm, 10 min) and washed with de-ionized water two times. 10 nmol of internal standard (tridecanoic acid, 13:0 acid) was added to the cell pellet, and lipids were transmethylated directly by incubation with 1 mL of 1 N HCl in methanol for 30 min at 80 °C. After methylation, 1 mL of 0.9% NaCl and 1 mL of n-hexane were added. The mixture was vortexed and centrifuged to achieve phase separation. The upper phase (hexane phase) was collected. The extraction was repeated 2 times with 1 mL of n-hexane each. Pooled extracts were

evaporated to dryness under a stream of nitrogen gas and re-dissolved in 100 µL hexane and transferred to autosampler vials for analysis by GC-MS. Detailed conditions are presented in section 2.3.3.1.3.

3. RESULTS

3.1 Characterization of *Arabidopsis HPCL* gene

Because it is the side chain of chlorophyll, phytol is considered the most abundant isoprenoid molecule in the biosphere. As free phytol has detergent-like characteristics and therefore is toxic to membranes (Dörmann, 2007), plants have developed different ways to store or metabolize phytol to minimize the harm of free phytol. Phytyl can be stored in the form of FAPE which is an intermediate sink of phytol. Two phytyl ester synthases, namely PES1 and PES2, were identified in *Arabidopsis* (Lippold et al., 2012). Phytol-diphosphate is produced from two sequential phosphorylation reactions catalyzed by the phytol kinase VTE5 and the phytyl-phosphate kinase VTE6 and provides the prenyl side chain for the synthesis of tocopherol and phylloquinol (Gross et al., 2006; Valentin et al., 2006; vom Dorp, 2015). Plants presumably harbor an effective phytol catabolism pathway. It is reasonable to hypothesize that the degradation of phytol follows a similar route as described for humans. HPCL (hydroxy-phytanoyl-CoA lyase) plays a vital role in human phytol degradation (Casteels et al., 2007). HPCL can catalyze the conversion of 2-hydroxy-phytanoyl-CoA to pristanal and formyl-CoA in a decarboxylation reaction.

The enzyme catalyzing the decarboxylation of 2-hydroxy-phytanoyl-CoA, one of hypothetical phytol degradation intermediates in plants, was previously unknown. The *Arabidopsis* gene At5g17380, a member of the decarboxylase family, was identified as a candidate for 2-hydroxy-phytanoyl-CoA decarboxylase employing the NCBI database and it was designated At*HPCL*. Orthologous sequences of At*HPCL* could be found in *Caenorhabditis elegans*, plants (*Oryza sativa*, rice; *Physcomitrella patens*; *Solanum tuberosum*, potato; *Selanigella moellendorfii*), fruit fly, zebrafish, *Escherichia coli*, *Saccharomyces cerevisiae* and *Homo sapiens* (Fig. 3.1). The At*HPCL* gene contains two exons separated by one intron. The open reading frame includes 1716 bp encoding a polypeptide of 572 amino acids. The orthologous *HPCL* sequence in yeast (*Saccharomyces cerevisiae*) was previously designated *PXP1* (Nötzel et al., 2016). Amino acid sequences of AtHPCL (At-Q9LF46), HsHPCL (Hs-Q9UJ83) and ScPXP1 (Sc-P39994) were

compared using ClustalW (Fig. 3.2). All three proteins harbored the conserved thiamin pyrophosphate (TPP)-binding sequence [LIVMF]-[GSA]-X(5)-P-X(4)-[LIVMFYW]-X-[LIVMF]-X-G-D-[GSA]-[GSAC] in the C-terminal half of the protein (accession PS00187, https://prosite.expasy.org). In contrast to the AtHPCL and ScPXP1 sequences, HsHPCL harbored an insertion of 4 amino acids within the TPP-binding sequence, instead of 5 amino acids.

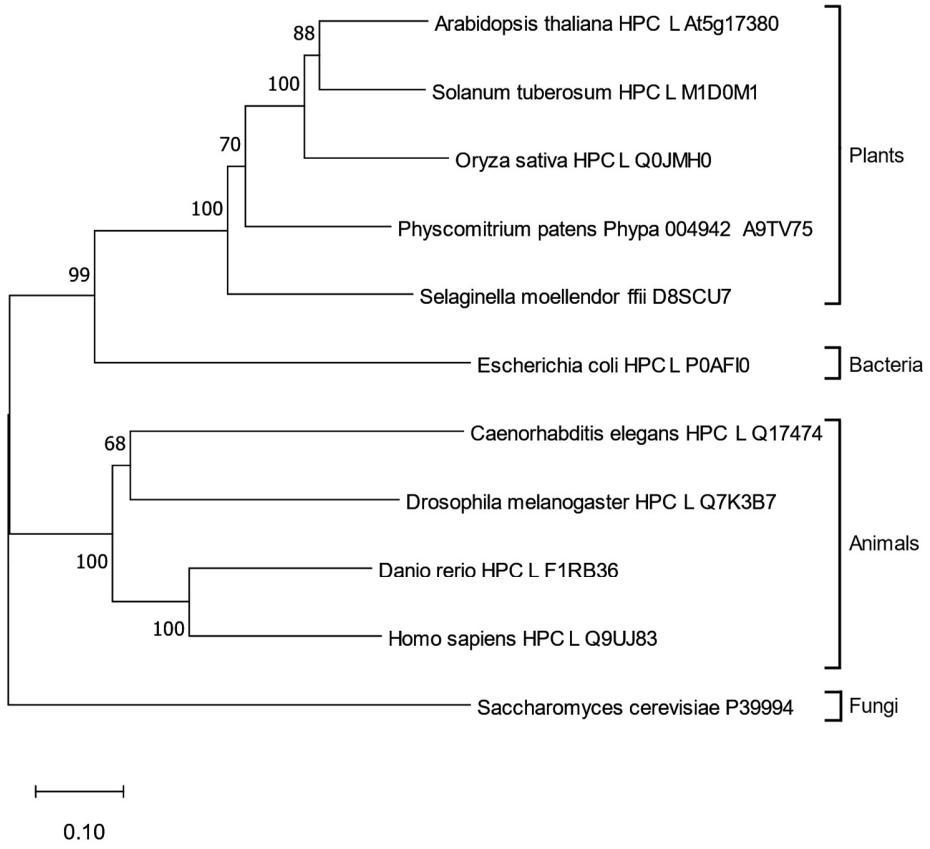

Figure. 3.1 The phylogenetic relationship of 2-hydroxy-acyl-CoA lyase proteins from different organisms.

The phylogenetic tree was generated with amino acid sequences (UniProtKB accessions) of HPCL sequences using MegaX. Sequences were aligned with ClustalW and the phylogenetic tree constructed using the neighbor-joining method with the bootstrap test of 500 replications (Felsenstein, 1985; Saitou & Nei, 1987). At, *Arabidopsis thaliana*; Ce, *Caenorhabditis elegans*; Dm, *Drosophila melanogaster*, fruit fly; Dr, *Danio rerio*, zebrafish; Ec, *Escherichia coli*; Hs, *Homo*

sapiens; Os, *Oryza sativa*, rice; Pp, *Physcomitrella patens*; Sc, *Saccaromyces cerevisiae*, yeast; Sm, *Selanigella moellendorfii*; St, *Solanum tuberosum*, potato.

Figure. 3.2 Sequence comparison of AtHPCL (At-Q9LF46), Hs-HPCL (Hs-Q9UJ83) and ScPXP1 (Sc-P39994) using ClustalW.

Identical amino acids and the conserved TPP-binding sequence ([LIVMF]-[GSA]-X(5)-P-X(4)-[LIVMFYW]-X-[LIVMF]-X-G-D-[GSA]-[GSAC]) are highlighted in yellow and red, respectively.

3.1.1 The Subcellular Localization of AtHPCL.

The HPCL proteins from human (HsHPCL) and yeast (ScPXP1) have previously been shown to localize to the peroxisomes (Foulon et al., 1999; Nötzel et al., 2016). HsHPCL and ScPXP1 both carry tripeptide sequences at their C-terminus, i.e. SNM and PRL, respectively, which are homologous to the conserved peroxisomal targeting (PTS1) sequences [SA][KR][LMI] (Chowdhary et al., 2012) (Fig. 3.2). On the other hand, the AtHPCL protein lacks four amino acids at its C-terminus,

compared with the human and yeast proteins, and this deletion includes the region of the PTS1 tripeptide sequence. The last three amino acids of AtHPCL are therefore HKN, with only the second amino acid (K) matching the PTS1 consensus sequence. The consensus prediction of the SUBA4 database (https://suba.live) for AtHPCL was “peroxisome” (Hooper et al., 2014, 2017). The ARAMEMNON database predicted that AtHPCL harbors at least one transmembrane (TM) domain derived from the consensus of 18 prediction programs (Fig. 3.3) (Schwacke et al., 2003).

Because the peroxisome is the organelle where fatty acid degradation happens in plants, it was possible that that AtHPCL is localized to peroxisomes. To study the subcellular localization of AtHPCL experimentally, the cDNA of AtHPCL was N‐terminally fused to the enhanced green fluorescent protein (eGFP) and the construct was introduced into *A.tumefaciens.* The bacteria were used to infiltrate *Nicotiana benthamiana* leaves, together with a cyan fluorescent protein carrying a C-terminal SKL fusion (CFP-SKL), which is an established marker for the peroxisome (Falter et al., 2019). The subcellular localization was studied by imaging the fluorescent signals from infiltrated leaf mesophyll cells with the confocal fluorescence microscopy. Fluorescence signals only appeared when *Nicotiana benthamiana* leaves were agro-infiltrated. When only eGFP-AtHPCL was used for the transformation, punctuate structures were observed. Similarly, when only CFP-SKL was used for the transformation, punctuate structures could be observed. When eGFP-AtHPCL and CFP-SKL were co-expressed in *Nicotiana benthamiana* leaves, the eGFP-AtHPCL construct showed bright, punctate structures which were co-localized with the CFP-SKL fluorescence but different from chlorophyll autofluorescence (Fig. 3.4) (Falter et al., 2019). Taken together, these results show that AtHPCL is localized to peroxisomes.

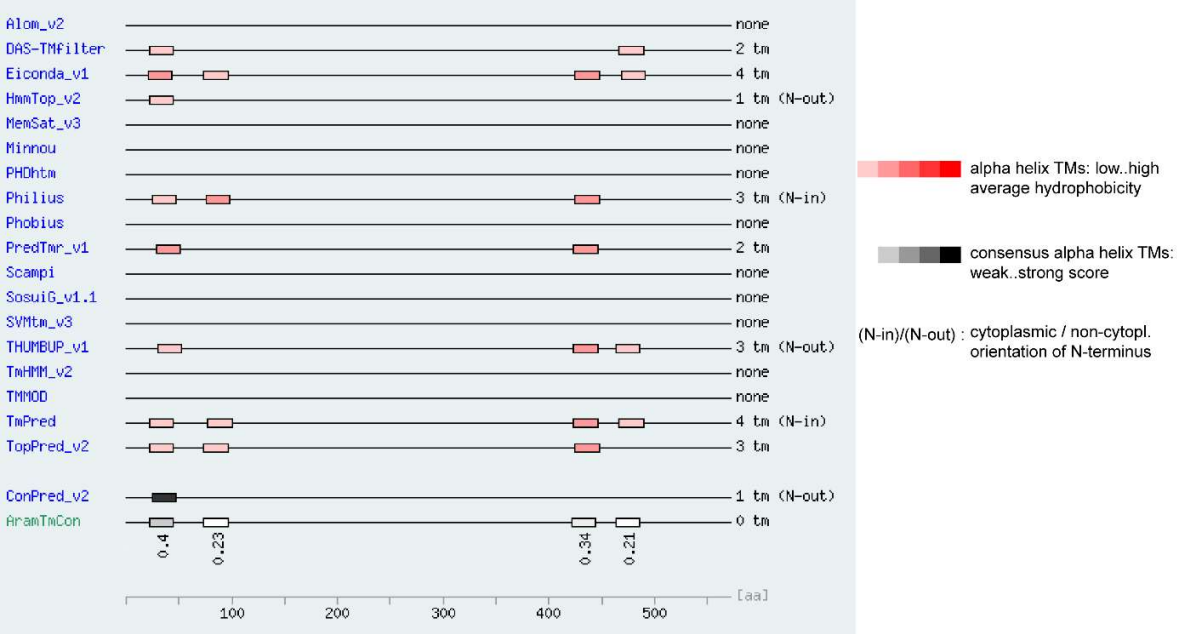

Figure. 3.3 ARAMEMNON database prediction for transmembrane domains of AtHPCL.

The topology of AtHPCL depicting the transmembrane spans. The 18 individual prediction programs are shown in blue letters, and the combined consensus prediction are in green letters and the boxes joined by lines are the transmembrane domains predicted by individual programs. The alpha helix TMs are highlighted as pink boxes whereas the combined consensus alpha helices are depicted as grey boxes.

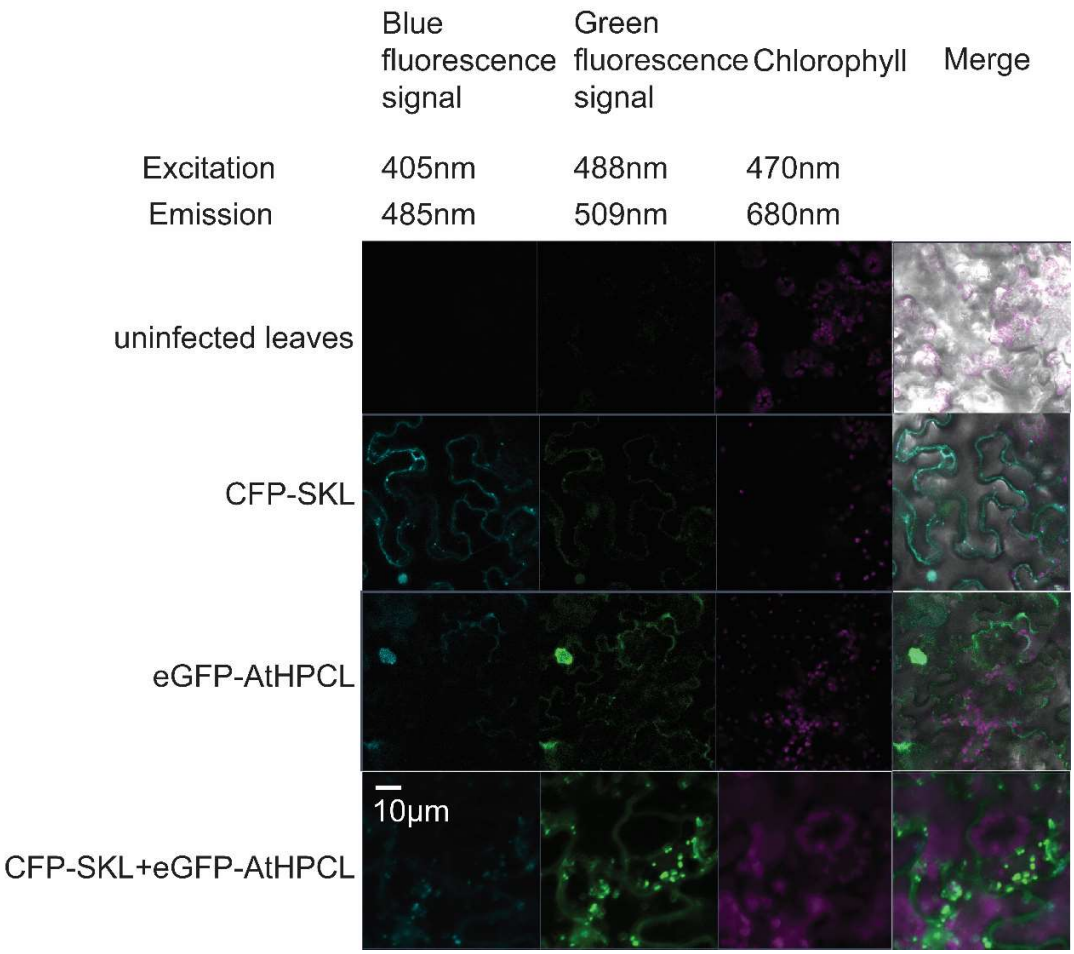

Figure. 3.4 The subcellular location of AtHPCL

The eGFP-AtHPCL fusion protein was transiently expressed in *Nicotiana benthamiana* leaves in combination with the peroxisomal marker CFP-SKL (Falter et al., 2019). The images show CFP fluorescence, GFP fluorescence, chloroplast autofluorescence and a merged image of the three channels. Bar = 10 μm.

3.1.2 Heterologous AtHPCL Expression

3.1.2.1 The Choice of Substrates

To study the enzymatic function of AtHPCL, a substrate supplementation experiment with living cells expressing AtHPCL, and an *in vitro* enzyme assay with recombinant AtHPCL or *Arabidopsis* peroxisomal proteins were performed. AtHPCL is a putative 2-hydroxy-acyl-CoA lyase, which converts 2-hydroxy-acyl-CoA lyase into the (n-1) aldehyde and formyl-CoA. In the supplementation

experiment, 2-hydroxy palmitic acid (HO-16:0 acid, TCI, Tokyo, Japan) was added to living cells (*E.coli*, *S.cerevisiae*, Sf9 cells) expressing AtHPCL. 2-hydroxy-palmitic acid would be converted into 2-hydroxy-palmitoyl-CoA by cellular acyl-CoA synthase, which could then be converted by AtHPCL into pentadecanal (15:0 aldehyde). Afterwards pentadecanal was extracted, derivatized with methoxylamine HCl and quantified by GC-MS to evaluate the enzyme activity. In the *in vitro* enzyme assay, cells were disrupted and the microsomal fraction was isolated and used in the enzyme assay. Also, peroxisomal proteins were extracted and purified from leaves of *Arabidopsis* wild type Col-0 and *hpcl* mutant plants (*hpcl-1*, *hpcl-2*, *hpcl-3*) and used in the *in vitro* enzyme assay. For enzyme assays, 2-hydroxy-acyl-CoA, not 2-hydroxy-fatty acid, was used as the substrate. I also tried to chemically synthesize 2-hydroxy-palmitoyl-CoA from 2-hydroxy-palmitic acid. However, this approach failed (data not shown), probable due to the presence of the hydroxy group at the β carbon, which inhibited the nucleophilic attack. Therefore, I used commercially available 2-hydroxy-stearoyl-CoA (HO-18:0-CoA, Larodan, Solna, Sweden) as the substrate and the corresponding (n-1) aldehyde, heptadecanal (17:0) was extracted, derivatized with methoxylamine HCl and quantified by GC-MS to evaluate the enzyme activity (Fig. 3.5). `

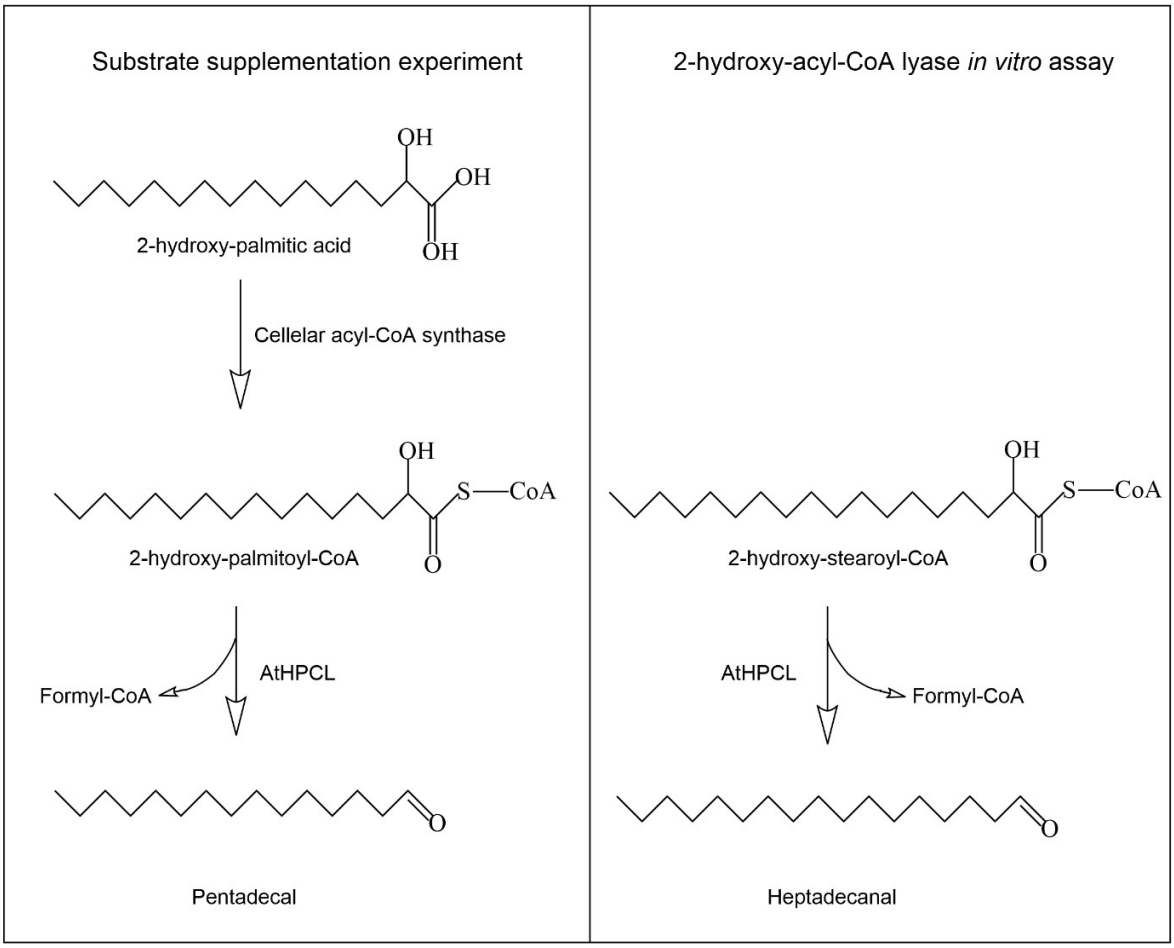

Figure. 3.5 The substrate supplementation experiment and the *in vitro* enzyme assay.

3.1.2.2 Expression of AtHPCL in *E.coli*.

To study the activity of AtHPCL, the pQE81L-6xHis-AtHPCL and pET43b-Nus-AtHPCL-6xHis constructs and corresponding empty vectors (ev) were introduced into *E.coli* protein expression strain Bl21pLySs. To pQE81L and pET43b vectors, a His6 tag was added at the N- and C- terminus of the ORF, respectively. In addition, the pET43b vector carried a Nus tag at the N-terminus, which increased the protein solubility in the aqueous phase. The size of AtHPCL expressed from pQE81L-6xHis-AtHPCL and pET43b-Nus-AtHPCL-6xHis were 63kDa and 123.9 kDa, respectively. AtHPCL expressed in *E.coli* could be identified in SDS-PAGE (Fig. 3.6) and Western blot analysis using the His6 tag detector kit (Fig. 3.7). Therefore, expression of AtHPCL in *E.coli* was successful.

Next, 2-hydroxy-palmitic acid was supplemented to cultures of *E.coli* expressing AtHPCL. *E.coli* continued growing for 2 h in the presence of 2-hydroxy-palmitic acid and pentadecanal (15:0 aldehyde) was extracted from cells with the addition of hexadecanal (16:0 aldehyde) as the internal standard. Pentadecanal was derivatized with methoxylamine HCl and quantified by GC-MS to evaluate the enzyme activity. There was no significant activity difference between AtHPCL and empty vector (ev) containing cells (Fig. 3.8).

For the *in vitro* enzyme assay, *E.coli* cells were ruptured, cell debris was removed by low-speed centrifugation and microsomal protein was enriched by ultracentrifugation. The membrane fraction was resuspended in homogenization buffer and tested for 2-hydroxy-stearoyl-CoA lyase activity. There was no significant activity difference between AtHPCL and empty vector (ev) (Fig.3.9).

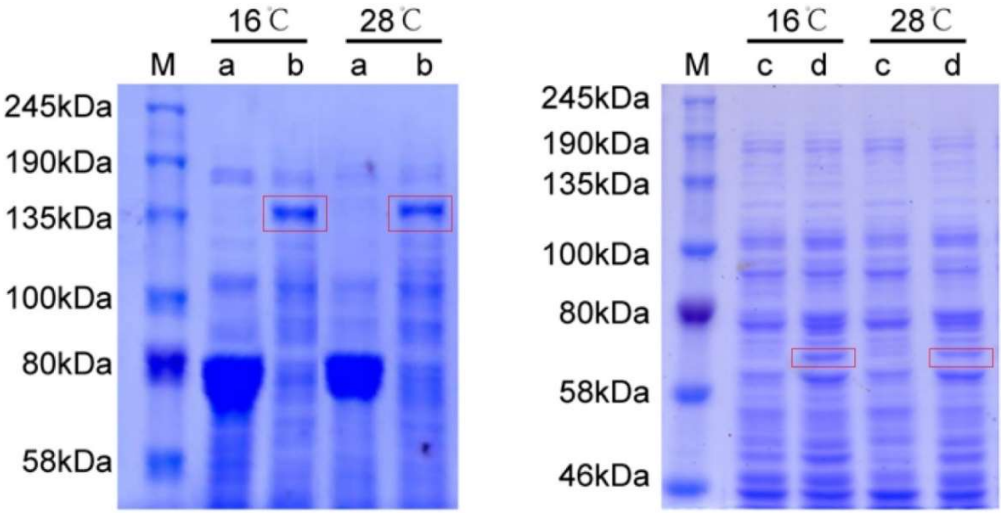

Figure. 3.6 Expression of AtHPCL in *E.coli*.

AtHPCL expressed in *E.coli* can be observed by polyacrylamide gel electrophoresis (SDS-PAGE), after staining with Coomassie brilliant blue R250. M: protein standard. a: pET43b-ev; b: pET43b-AtHPCL; c: pQE81L-ev; d: pQE81L-AtHPCL; ev: empty vector. Red boxes indicate the heterologously expressed AtHPCL protein. AtHPCL expression was induced with IPTG at 16 °C and 28 °C as indicated.

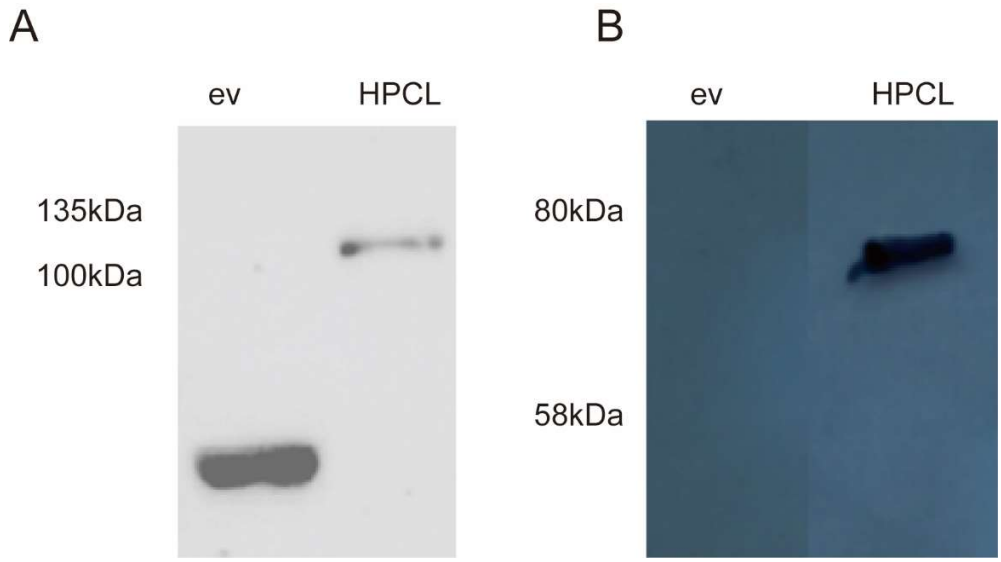

Figure. 3.7 Expression of AtHPCL in *E.coli*.

AtHPCL expressed in *E.coli* can be detected by Western blot using the His tag detector kit. Proteins were separated on a polyacrylamide gel and transferred onto a nitrocellulose membrane. The blots were developed with the ECL prime western blot detection kit. The chemical inflorescence signals of protein binding were detected with X-ray film in the dark room or with a Chemiluminescence documentation system. A. AtHPCL expressed from pET43b vector. B. AtHPCL expressed from pQE81L vector. ev: empty vector.

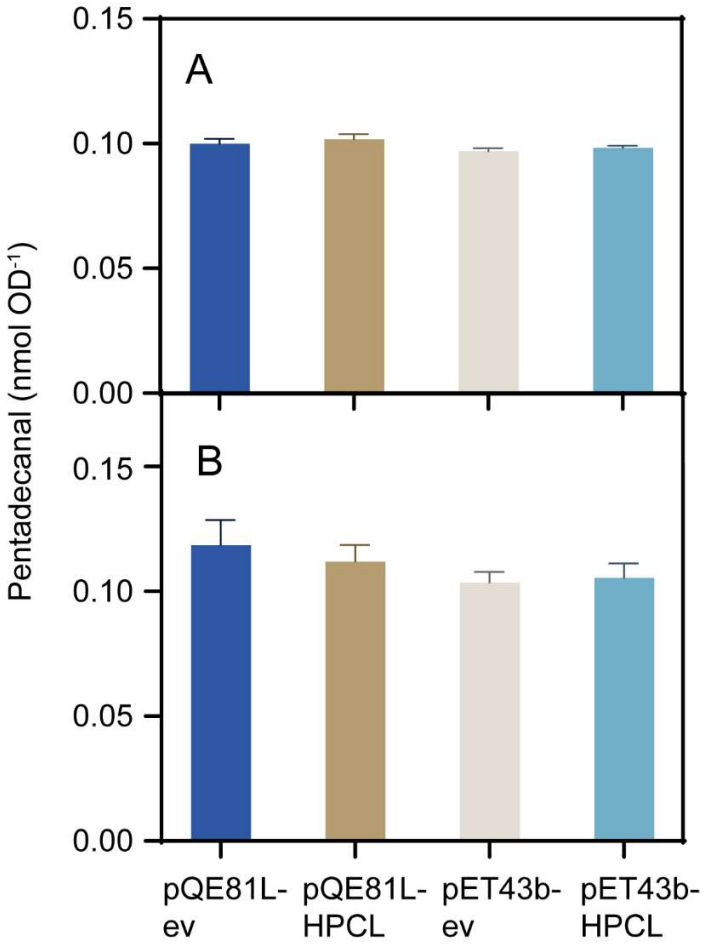

Figure. 3.8 Substrate supplementation assay with *E.coli*.

2-hydroxy-palmitic acid was supplemented to *E.coli* cultures expressing AtHPCL. After incubation, pentadecanal (15:0 aldehyde) was extracted from the cells, derivatized with methoxylamine HCl and measured by GC-MS to evaluate enzyme activities. A. Protein expression was induced at 16°C. B Protein expression was induced at 28°C. Pentadecanal concentrations were normalized to OD_{600nm}. In both cases, there was no activity difference between AtHPCL and control (ev). ev: empty vector. Mean ± SD; n=3.

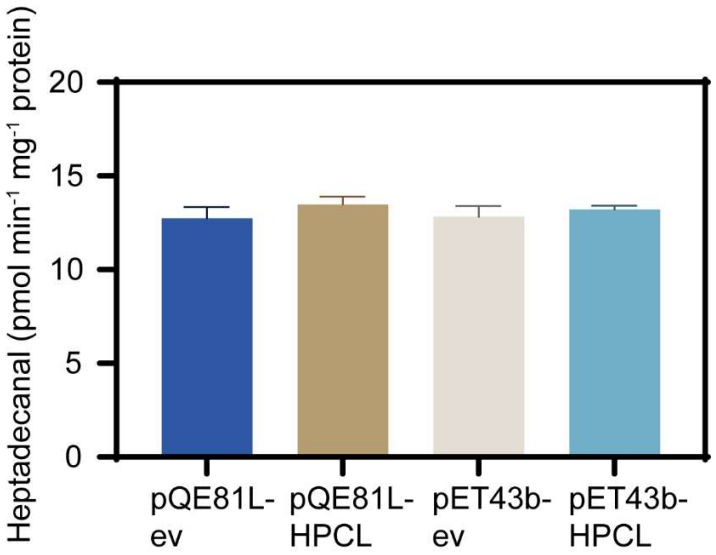

Figure. 3.9 *In vitro* 2-hydroxy-acyl-CoA lyase assay with protein expressed in *E.coli*.

E.coli cells were ruptured, cell debris was removed by low-speed centrifugation and microsomal protein was enriched by ultracentrifugation. The membrane fraction was resuspended in homogenization buffer and tested for the 2-hydroxy-stearoyl-CoA (2-hydroxy-18:0 acyl-CoA) lyase activity. Heptadecanal (17:0 aldehyde) was extracted, derivatized with methoxylamine HCl and measured via GC-MS to evaluate enzyme activities. There was no activity difference between AtHPCL and control. Mean±SD, n=3. ev, empty vector, control.

3.1.2.3 Expression of AtHPCL in the Wheat Germ Cell-Free *in vitro* Expression System

The wheat germ cell-free *in vitro* expression technology was initially developed for production of eukaryotic proteins (Endo & Sawasaki, 2003; Tsuboi et al., 2008). A commercial kit of this technology was obtained from Biotechrabbit (Hennigsdorf, Germany). To express AtHPCL in the cell-free system, the cDNA of AtHPCL was cloned into pIVEX1.3 and pIVEX1.4. In the pIVEX1.3 and pIVEX1.4 the ORF is cloned for expression under the control of a T7 promotor. The minor difference is that pIVEX1.3 has a His6 tag coding sequence at the C-terminus of the ORF, while for pIVEX1.4 the His6 tag coding sequence is at the N-terminus of the ORF. The

proteins expressed from pIVEX1.3 and pIVEX1.4 had a size of 63 kDa and 64 kDa, respectively and could be detected in Western blot with a His-tag detector kit (Fig. 3.10). Afterwards, AtHPCL expressed in the cell-free system was tested for the 2-hydroxy-acyl-CoA activity *in vitro*. The substrate was 2-hydroxy-stearoyl-CoA, and heptadecanal was extracted, derivatized with methoxylamine HCl and measured via GC-MS to evaluate enzyme activities. AtHPCL had no significant 2-hydroxy-acyl-CoA lyase activity compared to the control (pIVEX-GUS) (Fig. 3.11).

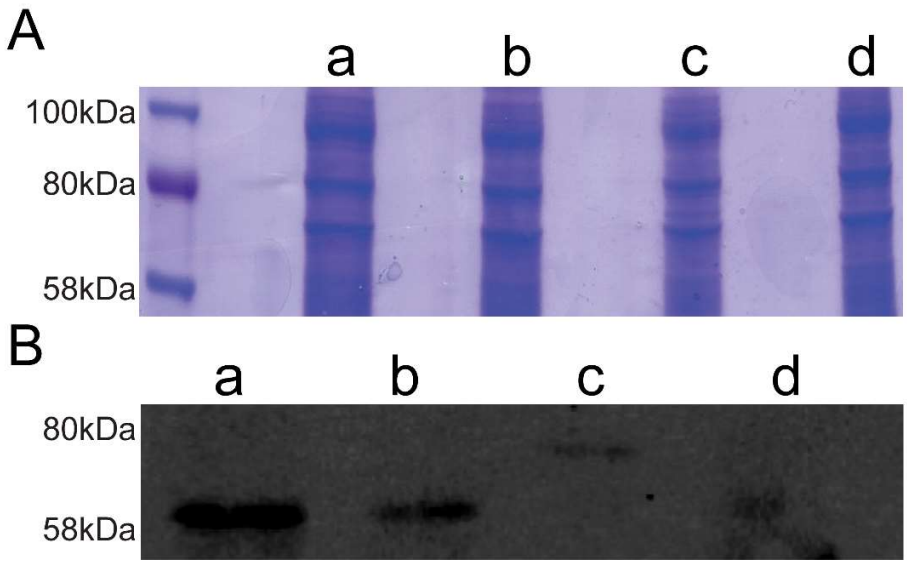

Figure. 3.10 Expression of AtHPCL in the wheat germ cell-free *in vitro* expression system.

A. AtHPCL expressed in the wheat germ cell-free *in vitro* expression system was in low concentration and could not be detected by polyacrylamide gel electrophoresis (SDS-PAGE), after staining with Coomassie brilliant blue R250.

B. AtHPCL expressed in the wheat germ cell-free *in vitro* expression system can be detected by Western blot using the His tag detector kit. Proteins were separated on a polyacrylamide gel and transferred onto a nitrocellulose membrane. The chemical fluorescence signals of protein binding were detected with X-ray film in the dark room. a, pIVEX1.3-HPCL; b, pIVEX1.4-HPCL; c, pIVEX-GUS; d, pIVEX1.3-ev. ev, empty vector.

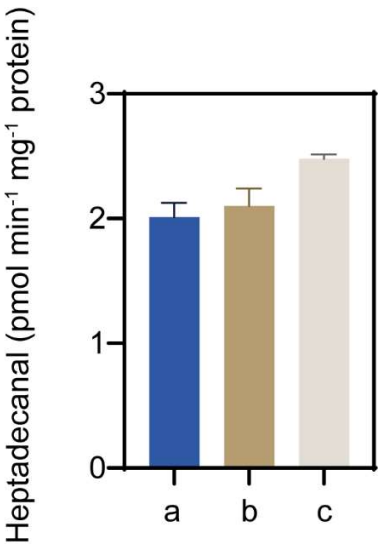

Figure. 3.11 2-Hydroxy-acyl-CoA lyase *in vitro* assay with AtHPCL expressed in wheat germ cell-free *in vitro* expression system.

AtHPCL was expressed in the wheat germ cell-free *in vitro* expression system and tested in the 2-hydroxy-acyl-CoA lyase *in vitro* assay. The substrate was 2-hydroxy-stearoyl-CoA. Heptadecanal (17:0 aldehyde) was extracted, derivatized with methoxylamine and measured via GC-MS. There was no significant activity difference between AtHPCL and control. Mean±SD, n=3. a, pIVEX1.3-HPCL; b, pIVEX1.4-HPCL; c, pIVEX-GUS.

3.1.2.4 Expression of AtHPCL in *Spodoptera frugiperda* (Sf9) Cells

The prokaryotic expression system (*E.coli*) did not produce active protein, possibly due to the lack of mechanism of protein folding and modification, i.e. glycosylation, methylation and disulfide bond forming. The insect cell expression system might produce recombinant proteins with correct folding and modification and is a powerful tool for protein research. One commonly used insect cell line is the Sf9 cell line from *Spodoptera frugiperda*. The Sf9 cells line is a clonal isolate of *Spodoptera frugiperda* Sf21 cells (Vaughn et al., 1977). To express AtHPCL in Sf9 cells, the cDNA of AtHPCL harboring an N-terminally fused His6 tag was cloned into the baculovirus vector pFastBac1 and introduced into DH10Bacα *E.coli* cells

to produce the recombinant bacmid which was then transfected into Sf9 cells. Recombinant bacmid DNA is very large in size (>135kbp). As restriction digestion and sequencing are very difficult to perform with DNA of this size, PCR was performed to verify the presence of the At*HPCL* cDNA in the bacmid. PCR with pUC/M13 forward and reverse primers that hybridize to the flanking sequences of the *att*Tn7 produced a product of 4 kb. Also, PCR with the pUC forward and AtHPCL reverse primers gave a positive band. Similarly, PCR with pUC reverse and AtHPCL forward primers could produce a positive band (Fig. 3.12). Therefore, the cDNA of AtHPCL was successfully transposed into the bacmid.

Afterwards Sf9 cells were transfected with bacmid-AtHPCL or bacmid-GUS (control). Transfected and untransfected Sf9 cells were observed under an optical microscope. Compared to the untransfected Sf9 cells, transfected Sf9 cells appeared larger and granular and had larger nuclei (Fig. 3.13 A). Transfected cells stopped dividing 4 days after transfection as they started to die and rupture. AtHPCL expressed in Sf9 cells is 63kDa and shows a strong band in the Western blot using the His6 tag detector kit, while the GUS protein expressed in Sf9 cells shows no band due to the lack of His6 tag (Fig. 3.13 C). To evaluate activities of enzymes produced from Sf9 cells, a GUS assay was performed. GUS expressed in Sf9 cells converted the substrate X-glucuronide into blue products in 20 minutes. AtHPCL and untransfected insect cells did not harbor GUS activity (Fig. 3.13 B).

For the 2-hydroxy-acyl-CoA lyase *in vitro* enzyme assay, Sf9 cells were transfected with Passage3 virus stock and continued growing for another 4-5 days. Cells were harvested by centrifugation and disrupted by a Precellys homogenizer. Microsomal proteins were isolated and enriched by ultracentrifugation and employed in the *in vitro* enzyme assay. The substrate was 2-hydroxy- stearoyl-CoA, and the product heptadecanal (17:0 aldehyde) was derivatized with methoxylamine HCl and quantified to evaluate enzyme activity. There was no significant activity difference between AtHPCL and control (GUS) (Fig. 3.14).

Alternatively, Sf9 cultures were supplemented with 2-hydroxy-palmitic acid and continued growing for another 2 h. Afterwards, pentadecanal (15:0 aldehyde) was extracted from cells and media, derivatized with methoxylamine HCl and quantified

to evaluate enzyme activities. Still, there was no significant activity difference between AtHPCL and control (GUS) (Fig. 3.15).

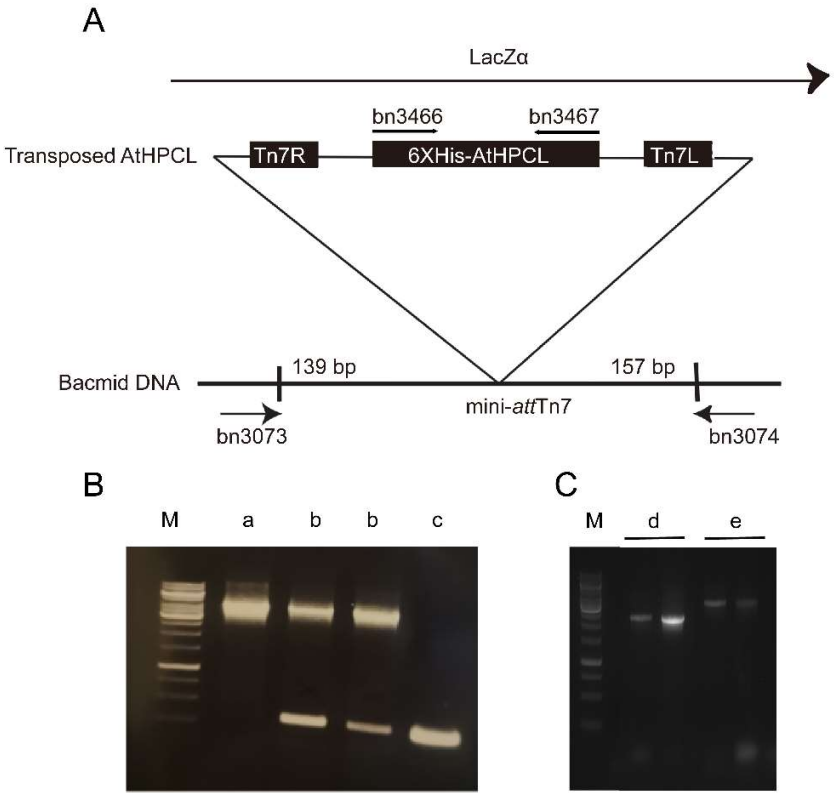

Figure. 3.12 Confirmation of the cloning of the recombinant bacmid carrying AtHPCL via PCR.

A. The recombinant bacmid structure (only the transposed region and flanking sequences are shown). bn3073, bn3074: Primers hybridizing to the flanking sequences. bn3466, bn3467: Primers hybridizing to the AtHPCL sequence. Modified from Bac-to-Bac™ Baculovirus Expression System USER GUIDE. Arrows indicate primers or the LacZα gene.

B. Screening of the recombinant bacmid with primers hybridizing to the *att*Tn7 flanking sequence. a: transposed bacmid; b: transposed bacmid + untransposed bacmid; c: untransposed bacmid.

C. Screening of the recombinant bacmid carrying the right insert. d: bn3466 + bn3074; e: bn3467 + bn3073. The PCR products were separated on an agarose gel, stained with ethidium bromide and then observed under ultraviolet light.

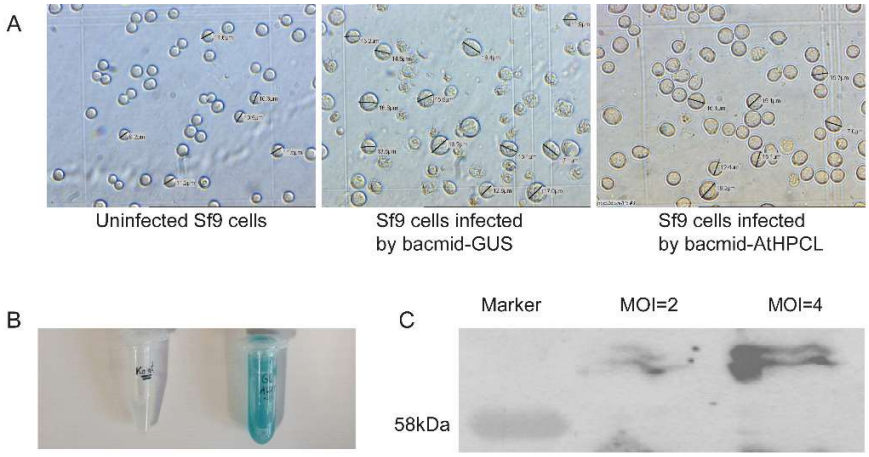

Figure. 3.13. Sf9 cells after infection and expression of proteins in Sf9 cells.

A. 4 days after transfection, Sf9 cells were observed under an optical microscope. Compared to the untransfected Sf9 cells, transfected Sf9 cells appeared larger and granular and had larger nuclei.

B. GUS enzyme assay. The left tube shows uninfected cells. The right tube shows Sf9 cells infected by bacmid-GUS. 5 μL of X-Glucuronide (20mg/mL solution in DMSO) and 50 μL insect cell culture were mixed and incubated at room temperature for 20 min.

C. AtHPCL expressed in Sf9 cells was detected in a Western blot using the His6 tag detector kit. MOI: multiplicity of Infections.

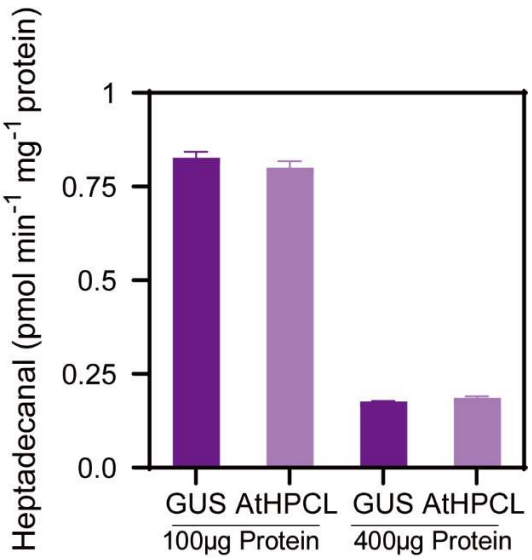

Figure. 3.14 *In vitro* assay for 2-Hydroxy-acyl-CoA lyase with protein expressed in Sf9 cells.

Total protein was extracted from Sf9 cells, and microsomal protein purified via ultracentrifugation and tested in the 2-hydroxy-acyl-CoA lyase assay. The substrate was 2-hydroxy-stearoyl-CoA. After incubation, heptadecanal (17:0 aldehyde) was extracted, derivatized with methoxylamine and measured via GC-MS to evaluate enzyme activities. Reactions were set at different protein amounts, namely 100 µg and 400 µg as shown on the x-axis. In both cases, there was no significant activity difference between AtHPCL and the control (GUS). Mean ± SD; n=3.

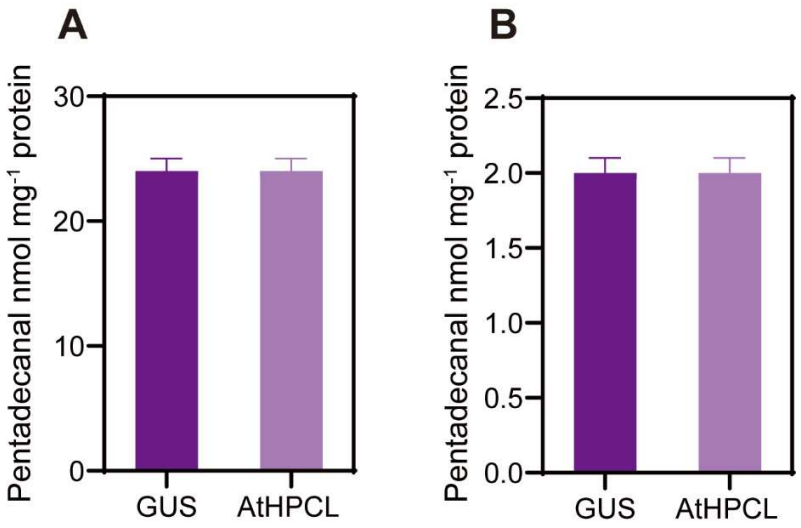

Figure. 3.15 Substrate feeding assay with Sf9 cells.

2-Hydroxy-palmitic acid was supplemented to Sf9 cell cultures expressing AtHPCL. After incubation, pentadecanal (15:0 aldehyde) was extracted from cells (A) and media (B), derivatized with methoxylamine HCl and quantified via GC-MS to evaluate enzyme activities. In both cases, there was no significant activity difference between AtHPCL and control. Mean ± SD; n=3.

3.1.3 Isolation of *A. thaliana* Mutant Lines

Three *Arabidopsis* HPCL T-DNA insertion lines of At*HPCL* gene were obtained and designated *hpcl-1*, *hpcl-2* and *hpcl-3*, respectively. *hpcl-1* (SALK_142717) and *hpcl-3* (SALK_001425C) were obtained from the NASC (Nottingham, UK). The T-DNA line *hpcl-2* (SAIL_343D06/CS816002) was obtained from Prof. Kimitsune Ishizaki (Kobe University, Japan). Homozygous mutant seedlings were selected by PCR of genomic DNA. The genomic sequence around the insertion site was amplified with the primer pairs bn2895/bn2896, bn2889/bn2890 and bn2897/bn2898 for *hpcl-1*, *hpcl-2* and *hpcl-3*, respectively. The T-DNA insertions in the mutants were amplified using the primer combinations bn2880/ bn2896, bn2882/bn 2890 and bn2880/bn2898 for *hpcl-1*, *hpcl-2* and *hpcl-3*, respectively (Fig. 3.16).

To assess the expression level of AtHPCL in the mutant lines, the AtHPCL

transcript abundance was determined by RT-PCR. Actin (ACT2) was used as the control. It was found that the expression of AtHPCL in *hpcl-1* was undetectable, while *hpcl-2* and *hpcl-3* still showed residual expression (Fig. 3.17). These results further indicated that *hpcl-1* represented a null allele in agreement with the localization of the insertion in the first exon. In contrast, *hpcl-2* and *hpcl-3* still showed considerably AtHPCL transcript abundance, in line with the scenario that the insertions in these lines did not abolish expression. This was in good agreement with results from section 3.1.3 (Fig. 3.17), that *hpcl-1* completely lost enzymatic activity, while *hpcl-2* and *hpcl-3* still harboured residual activities.

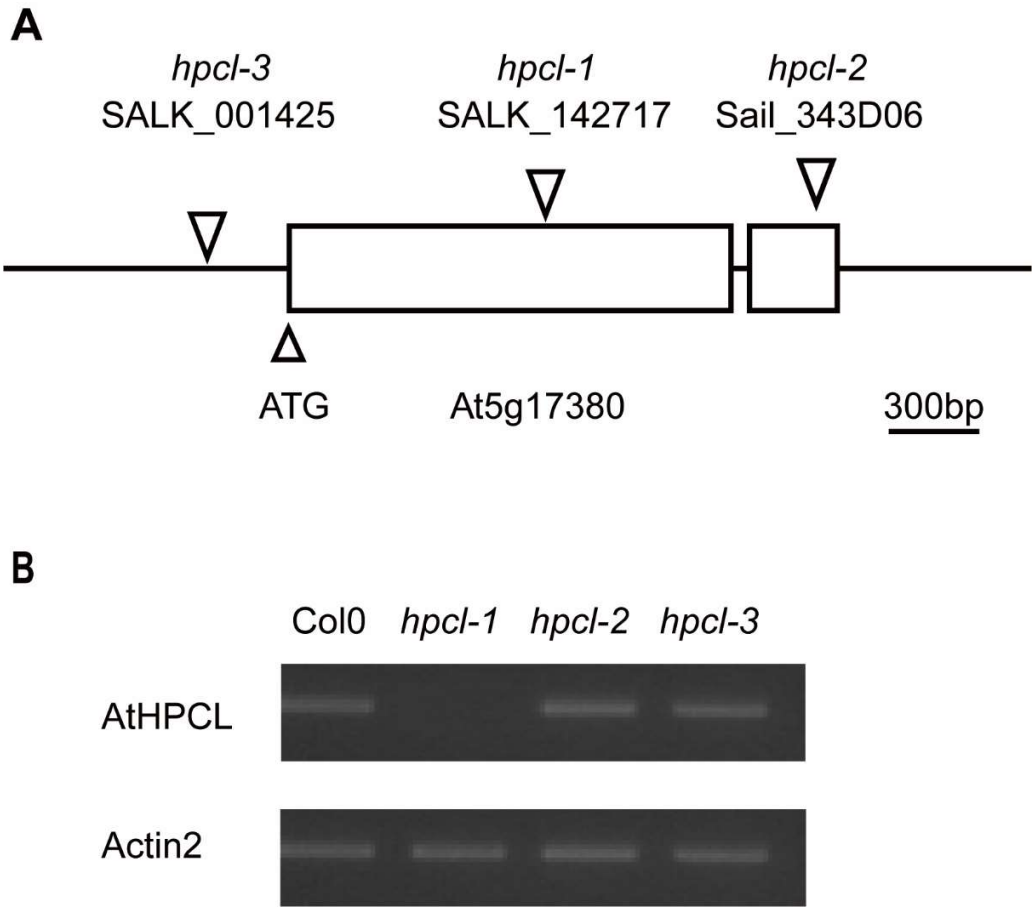

Figure. 3.16 Insertional mutants of At*HPCL* and expression analysis.

A. The gene structure of T-DNA insertion lines of At*HPCL* (locus At5g17380). Exon (boxes) and intron (lines) structure of the *Arabidopsis HPCL* gene (locus At5g17380) with the positions of T-DNA insertion sites in the *hpcl* mutant alleles.

Bar = 300 bp.

B. Expression analysis of At*HPCL* in *Arabidopsis hpcl* mutant leaves. cDNA was synthesized from RNA extracted from *Arabidopsis* leaves. The RT-PCR was performed and products were separated by agarose gel electrophoresis containing ethidium bromide. Actin2 was used as control. *hpcl-1* was a null mutant without any expression.

3.1.4 Peroxisome Isolation

To study the enzymatic function of AtHPCL, peroxisomes were isolated and purified from leaves of *Arabidopsis* wild type (Col-0) and three *hpcl* mutants plants (*hpcl-1*, *hpcl-2* and *hpcl-3*). Peroxisomal proteins were used for *in vitro* 2-hydroxy-acyl-CoA lyase (HACL) assays in the presence of the cofactor TPP and the substrate 2-hydroxy-stearoyl-CoA, which was expected to be converted into heptadecanal (17:0 aldehyde). Heptadecanal was extracted, derivatized into aldehyde-methyloximes with methoxylamine HCl and quantified by GC-MS. In enzyme assays with peroxisomal protein from Col-0 WT, considerable amounts of heptadecanal were detected, indicating that Col-0 harbored 2-hydroxyl-acyl-CoA lyase (HACL) activity (Fig. 3.16). When TPP was omitted from the assay, no activity was observed, indicating that the cofactor was essential for enzyme activity (data not shown). No activity was detected in *hpcl-1* peroxisomal proteins, while the activities in persoxisomal proteins from *hpcl-2* and *hpcl-3* were strongly reduced compared with Col-0. These results showed that AtHPCL harbored HACL activity and that the entire HACL activity in Col-0 peroxisomes was derived from AtHPCL. These results confirmed that *hpcl-1* represented a null mutation, while *hpcl-2* and *hpcl-3* showed residual gene activity.

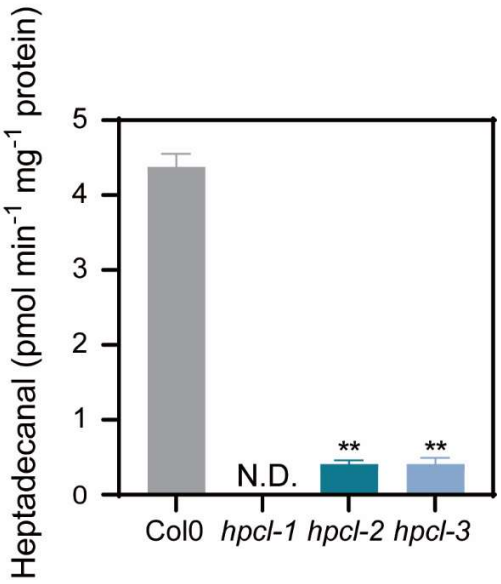

Figure. 3.17 2-Hydroxy-acyl-CoA lyase *in vitro* assay with *Arabidopsis* peroxisomes

Peroxisomes were isolated from *Arabidopsis* Col-0, *hpcl-1, hpcl-2* and *hpcl-3* leaves and used for the *in vitro* 2-hydroxy-acyl-CoA enzyme assay. The substrate was 2-hydroxy-stearoyl-CoA. Heptadecanal (17:0 aldehyde) was extracted, derivatized with methoxylamine HCl and quantified with GC-MS. Mean ± SD; n=3; 2-way ANOVA with Tuckey test; letters indicate significant differences; **, $p < 0.01$; n.d., not detected.

3.2 Characterization of *Arabidopsis* Mutant Lines

3.2.1 The Chlorosis of *hpcl* and *pahx* Mutants under Stress was Less Pronounced Compared with Col-0

The aim of this study was to investigate the phytol degradation pathway in plants. In section 3.1, it was shown that AtHPCL had 2-hydroxy-acyl-CoA lyase activity. But it was not clear whether AtHPCL was involved in phytol metabolism. Also, AtPAHX was proved to have the capacity to convert phytanoyl-CoA into 2-hydroxy phytanoyl-CoA *in vitro*, which was a hypothetical step in plant phytol degradation (Araújo et al., 2011). But the role of AtPAHX in phytol degradation remained

unclear.

To study the roles of AtHPCL and AtPAHX during phytol degradation, 3-weeks old *Arabidopsis* seedlings of wild type Col-0 and *pahx* and *hpcl* mutants were transferred onto synthetic medium with (Control) or without nitrogen (-N). After four days, leaves of Col-0 plants started to turn yellow, but *hpcl-1*, *hpcl-2*, *hpcl-3*, *pahx-1*, *pahx-2* and *pahx-3* plants were still green. After 8 days of nitrogen deprivation, Col-0 plants were completely yellow, while *hpcl-2* and *hpcl-3* plants were slightly yellow, and chlorosis in *hpcl-1*, *pahx-1*, *pahx-2* and *pahx-3* had just started (Fig. 3.18). Chlorophyll was measured photometrically. The chlorophyll contents of WT and mutant plants grown under full nutrition were very similar, with only slight differences on day 4. When plants were grown under nitrogen deprivation, the chlorophyll contents of the mutants remained higher on days 4 and 8, compared with the WT. On day 8, the chlorophyll content of *hpcl-1*, *pahx-1*, *pahx-2* and *pahx-3* were almost 2-fold higher compared with WT, while it was only slightly higher in *hpcl-2* and *hpcl-3*, in line with the scenario that *hpcl-1* represents a stronger allele compared with *hpcl-2* and *hpcl-3* (Fig. 3.19). Therefore, *hpcl-1*, *pahx-1*, *pahx-2* and *pahx-3* showed a strong stay-green phenotype during nitrogen deprivation, while chlorosis of *hpcl-2* and *hpcl-3* was also delayed compared with WT Col-0.

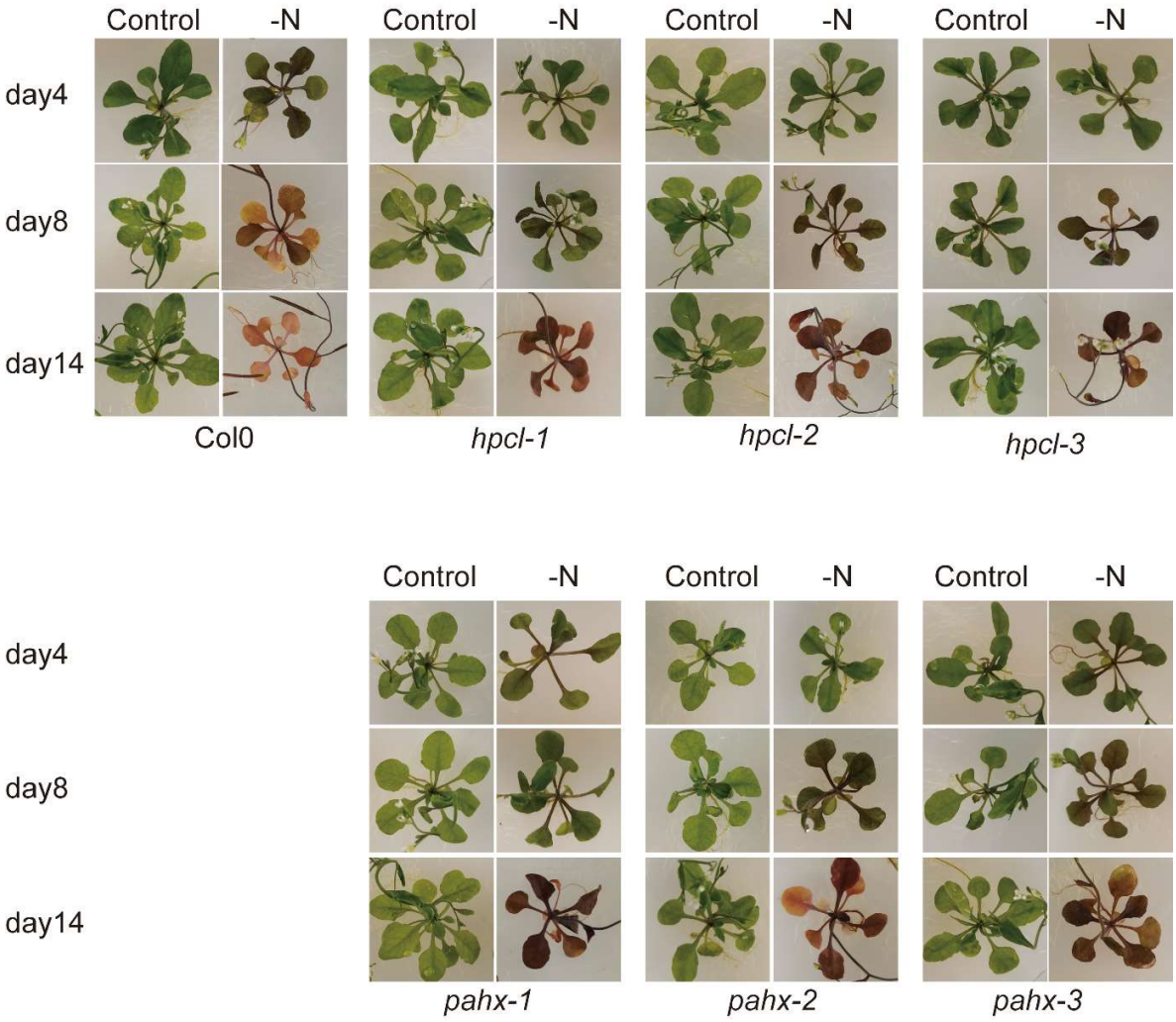

Figure. 3.18 Visible phenotype of *Arabidopsis hpcl* and *pahx* under nitrogen deprivation

Arabidopsis wild type Col-0, *hpcl* and *pahx* mutants were germinated on MS medium containing 2% sucrose. 3 weeks old plants were transferred onto synthetic medium without nitrogen (-N) or with nitrogen (Control). Plants continued growing for 14 days. Visible phenotypes were observed regularly.

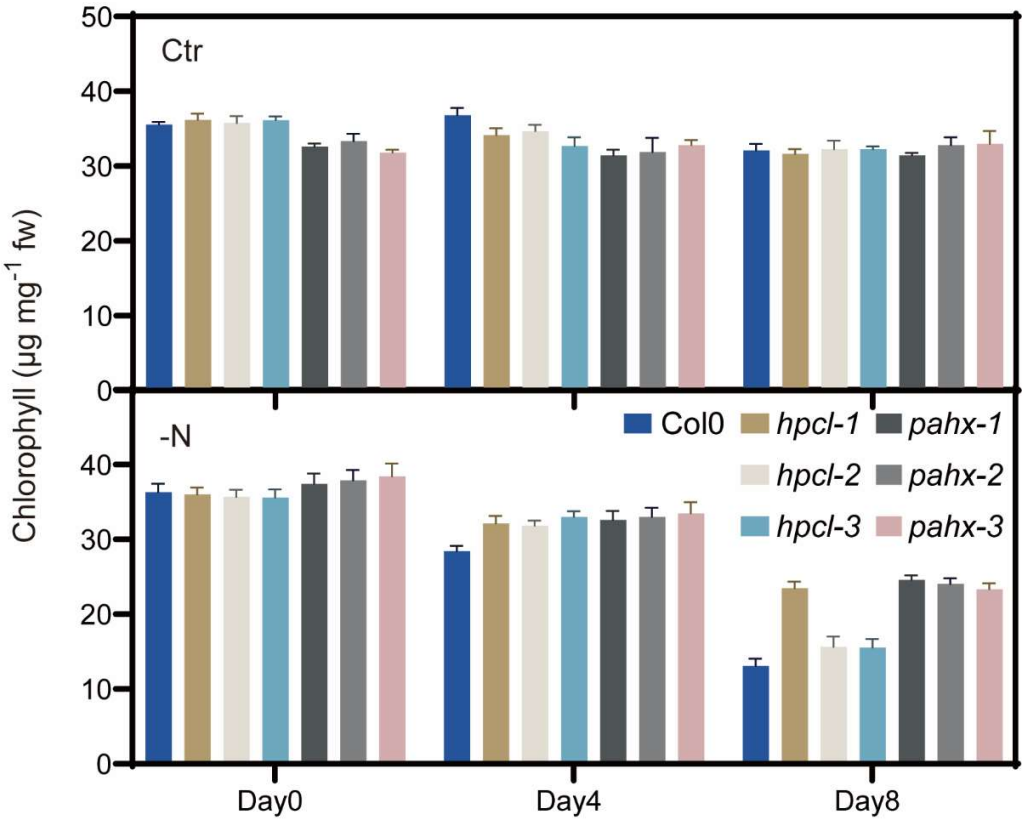

Figure. 3.19 Chlorophyll contents of *hpcl* and *pahx* under nitrogen deprivation

Chlorophyll from Col-0 and *hpcl* and *pahx* were measured photometrically. Day0, day4 and day8 indicated the days that plants were grown on the synthetic medium without nitrogen (-N) or with nitrogen (Ctr). Mean±SD, n=3.

3.2.2 Phytol Incorporation into FAPE and Tocopherol was Increased in *hpcl* and *pahx*

To study the role of AtHPCL on the phytol metabolism, phytenal, free phytol, FAPE and tocopherol were measured in plants growing on nitrogen-deprived medium via mass spectrometry. Previous results showed that free phytol was the precursor for the synthesis of FAPE and tocopherol (Lippold et al., 2012; Valentin et al., 2006; vom Dorp et al., 2015). The phytyl ester synthases PES1 and PES2 contributed most of FAPE synthase activities (Lippold et al., 2012; Wehler, 2017). ER-localized WSD6 could also use phytol as the alcohol donor to synthesize long chain fatty

acid phytyl esters *in vitro* (Patwari, 2019). FAPE was a temporary “phytol sink”, because plants could accumulate FAPE under stress and degrade most FAPE when stress was removed (vom Dorp, 2015). Free phytol could be phosphorylated by VTE5 giving rise to phytol-phosphate. Phytol-phosphate could be phosphorylated by VTE6 yielding phytol-diphosphate. Phytol-diphosphate was the intermediate in the biosynthesis of tocopherol and phylloquione. Therefore, the increase of contents of FAPE and tocopherol indicates that phytol catabolism is inhibited and thus, more phytol is incorporated into FAPE and tocopherol.

This section showed that when plants were grown under nitrogen deprivation, the amounts of tocopherol and FAPE were increased in Col-0, *hpcl* and *pahx*. The amounts of tocopherol and FAPE accumulated to even higher amounts in the *hpcl* and *pahx* mutants compared with Col-0. This showed that the deletions of AtHPCL and AtPAHX resulted in more phytol entering the synthesis pathway of tocopherol and FAPE (Fig. 3.20, 3.21).

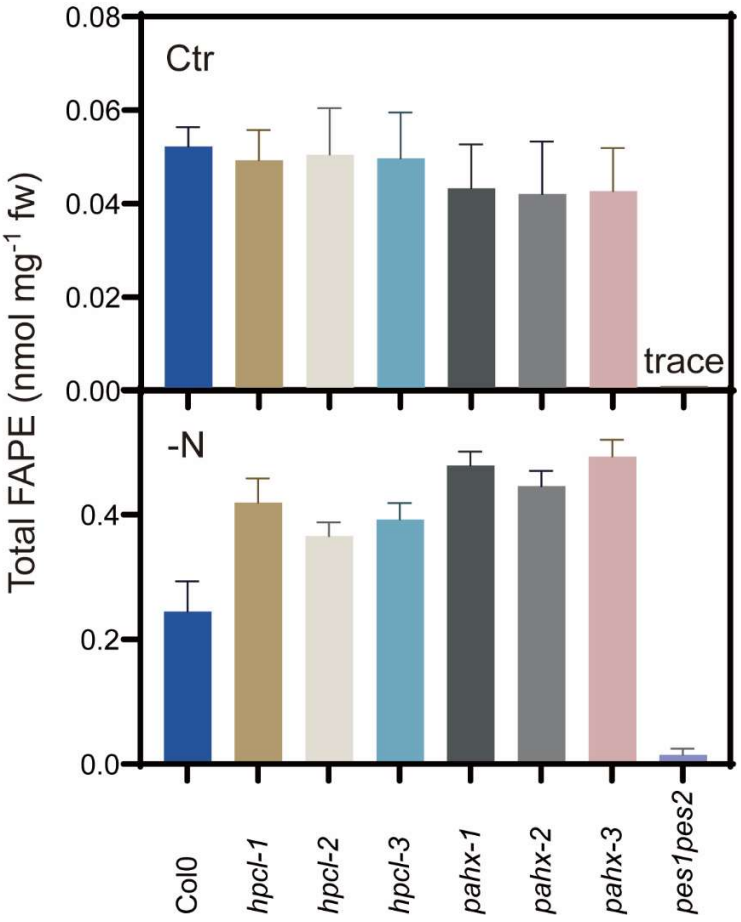

Figure. 3.20 Total FAPE was extracted and measured in *hpcl* and *pahx* under nitrogen deprivation.

Total FAPE was extracted from Col-0 and *hpcl* and *pahx* mutants and measured via Q-TOF direct infusion mode. Plants were grown on the synthetic medium without nitrogen (-N) or with nitrogen (Ctr). Mean ± SD, n=3.

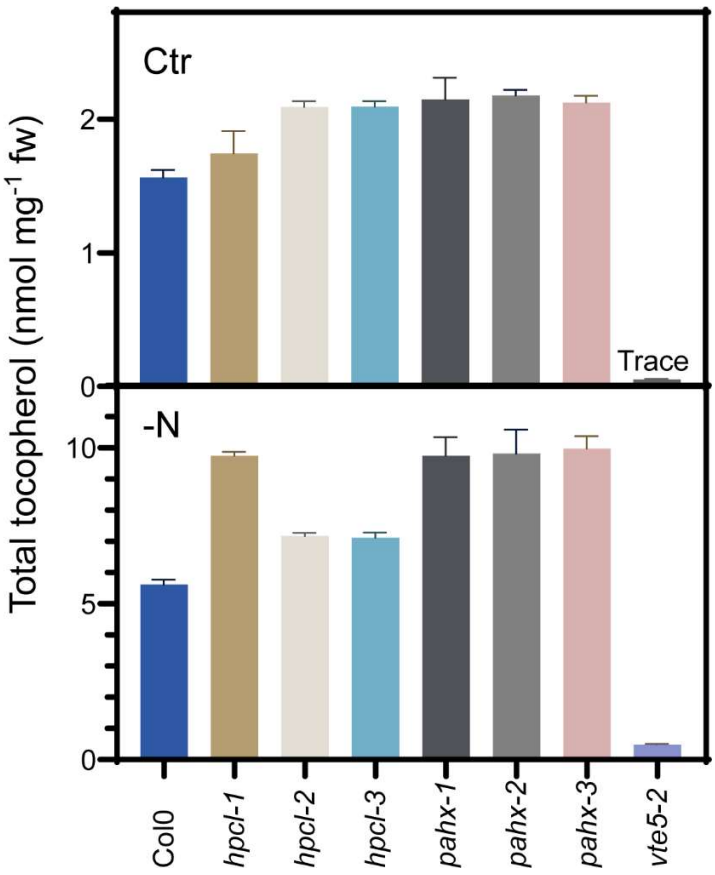

Figure. 3.21 Total tocopherol contents of *hpcl* and *pahx* mutants under N deprivation

Total tocopherol (α, β, γ, δ) was extracted from Col-0 and *hpcl* and *pahx* and measured via HPLC. Plants were grown on the synthetic medium without nitrogen (-N) or with nitrogen (Ctr). fw: fresh leaf weight. Mean ± SD, n=4.

3.2.3 Degradation of Phytol was Suppressed in *hpcl* and *pahx*

A recent study showed that plants accumulated phytenal under stress and the phytenal was indeed derived from the phytol moiety of chlorophyll (Gutbrod et al., 2021). Under nitrogen deprivation, free phytol increased in Col-0, *hpcl* and *pahx*, and it accumulated to higher amounts in *hpcl-1* compared to Col-0. Phytol contents in *hpcl-2* and *hpcl-3* were lower than *hpcl-1*, but higher than Col-0 (Fig. 3.22). Similarity, phytenal increased in Col-0, *hpcl* and *pahx* under nitrogen deprivation. The amounts of phytenal were higher in *hpcl-2* and *hpcl-3*, compared with WT, but

it was even more increased in *hpcl-1* (Fig. 3.23). Therefore, the deficiency in AtHPCL and AtPAHX resulted in an increase in the phytol and phytenal in *hpcl* and *pahx* mutants under stress, indicating that the phytol catabolic pathway was affected when AtHPCL or AtPAHX was deleted.

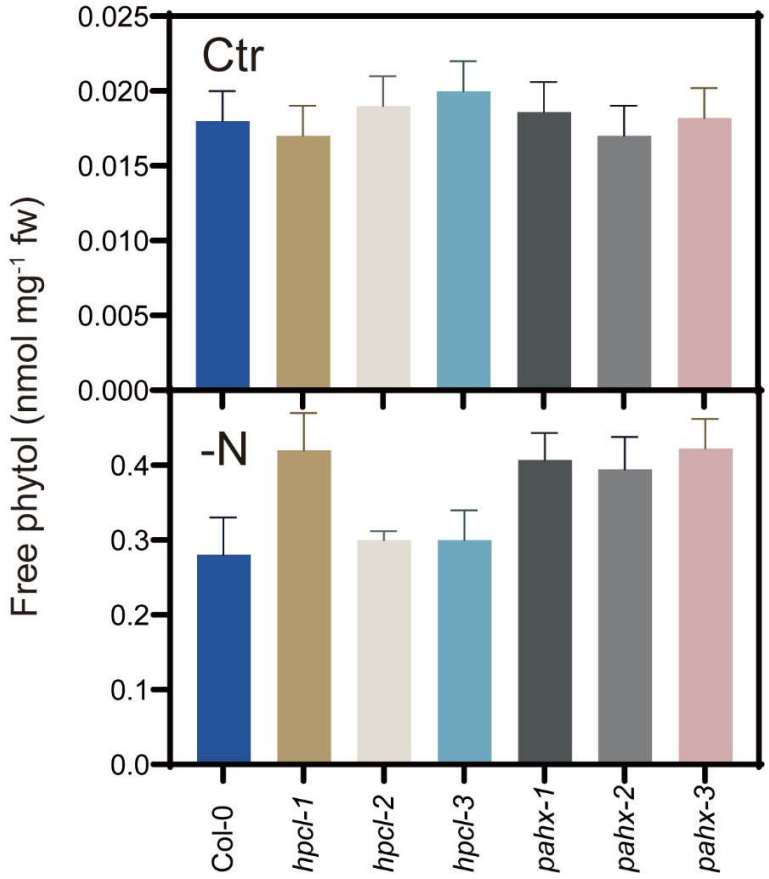

Figure. 3.22 Free phytol contents of *hpcl* and *pahx* under nitrogen deprivation

Free phytol was extracted from Col-0 and *hpcl* and *pahx*, derivatized with MSTFA and measured via GC-MS with helium as the carrier gas. Plants were grown on the synthetic medium without nitrogen (-N) or with nitrogen (Ctr). Mean ± SD, n=3.

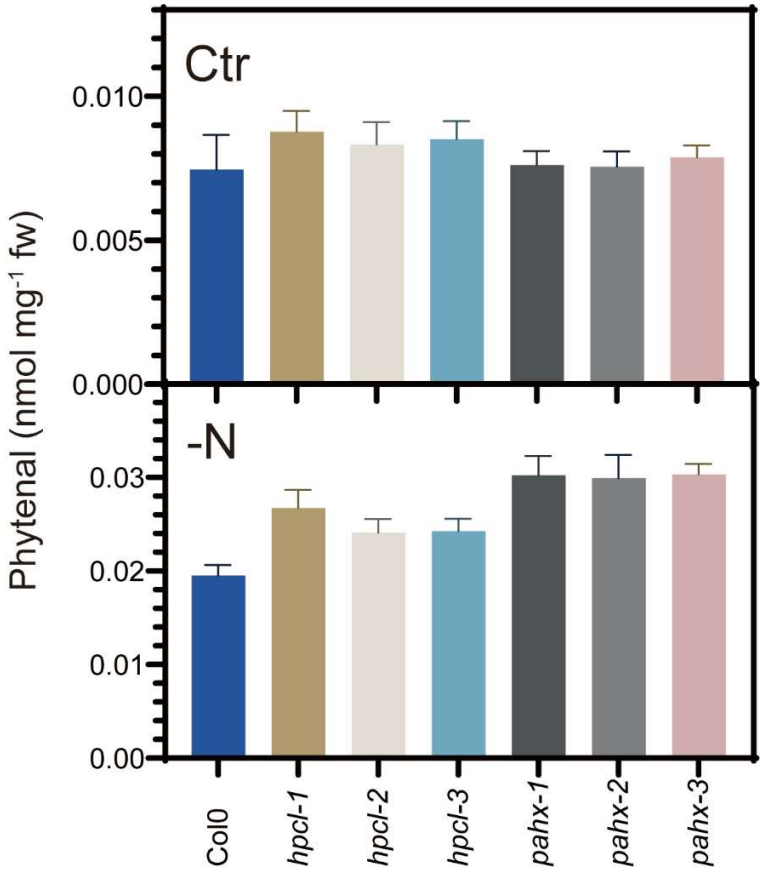

Figure. 3.23 Phytenal contents of *hpcl* and *pahx* under nitrogen deprivation
Phytenal was extracted from Col-0, *hpcl* and *pahx*, derivatized with methoxylamine HCl and measured via GC-MS with helium as the carrier gas. Plants were grown on the synthetic medium without nitrogen (-N) or with nitrogen (Ctr). Mean±SD, n=3.

3.2.4 Exogenous Phytol Follows A Similar Metabolic Pathway Compared with Phytol Released during Nitrogen Deprivation in Col-0, *hpcl* and *pahx*

Alternatively, exogenous phytol was supplemented to Col-0 and *hpcl* and *pahx* seedlings of 3 weeks. After an incubation of 12 h, lipids (phytenal, FAPE and tocopherol) were extracted and quantitatively measured. It was found that exogenous phytol was oxidized to phytenal or incorporated into FAPE and tocopherol in Col-0, *hpcl* and *pahx*. Also, the oxidation and incorporation of phytol in *hpcl* and *pahx* were stronger than Col-0. Taken together, the results shown in

the above sections proved that AtHPCL and AtPAHX were indeed involved in phytol degradation in plants (Fig. 3.24, 3.25, 3.26).

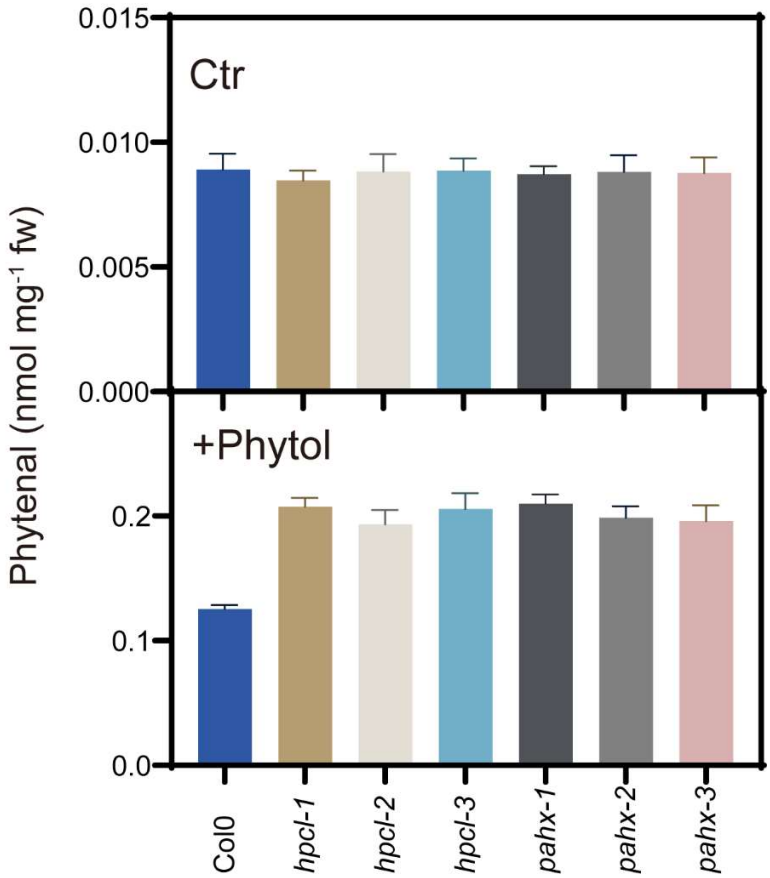

Figure. 3.24 Phytenal contents of *hpcl* and *pahx* after phytol feeding

Plants were germinated on MS medium containing sucrose. 3 weeks old seedling were transferred into Erlenmeyer flasks with MES-KOH buffer (pH=6.5). Phytol was supplemented at a final concentration of 0.1%. After 12 h, phytenal was extracted from leaves, derivatized with methoxylamine and measured with GC-MS. Mean ± SD, n=3.

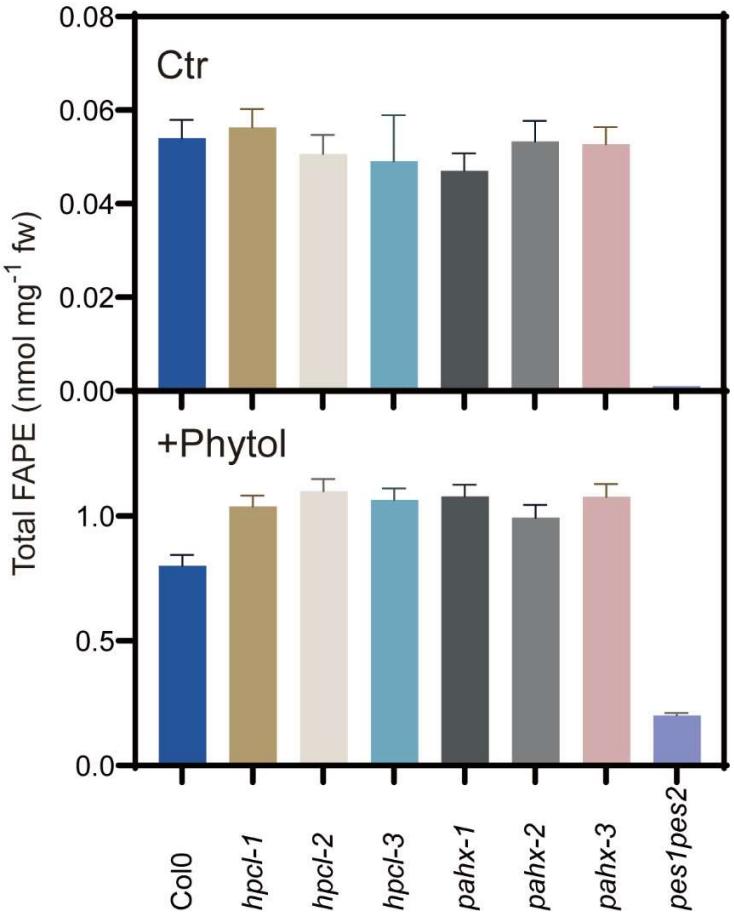

Figure. 3.25 FAPE contents of *hpcl* and *pahx* mutants after phytol feeding

Plants were germinated on MS medium containing sucrose. 3 weeks old seedling were transferred into Erlenmeyer flasks with MES-KOH buffer (pH=6.5). Phytol was supplemented at a final concentration of 0.1%. After 12 h, total FAPE was extracted from leaves, purified via solid phase extraction and measured with Q-TOF direct infusion mode. Mean ± SD, n=3.

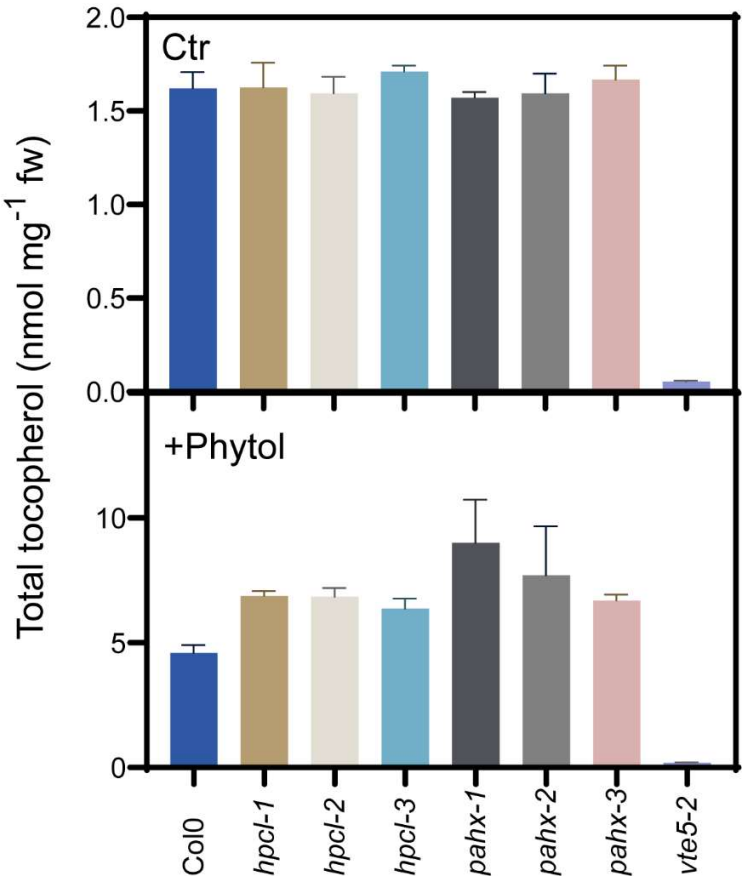

Figure. 3.26 Total tocopherol contents of *hpcl* and *pahx* mutants after phytol feeding

Plants were germinated on MS medium containing sucrose. 3 weeks old seedling were transferred into Erlenmeyer flasks with MES-KOH buffer (pH=6.5). Phytol was supplemented at a final concentration of 0.1%. After 12 h, total tocopherol was extracted from leaves, purified via solid phase extraction and measured with HPLC. Mean±SD, n=4.

3.2.5 Complementation of the Yeast Δ*mpo1* and Δ*pxp1* Mutants with AtHPCL

The orthologous HPCL sequence from yeast (*Saccharomyces cerevisiae*) was designated PXP1 (Nötzel et al., 2016). Recent results showed that another gene, ScMPO1, provided most of the 2-hydroxy fatty acid degradation capacity in yeast (Seki et al., 2019). In contrast to ScPXP1 which presumably employs CoA thioesters as the substrate, the ScMPO1 uses free 2-hydroxy-fatty acids, which are directly converted into (n-1) fatty acids and carbon dioxide without the occurrence of aldehydes as intermediates and the thiamine pyrophosphate as the cofactor.

ScPXP1 (YEL020C) is localized to peroxisomes and carries a C-terminal peroxisome target tripeptide PRL (Nötzel et al., 2016). PXP1 is well-conserved in fungi and has low similarities with *Saccharomyces cerevisiae* pyruvate decarboxylases. *Saccharomyces cerevisiae* has 3 pyruvate decarboxylase isozymes, namely Pdc1, Pdc5 and Pdc6, which are very similar in sequence (Fig. 3.27). ScPXP1 has a conserved thiamine-pyrophosphate (TPP) binding sequence, which is in line with its proposed TPP-dependent 2-hydroxy-acyl-CoA lyase function. The ScPXP1 gene contains one exon, which encodes a protein of 560 amino acids.

ScMPO1 (YGL010W) is localized to the ER, in line with its function in the degradation of phytosphingosine (PHS), which is the intermediate of sphingolipid metabolism (Kondo et al., 2014; Seki et al., 2019). The ScMPO1 gene has one exon and encodes a protein with 174 amino acids, which is much smaller than ScPXP1 and AtHPCL. According to previous studies, deletions of ScPXP1 or ScMPO1 from *S.cerevisiae* did not lead to obvious phenotypes (Seki et al., 2019). Nevertheless, mild impairment of growth could be observed between Δ*pxp1* and wild type when *S.cerevisiae* was grown on oleate medium, indicating that PXP1 was involved in peroxisome functions or metabolisms, because oleate was specifically toxic to strains with peroxisomal defects (Seki et al., 2019). Yeast mutant cells of Δ*pxp1* and Δ*mpo1* were obtained from stock centers (Euroscarf, Oberursel, Germany). The Δ*pxp1* and Δ*mpo1* mutants both were defective in the synthesis of uracil, which made them unable to grow on synthetic medium without

uracil. The YEL020C gene of Δ*pxp1* and the YGL010W gene of Δ*mpo1* were mutagenized by recombination with a *Kan*MX cassette, which permitted efficient selection of transformants resistant against geneticin (G418) (Wach et al., 1994).

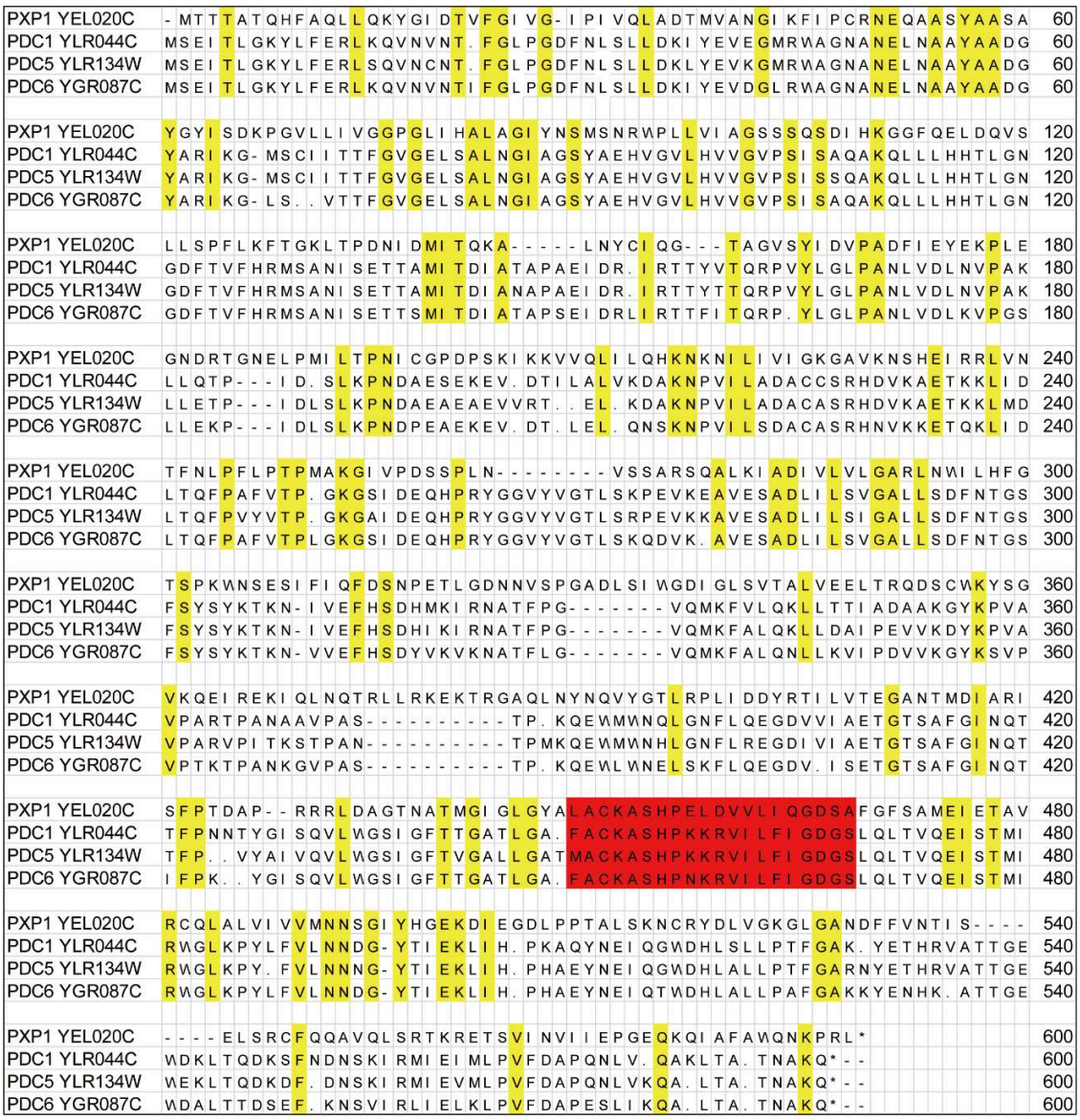

Figure. 3.27. Protein sequence comparison of ScPXP1 and *S.cerevisiae* pyruvate decarboxylase using ClustalW.

Identical amino acids and the conserved TPP-binding sequence ([LIVMF]-[GSA]-X(5)-P-X(4)-[LIVMFYW]-X-[LIVMF]-X-G-D-[GSA]-[GSAC]) were highlighted in yellow and red, respectively.

3.2.5.1 Generation of Yeast Strains Δ*mpo1* and Δ*pxp1* Expressing AtHPCL

The cDNA of AtHPCL was cloned into the yeast expression vector pDR196 and the construct was introduced into Δ*pxp1* and Δ*mpo1* mutants to address the question whether AtHPCL can complement the deficiencies in growth or in 2-hydroxy-acyl-CoA or 2-hydroxy-fatty acid lyase activities, respectively. For the control, an empty vector (ev) was introduced into yeast cells instead of pDR196-AtHPCL. To select *S.cerevisiae* colonies carrying pDR196-AtHPCL, PCR screening was performed. Total DNA (genomic DNA and plasmid DNA) was used as template for the PCR. When primers hybridized to the 5' and 3' ends of AtHPCL, Δ*pxp1*: AtHPCL and Δ*mpo1*: AtHPCL could be amplified. When primers hybridized to the coding sequence of the *MPO1* gene, wild type, Δ*pxp1*: ev and Δ*pxp1*: AtHPCL gave positive bands. When primers hybridized to the coding sequence of the *PXP1* gene, wild type, Δ*mpo1*: ev and Δ*mpo1*: AtHPCL gave positive bands. Therefore, I confirmed that correct plasmids were introduced into *S.cerevisiae* (Fig. 3.28). Moreover, the AtHPCL protein expressed in *S.cerevisiae* could be observed with SDS-PAGE (Fig. 3.29). Taken together, this section shows that AtHPCL was successfully expressed in *S.cerevisiae* and that Δ*pxp1* and Δ*mpo1* were deleted from S.*cerevisiae* successfully.

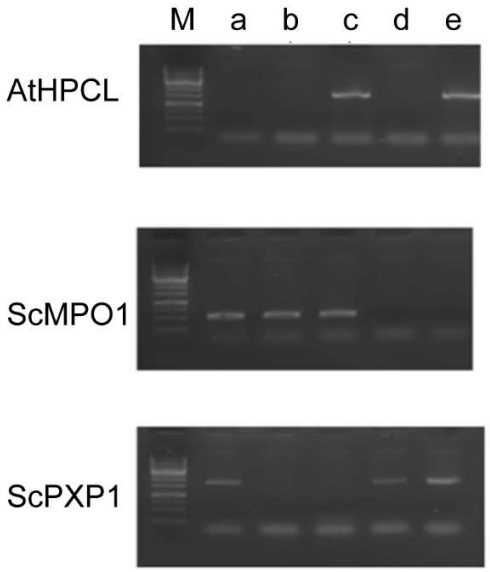

Figure. 3.28 Genotyping of *S.cerevisiae* mutants carrying pDR196-AtHPCL or pDR196-ev

PCR was used to identify yeast mutants carrying the At*HPCL* cDNA on the plasmid pDR196. AtHPCL, ScMPO1 and ScPXP1: primers hybridizing to the *Arabidopsis HPCL* cDNA, *S.cerevisiae MPO1* gene and *S.cerevisiae PXP1* gene, respectively. a, wt:ev; b, Δ*pxp1*:ev; c, Δ*pxp1*: AtHPCL; d, Δ*mpo1*: ev; e, Δ*mpo1*: AtHPCL. ev: empty vector. wt: wild type. M, gene ruler 1kb.

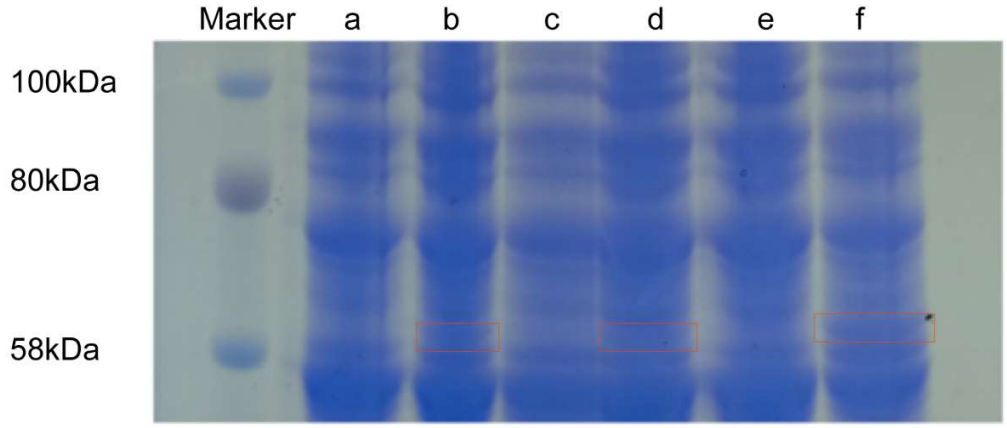

Figure. 3.29 Expression of AtHPCL in *S. cerevisiae*

AtHPCL expressed in *S. cerevisiae* can be observed by polyacrylamide gel electrophoresis (SDS-PAGE)，after staining with Coomassie brilliant blue. The orange boxes highlight the band for AtHPCL. M: protein standard. a, wt:ev; b, wt:AtHPCL; c, Δ*pxp1*:ev; d, Δ*pxp1*: AtHPCL; e, Δ*mpo1*:ev; f, Δ*mpo1*: AtHPCL. ev: empty vector. wt: wild type.

3.2.5.2 The Growth Retardation of Δ*pxp1* was Complemented by AtHPCL

In line with previous studies, Δ*mpo1*: ev and Δ*mpo1*: AtHPCL grew very similarly like wild type cells on synthetic medium lacking uracil. However, Δ*pxp1*: ev showed a strong growth retardation compared with Δ*mpo1* and WT yeast. The growth deficiency of Δ*pxp1* was fully recovered by heterologous expression of AtHPCL, indicating that ScPXP1 and AtHPCL are functionally related. Expression of AtHPCL did not alter the growth of WT or Δ*mpo1* cells (Fig. 3.30).

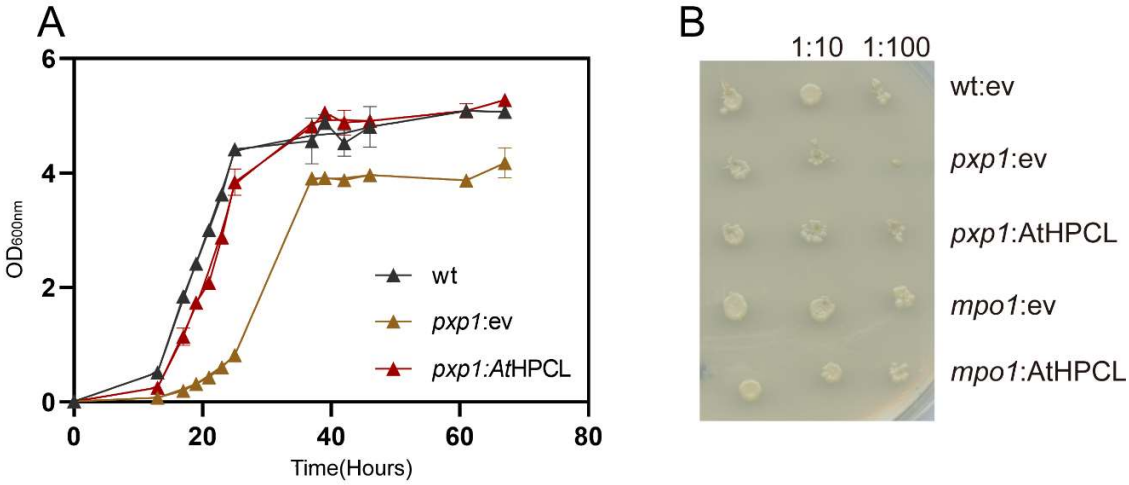

Figure. 3.30 Growth of *S.cerevisiae* Δpxp1 and Δmpo1 mutant cells in liquid culture and on solidified medium

A. Growth curves of yeast control and complemented Δ*pxp1* strains in liquid synthetic medium lacking uracil. The Δ*pxp1* mutant carrying an empty vector (ev) showed reduced growth compare with WT. This growth deficiency could be fully complemented by introduction of AtHPCL. Mean±SD, n=3.

B. Growth assay of yeast on solid synthetic medium lacking uracil. Yeast cells were harvested and diluted to an OD_{600nm} of 1.0. Serially dilutions of 1:10 were spotted on minimal medium lacking uracil and incubated at 28°C for 36 hours. While growth of Δ*pxp1*:ev was retarded, it was ameliorated by the introduction of AtHPCL. The growth of Δ*mpo1*:ev was not different from wt:ev, and it was also not different after introduction of At*HPCL* into Δ*mpo1*.

3.2.5.3 Lipid Alterations of Δ*pxp1* and Δ*mpo1* after the Introduction of AtHPCL

To study the function of AtHPCL on the enzymatic level, 2-hydroxy-palmitic acid was supplemented to the yeast cells growing in liquid cultures. In analogy to previous studies, 2-hydroxy-palmitic acid was expected to be converted into 2-hydroxy-palmityl-CoA by a *S.cerevisiae* acyl-CoA synthase and degraded to pentadecanal (15:0 aldehyde) via the PXP1 or AtHPCL reaction, and pentadecanal would subsequently be oxidized to pentadecanoic acid (15:0) by chemical oxidation or by an aldehyde dehydrogenase. Alternatively, 2-hydroxy-16:0 could directly be degraded by MPO1 resulting in pentadecanoic acid production. Pentadecanoic acid can be incorporated into phospholipids like phosphatidylcholine (PC). Therefore, the increase in molecular PC species with odd-chain fatty acids (e.g. 31:0, 31:1, 31:2) is indicative for the production of 15:0 from 2-hydroxy-16:0 acid.

Lipids were extracted from the yeast cells after 2-hydroxy-16:0 feeding and the relative amounts of the PC molecular species of 31:2, 31:1, 31:0, representing the acyl combinations of 15:1-16:1, 15:0-16:1/15:1-16:0 and 15:0-16:0, were measured by direct infusion mass spectrometry. It was shown that the amounts of 31:2, 31:1 and 31:0 molecular species were not altered in the Δ*pxp1*(ev) mutant compared with WT or the complemented mutant Δ*pxp1*(AtHPCL). However, the amounts of all three molecular species were decreased in the Δ*mpo1*(ev) cells, in agreement with previous results (Seki et al., 2019). Introduction of AtHPCL into the Δ*mpo1* mutant resulted in an increase in the odd-chain PC molecular species 31:1, indicating that AtHPCL can functionally complement the MPO1 deficiency (Fig. 3.31).

In an alternative strategy, yeast cells were grown in liquid synthetic medium with 2-hydroxy-palmitic acid in the presence or absence of thiamine pyrophosphate (TPP), and the product, pentadecanoic acid, measured directly. Cells were harvested and trans-methylated in methanolic HCl and fatty acid methyl esters (FAME) were measured by GC-MS. After 2-hydroxy-palmitic acid feeding, the amount of pentadecanoic acid in the Δ*pxp1*:ev was similar compared with WT cells,

independent of the addition of the cofactor TPP to the culture. When AtHPCL was expressed in Δ*pxp1*, the amount of pentadecanoic acid was slightly but significantly increased in the presence of TPP, in agreement with the scenario that AtHPCL activity is TPP-dependent. The amount of pentadecanoic acid was strongly decreased to background levels in the Δ*mpo1*:ev. This result indicates that the predominant amount of pentadecanoic acid in the total lipid extract is derived from MPO1, but not from PXP1. Introduction of AtHPCL into the Δ*mpo1* mutant resulted in an 8-fold increase in pentadecanoic acid content when cells were grown with TPP, but not in the absence of TPP. The amount of total pentadecanoic acid produced in Δ*mpo1*:AtHPCL cells (0.37 ± 0.04 nmol/OD_{600nm}, mean ± SD) did not reach the WT level (1.94±0.72 nmol/OD_{600nm}; mean ± SD) indicating that AtHPCL cannot fully compensate for the loss of MPO1 activity in the Δ*mpo1* mutant (Fig. 3.32).

Taken together, expression of AtHPCL in the Δ*pxp1* mutant resulted in the complementation of the growth deficiency. Expression of AtHPCL in Δ*pxp1*, which shows WT-like pentadecanoic acid accumulation, resulted in an increase in pentadecanoic acid in total fatty acids in the presence of TPP. The Δ*mpo1* mutant shows no growth deficiency compared with WT, but lacks pentadecanoic acid accumulation both in total fatty acids and PC molecular species. The deficiency in pentadecanoic acid production in Δ*mpo1* was complemented by expression of AtHPCL. Therefore, AtHPCL contributes to the conversion of 2-hydroxy-palmitic acid into pentadecanoic acid, presumably by converting 2-hydroxy-palmityl-CoA into pentadecanal which is further oxidized to pentadecanoic acid.

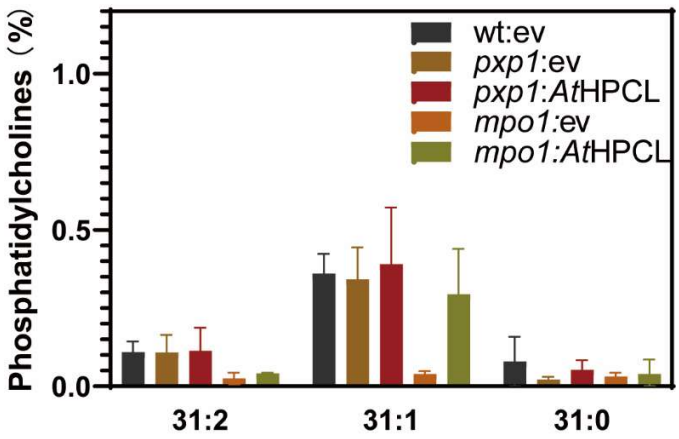

Figure. 3.31. Odd-chain molecular species of phosphatidylcholines from *S.cerevisiae* mutants

Yeast cells (WT, Δpxp1 and Δmpo1 expressing AtHPCL) growing in liquid culture were supplemented with 2-hydroxy-palmitic acid and the cofactor thiamine pyrophosphate (TPP). Lipids were extracted from the cell pellet and PC molecular species quantified by direct infusion mass spectrometry. The odd-chain molecular species 31:2, 31:1, 31:0 of PC contain different combinations of 15:0, 15:1, 16:0 and 16:1. Mean ± SD; n=3. The introduction of AtHPCL into Δ*mpo1* led to increasing of 31:1 phosphatidylcholine.

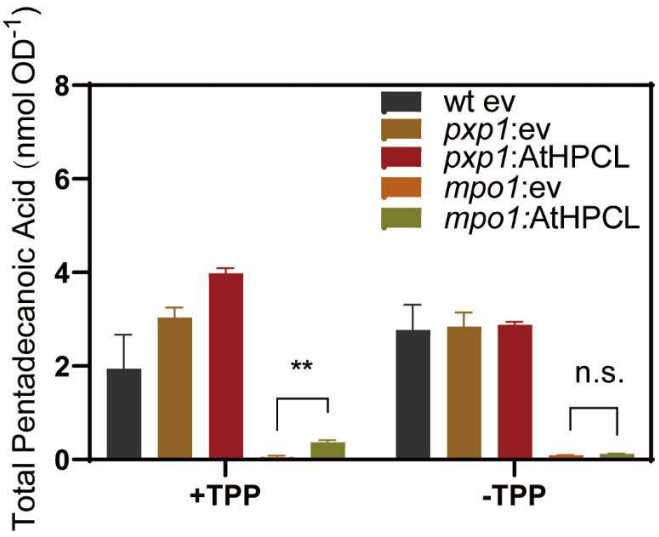

Figure. 3.32 Pentadecanoic acid contents of *S.cerevisiae*

Yeast cells (WT, Δpxp1 and Δmpo1 expressing AtHPCL) growing in liquid culture were supplemented with 2-hydroxy-palmitic acid in the presence or absence of thiamine pyrophosphate (TPP). Cells were harvested and lipids were trans-methylated in methanolic HCl and fatty acid methyl esters (FAMEs) were measured (normalizing to OD_{600nm}) by GC-MS. Mean ± SD; n=3. n.s., not significant.

3.2.6 Phytenal was the Only Detectable Long Chain Aldehyde

It has been proposed that phytol degradation in plants follows a similar pattern as described in *Homo sapiens*. In humans, free phytol was oxidized to phytenal by an unknown alcohol dehydrogenase (fatty alcohol oxidase). Phytenal was converted to 2-hydroxy-phytanoyl-CoA in a series of reactions (Mihalik et al., 1997; van den Brink et al., 2004, 2005). 2-Hydroxy-phytanoyl CoA was then cleaved by hydroxy-acyl-CoA lyase, yielding pristanal, a C19 isoprenoid aldehyde (Casteels et al., 2007; Jenkins et al., 2017; Mezzar et al., 2017) (Fig. 1.8). Formyl-CoA was released during this reaction. From phytol to pristanic acid, three aldehydes were involved, namely phytenal, phytanal and pristanal, respectively (Fig. 3.33). Phytenal was found in plants and originated from the phytol moiety in chlorophyll (Gutbrod et al., 2021). Nevertheless, phytanal and pristanal were never found in plants. It was therefore of interest to identify phytanal and pristanal, which would

help understanding the phytol degradation in plants. The straight chain isomers of pristanal and phytanal, i.e. nonadecanal (19:0 aldehyde) and eicosanal (20:0 aldehyde), respectively, could in principle also be present in tissue extracts and could interfere with the measurements of the isobaric aldehydes pristanal and phytanal. Therefore, I chemically synthesized nonadecanal, eicosanal, pristanal and phytanal standards and determined their chromatographic characteristics on Q-Trap LC-MS/MS. The two straight chain aldehydes also resulted in two peaks each with the same mass transitions as pristanal and phytanal. However, the straight chain aldehydes eluted ~1 min earlier than the isoprenoid aldehydes. Therefore, the two classes of aldehydes can be separated by LC-MS/MS, which made it possible to identify pristanal and phytanal in plant samples. Next, extracts from *Arabidopsis* wild type leaves (plants exposed to nitrogen deprivation) were analyzed by LC-MS/MS for the presence pristanal or phytanal. Analysis of C19:0 aldehyde-methyloximes (MRM 312/60) and C20:0 aldehyde-methyloximes (MRM 326/60) revealed broad peaks eluting at different retention times compared with the standards. Therefore, pristanal and phytanal could not be clearly identified in *Arabidopsis* leaves (Fig. 3.34).

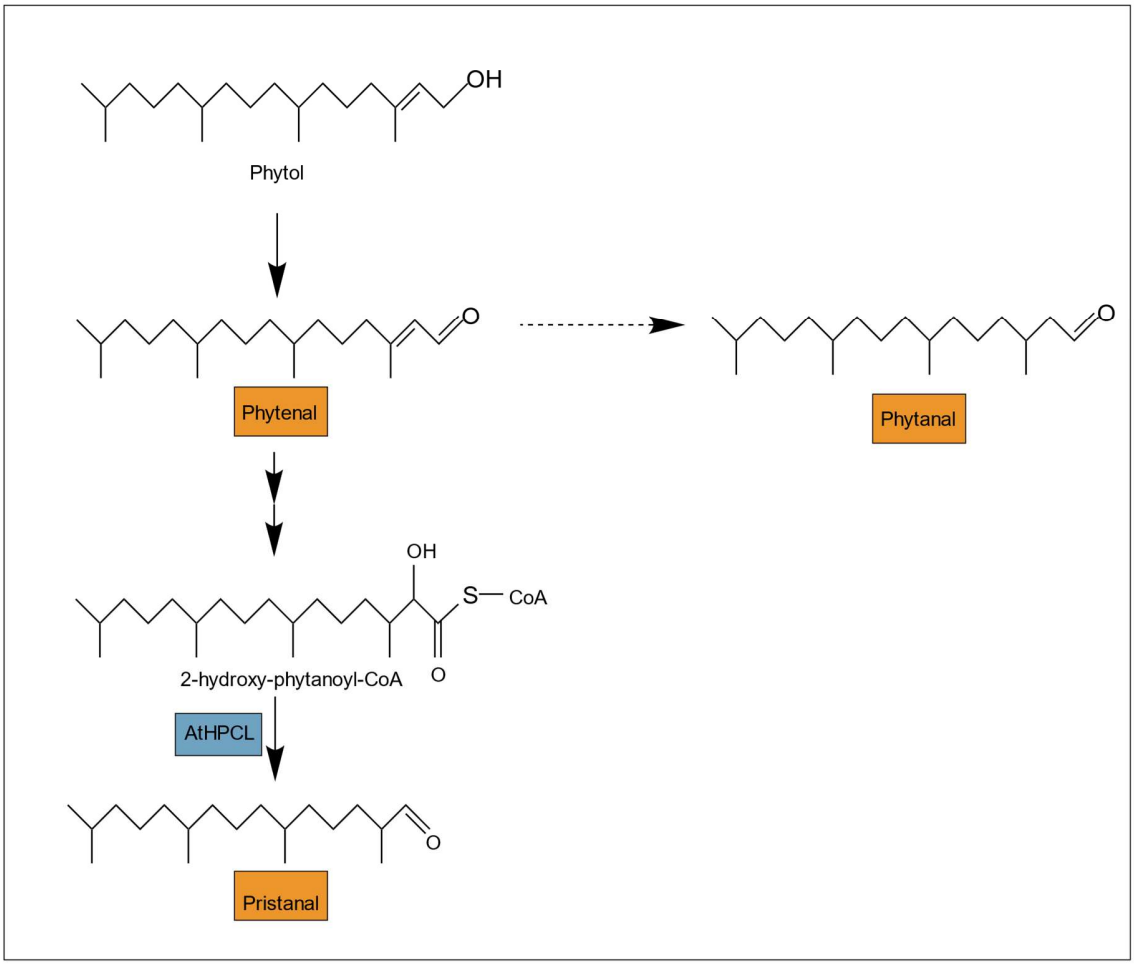

Figure. 3.33 The possible role of aldehydes in phytol degradation

Three aldehydes (phytenal, phytanal and pristanal) were proved/proposed to be involved in the phytol degradation. The hypothetical pathway was depicted. The dashed arrow indicates a theoretical reaction which has not been found in plants, during which phytenal is reduced to phytanal. In animals, the reduction step happens as the CoA ester form, namely, phytenoyl-CoA is reduced to phytanoyl-CoA.

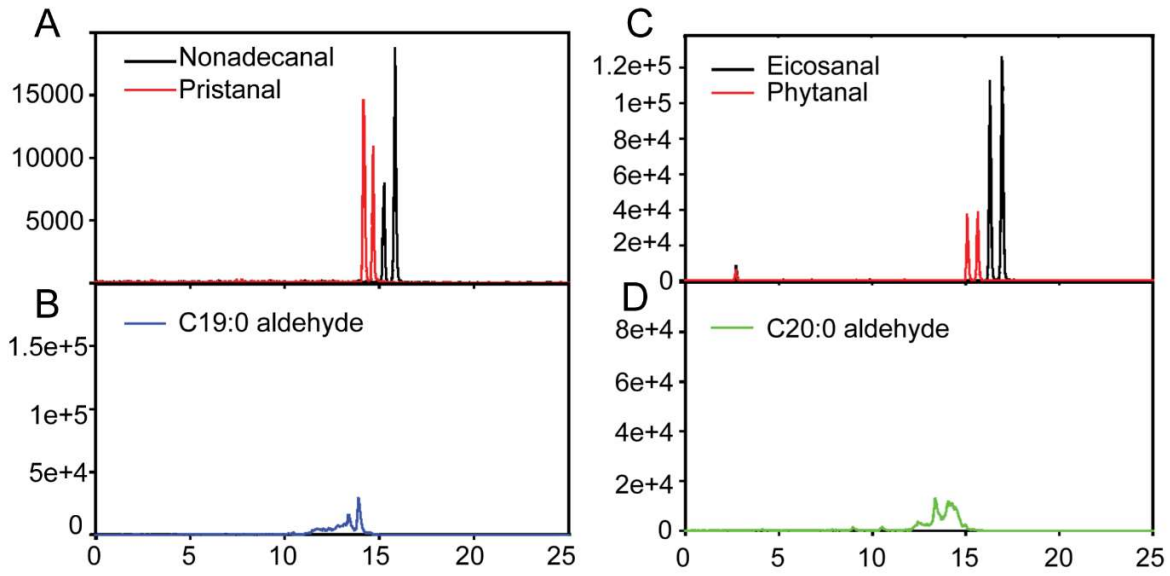

Figure. 3.34 Analysis of Nonadecanal, Pristanal, Eicosanal and Phytanal by LC-MS/MS.

Aldehydes standard mixtures or aldehyde extract from *Arabidopsis* leaves were derivatized with methyloxime and separated by LC-MS/MS on a Q-Trap instrument. A. Chromatograms for C19:0 aldehyde-methyloximes (MRM 312 → 60) of nonadecanal (black) and pristanal (red) standards. B. C19:0 aldehydes from *Arabidopsis* Col-0 leaves of plants grown under N deprivation. Aldehydes were derivatized with methoxylamine and analyzed for the presence of C19 aldehydes (MRM 312 → 60).

C. Chromatograms for C20:0 aldehyde-methyloximes (MRM 326 → 60) of eicosanal (black) and phytanal (red) standards. D. C20 aldehydes from *Arabidopsis* Col-0 leaves of plants grown under N deprivation. Aldehydes were derivatized with methoxylamine and analyzed for the presence of C20 aldehydes (MRM for 326 → 60).

3.2.7 α-Dioxygenases were not Involved in the Degradation of Phytol

An alternative phytol degradation pathway had previously been discussed which would not involve the participation of AtHPCL and AtPAHX. In this pathway, phytanic acid was converted by α-dioxygenase into 2-hydroperoxy-phytanic acid. 2-hydroperoxy-phytanic acid was very instable and could be reduced to 2-hydroxy-

phytanic acid by a peroxidase, and the free acid might be converted into its CoA ester. Another possible fate of 2-hydroperoxy-phytanic was the spontaneous enzymatic or non-enzymatic decarboxylation reaction giving rise to pristanal (Fig 1.8). *Arabidopsis* contains 2 α-dioxygenase genes, namely α-DOX1 and α-DOX2, respectively (Bannenberg et al., 2009; Hamberg et al., 1999). Single and double mutants of the two *Arabidopsis α-dox* genes were produced, but they show no obvious growth phenotype (Bannenberg et al., 2009).

To address the question that whether α-DOX1 and α-DOX2 are involved in phytol degradation, 3-weeks old *Arabidopsis* seedling of wild type Col-0, single mutants *α-dox1*, *α-dox2* and double mutant *α-dox1-α-dox2* were transferred onto synthetic medium without/with nitrogen. The author tried to identify phytanic acid, which was a possible substrate of α-DOX1 and α-DOX2. Also, nonpolar lipids (free phytol, FAPE and tocopherol) and aldehydes were analyzed in *Arabidopsis* leaves.

The straight chain isomer of phytanic acid, namely eicosanoic acid, could in principle also be present in leaves and could interfere with the measurement of the isobaric phytanic acid. Commercial standards of eicosanoic acid and phytanic acid were obtained, transmethylated and analyzed on GC-MS. The elution time of phytanic acid methyl ester (~20 min) was much earlier than eicosanoic acid methyl ester (~25 min). Also, the major fragment of phytanic acid methyl ester was m/z=73, while eicosanoic acid's major fragment was m/z=101 (Fig. 3.35). Therefore, I confirmed that phytanic acid methyl ester and eicosanoic acid methyl ester could be separated on GC-MS, which made the identification of phytanic acid possible. Next, leaves of *Arabidopsis α-dox1*, *α-dox2* and *α-dox1α-dox2* mutants exposed to nitrogen deprivation were transmethylated and analyzed by GC-MS for the presence of phytanic acid. No peaks were eluted at the time points which were corresponding to phytanic acid and eicosanoic acid methyl esters. Therefore, phytanic acid could not be identified in *Arabidopsis* leaves (Fig. 3.35).

Nitrogen-deprivation promotes leaf senescence. There was no difference in the kinetics of chlorosis between Col-0, *α-dox1*, *α-dox2* and *α-dox1α-dox2* (Fig. 3.36). Chlorophyll was measured photometrically. The chlorophyll contents of Col-0, *α-dox1*, *α-dox2* and *α-dox1 α-dox2* were very similar, indicating that deletions of α-

DOX1 and α-DOX2 do not affect chlorosis (Fig. 3.37). In the nitrogen deprivation condition, Col-0, *α-dox1*, *α-dox2* and *α-dox1 α-dox2* all accumulated phytol, phytenal, FAPE and tocopherol. The contents of phytol, phytenal, FAPE and tocopherol in Col-0, *α-dox1*, *α-dox2* and *α-dox1 α-dox2* are very similar (Fig. 3.38). Also, phytenal, FAPE and tocopherol were extracted from *Arabidopsis* leaves in the phytol supplement experiment. Exogenous phytol led to large increases of phytenal, FAPE and tocopherol in Col-0, *α-dox1*, *α-dox2* and *α-dox1α-dox2.* The contents of phytol, phytenal, FAPE and tocopherol in Col-0, *α-dox1*, *α-dox2* and *α-dox1α-dox2* showed no significant difference. The experiment to identify phytanic acid in the phytol supplement experiment failed, too. Taken together, these results showed that *α-DOX1* and *α-DOX2* were not involved in phytol degradation (Fig. 3.39).

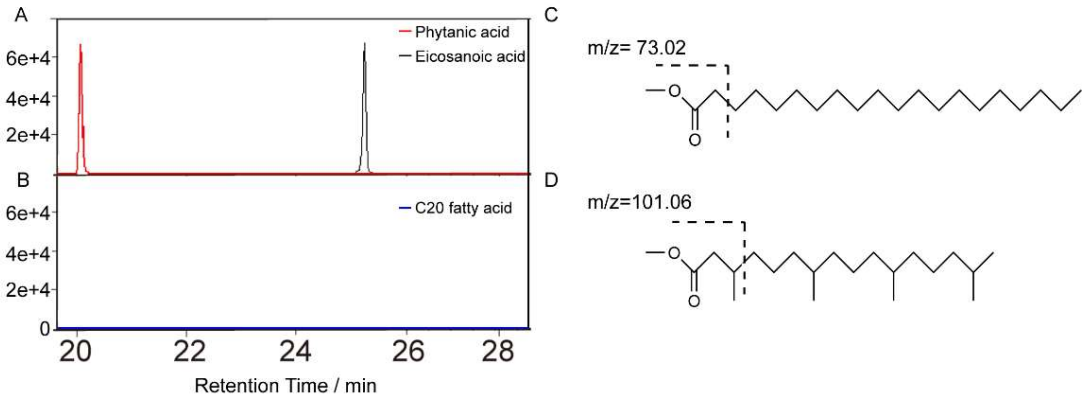

Figure. 3.35 Analysis of eicosanoic acid and phytanic acid by GC-MS in *Arabidopsis α-dox1α-dox2* leaves under nitrogen deprivation

Fatty acid standards or fatty acids from *Arabidopsis* leaves were transmethylated in methanolic HCl and separated by GC-MS.

A. Chromatograms for C20:0 fatty acids of eicosanoic acid (black) and phytanic acid (red) standards.

B. Fatty acids from *Arabidopsis α-dox1α-dox2* leaves of plants grown under nitrogen deprivation eluting at the range of eicosanoic acid and phytanic acid.

C. Structure of eicosanoic acid methyl ester indicating the major fragment of m/z 73 originating from the loss of the $C_3H_5O_2$ group.

D. Structure of phytanic acid methyl ester indicating the major fragment of m/z 101

originating from the loss of the $C_5H_9O_2$ group.

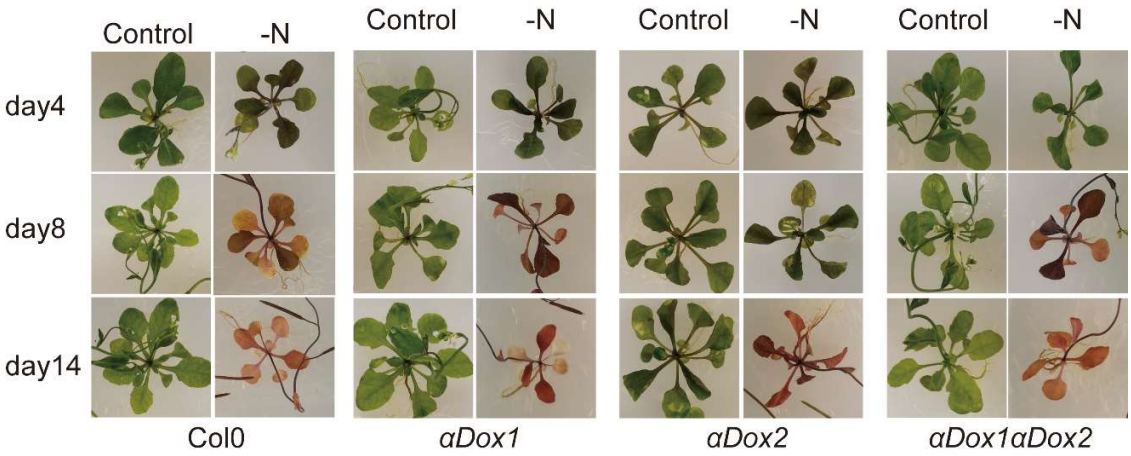

Figure. 3.36 Visible phenotype of *Arabidopsis* α-dox1, α-dox2 and α-dox1-α-dox2 plants under nitrogen deprivation

Arabidopsis wild type Col-0, α-dox1, α-dox2 and α-dox1-α-dox2 were germinated on MS medium containing 2% sucrose. 3 weeks old plants were transferred onto synthetic medium without nitrogen (-N) or with nitrogen (Control). Plants continued growing for 8 days. Visible phenotypes were observed regularly.

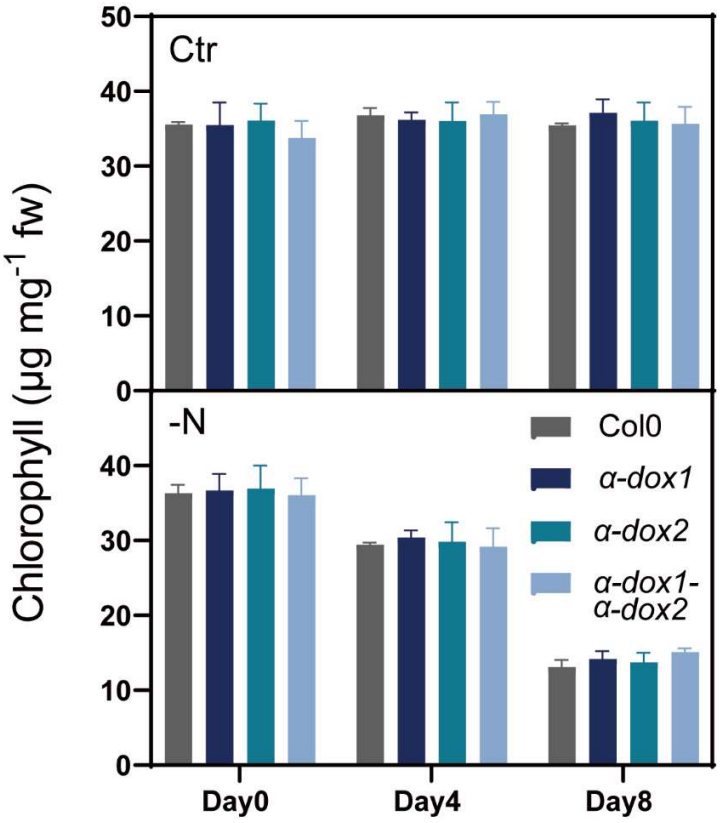

Figure. 3.37 Chlorophyll contents of *Arabidopsis α-dox1, α-dox2* and *α-dox1-α-dox2* under nitrogen deprivation

Chlorophyll from Col-0, *α-dox1, α-dox2* and *α-dox1-α-dox2* were measured photometrically. Day0, day4 and day8 indicated the days that plants were grown on the synthetic medium without nitrogen (-N) or with nitrogen (Ctr). Mean±SD, n=3.

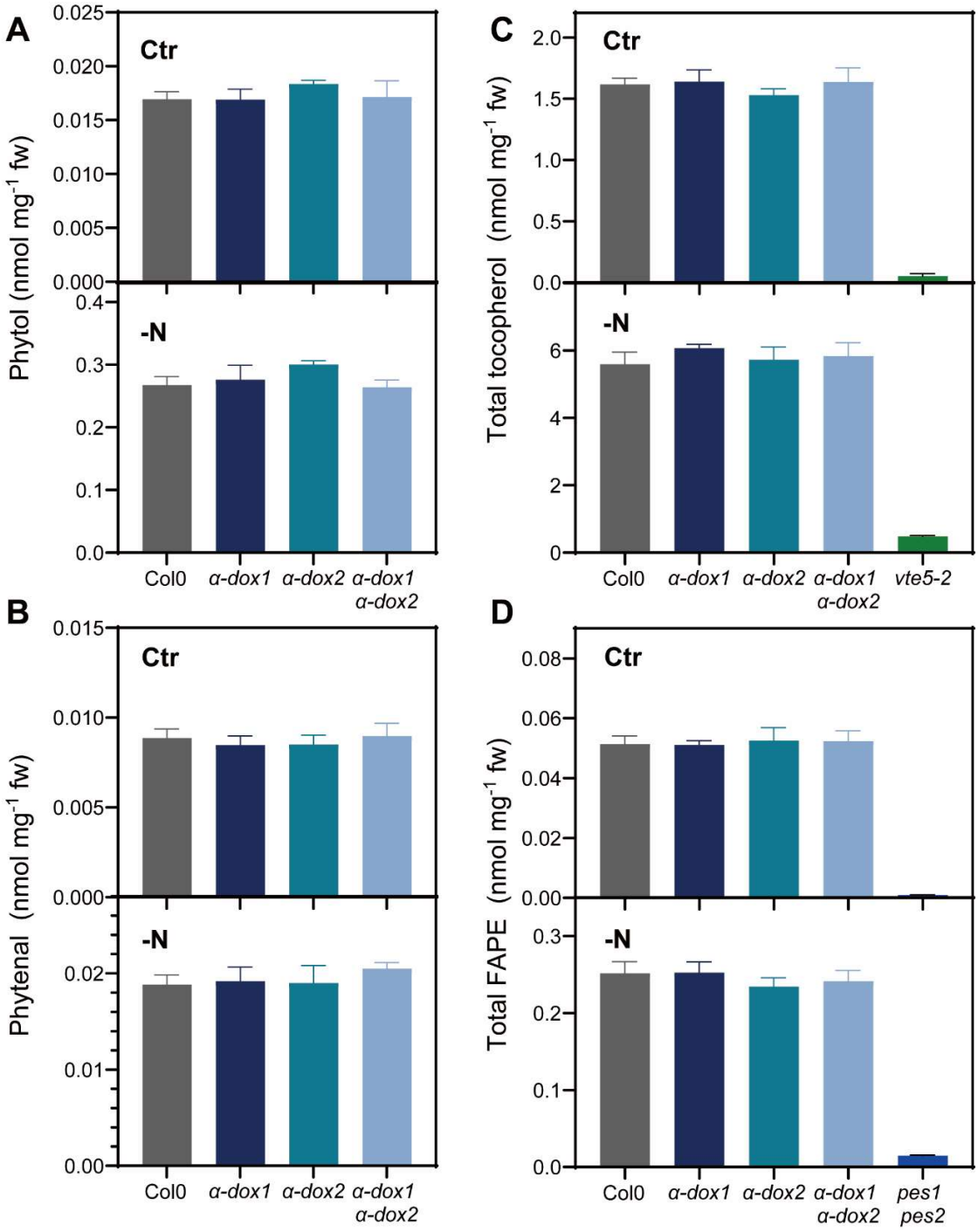

Figure. 3.38 Lipid compositions of *Arabidopsis α-dox1, α-dox2* and *α-dox1-α-dox2* mutant plants under nitrogen deprivation

Lipids were extracted from *Arabidopsis* wild type Col-0, *α-dox1*, *α-dox2* and *α-dox1-α-dox2* plants and quantified via mass spectrometry. Plants were grown on

synthetic medium without nitrogen (-N) or with nitrogen (Ctr). fw: fresh leaf weight. Mean±SD, n=3. Nonpolar lipids (free phytol, tocopherol and FAPE) were extracted and isolated via solid phase extraction.

A. Phytol was derivatized with MSTFA at 80 °C and quantified via GC-MS.

B. Aldehydes were extracted from leaf tissue, derivatized with methoxylamine HCl and quantified via GC-MS.

C. The different tocopherols forms (α, β, γ, δ) were separated and quantified by HPLC.

D. FAPE was quantified by direct infusion mass spectrometry on a Q-TOF instrument.

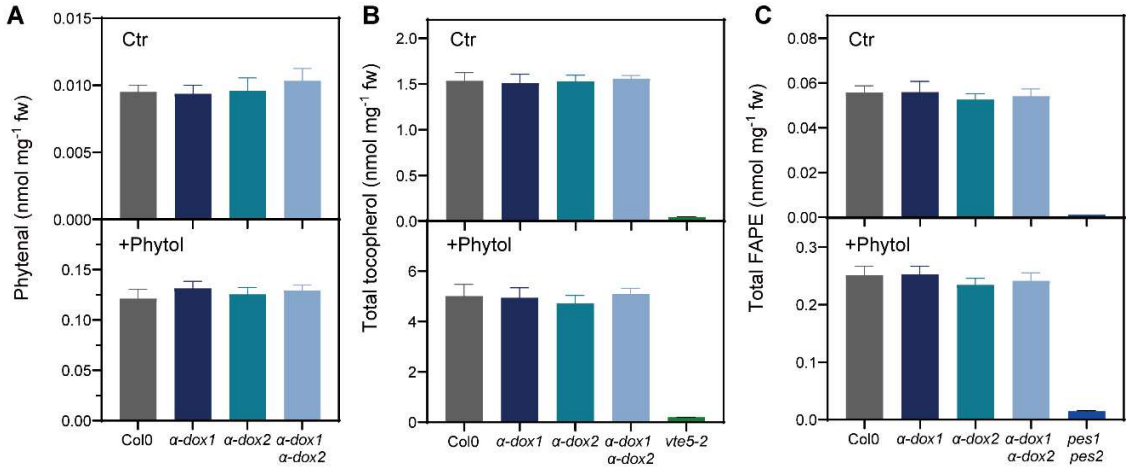

Figure. 3.39 Lipid compositions of *Arabidopsis α-dox1, α-dox2* and *α-dox1-α-dox2* after phytol supplementation

Lipids were extracted from *Arabidopsis* wild type Col-0, *α-dox1*, *α-dox2* and *α-dox1-α-dox2* and quantified via mass spectrometry. Plants were grown on MS medium containing 2 % sucrose and then transferred to Erlenmeyer flasks containing MES-KOH buffer (pH=6.5) and supplemented with phytol (0.1%, v:v) or without phytol (Ctr). fw: fresh leaf weight. Mean±SD, n=3. Nonpolar lipids (tocopherol and FAPE) were extracted and isolated via solid phase extraction.

A. Aldehydes were extracted from leaf tissue, derivatized with methoxylamine HCl and quantified via GC-MS. The internal standard (hexadecanal, 16:0 aldehyde) was spiked at the beginning of extraction.

B. Different forms of tocopherols (α, β, γ, δ) were separated and quantified by HPLC.

C. FAPE was quantified by direct infusion mass spectrometry on a Q-TOF instrument.

3.2.8 WSD6 Has *in vivo* Phytyl Ester Synthase Activity

Arabidopsis contains 11 genes belonging to the Acinetobacter-type wax ester synthase family, which are designated WSD1 to WSD11, respectively. *wsd1* showed reduced drought tolerance (Patwari, 2019). *wsd6* and *wsd7* grew similarly to WT, showing no wilting or chlorosis under control and drought conditions. Nevertheless, WSD6 and WSD7 expressed in Sf9 cells could use acyl-CoAs and alcohols to synthesize wax ester. Interestingly, WSD6 could use free phytol as alcohol donor to synthesize esters (Patwari, 2019). This result suggested that WSD6 might contribute to the synthesis of FAPE *in vivo*. To address this question, free phytol was supplemented to 3 weeks old *Arabidopsis* wild type Col-0 and *wsd1-2*, *wsd6-1*, *wsd6-2*, and *wsd7-2* mutant seedlings in MES-KOH buffer (pH=6.5). Afterwards, FAPEs were extracted, purified and quantitatively measured. Results showed that exogenous phytol led to the increase of FAPE content. It was notable that the increase of very long chain fatty acid (20:0 and 22:0) phytyl ester concentrations of *wsd6* mutants (*wsd6-1*, *wsd6-2*) was much lower than the wild type Col-0. Considering that plants synthesize very long chain fatty acids (20:0, 22:0) at the ER and that WSD6 also localizes to the ER, this result indicated that WSD6 contribute to the synthesis of FAPEs (Fig 3.40).

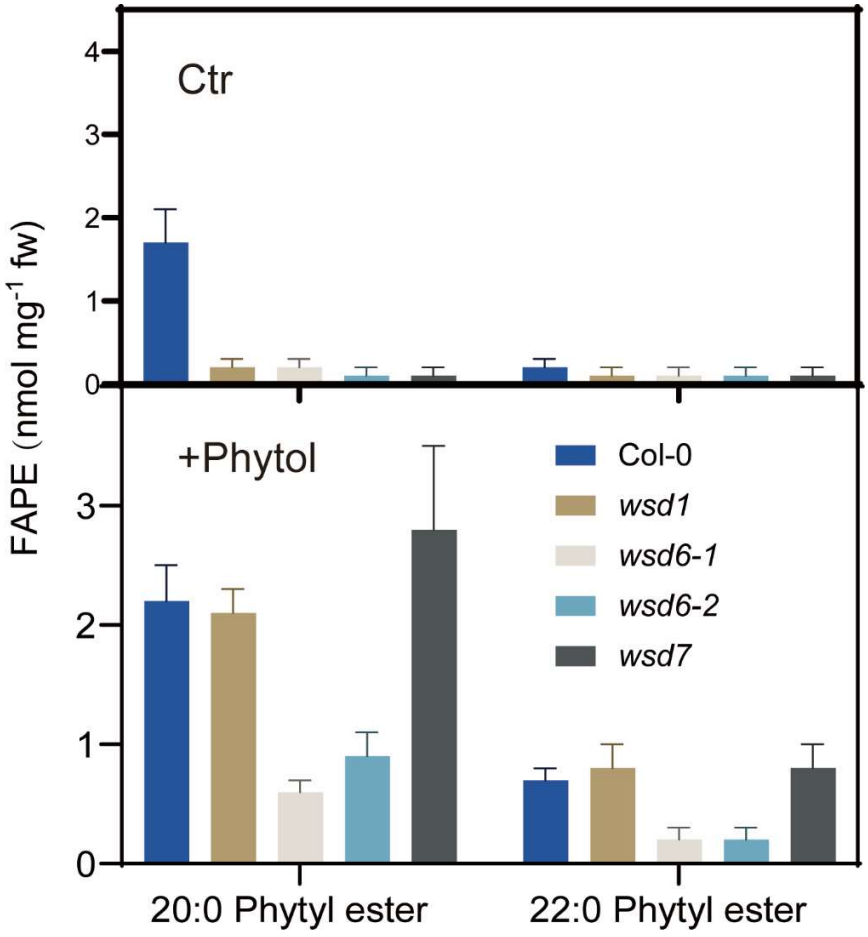

Figure 3.40 Very long chain fatty acid species of FAPEs from Col-0 and *wsd* mutant lines after phytol supplementation

Phytol was supplemented to *Arabidopsis* Col-0 and *wsd* mutant lines in MES-KOH buffer for 12 h. Afterwards, fatty acid phytyl esters (FAPEs) were extracted from leaves and measured via Q-TOF direct infusion. Very long chain fatty acid species were plotted. Mean±SD, n=3. Ctr: No phytol feeding, control.

4. DISCUSSION

Chlorophyll is the most abundant photosynthetic pigment in the biosphere. Chlorophyll is composed of a porphyrin ring head and a hydrophobic side chain, which are connected via an ester bond. During biotic or abiotic stress or during leaf senescence, metabolism shifts from anabolism to catabolism, and chlorophyll degradation is strongly increased (Guo et al., 2004). The first step of chlorophyll degradation is the removal of the Mg ion in the center of the porphyrin ring, releasing pheophytin a (Shimoda et al., 2016). Then the ester bond connecting the porphyrin ring and the phytol moiety is hydrolyzed by PPH (Schelbert et al., 2009), giving rise to pheophorbide a and free phytol. Free phytol can be incorporated into tocopherol (vom Dorp et al., 2015), fatty acid phytyl ester (Lippold et al., 2012) and phylloquinol (L. Wang et al., 2017). Besides PPH, plants harbor at least two other dephytylases, namely CLH and CLD, respectively. *Arabidopsis* CLH1 and CLH2 do not localize to the plastid but rather to the ER and tonoplast, and the *clh1 clh2* double mutant is still capable of chlorophyll breakdown, indicating that CLH may have physiological functions other than chlorophyll degradation or chlorophyll turnover, e.g. defense against insects (Schenk et al., 2007). *Arabidopsis* CLD1 is a thylakoid-localizing protein which has *in vivo* chlorophyll dephytylase activity (Lin et al., 2016). Based on the findings that 1) Massive chlorophyll degradation does not happen before the initiation of senescence and *CLD1* is highly expressed in green tissues; 2) The reduction or increase of CLD1 activity does not influence chlorophyll breakdown in dark-induced senescence leaves, Lin et al concluded that CLD1 is involved in chlorophyll turnover, rather than chlorophyll breakdown (Lin et al., 2016).

The degradation of phytol in plants is mostly elusive. I hypothesized that degradation of phytol in plants follows a similar pathway as in humans. In humans, HsPAHX and HsHPCL play vital roles in phytol degradation, because deletions of PAHX and/or HPCL may cause inheritable genetic diseases. The *Arabidopsis* genome contains one homolog each for PAHX and HPCL, which were designated AtPAHX and AtHPCL, respectively. AtPAHX was previously proven to harbor phytanoyl-CoA hydroxylase activity, while no research on AtHPCL has been

conducted so far (Araújo et al., 2011). The present research aims to study the phytol degradation pathway in the model plant *Arabidopsis* by 1) analyzing the subcellular localization and enzymatic function of AtHPCL; 2) characterizing *Arabidopsis* mutants potentially defective in phytol degradation or metabolism. Moreover, *S.cerevisiae* mutants which are defective in 2-hydroxy-acyl-CoA/fatty acid metabolism were characterized.

4.1 AtHPCL Is Localized to Peroxisomes

While many committed enzymes in phytol degradation of humans have been elucidated in depth, very little is known about phytol degradation in plants. In human cells, peroxisome-localized HsHPCL plays a vital role during phytol degradation. HsHPCL can convert 2-hydroxy-phytanoyl-CoA, which is the intermediate of phytol degradation, to pristanal. The activity of HsHPCL strongly depends on the presence of TPP (Casteels et al., 2007). The *Arabidopsis* genome contains one homolog of HsHPCL, which was designated AtHPCL. No enzymatic and localization studies about AtHPCL have been conducted before. AtHPCL has very high amino acid similarity with HsHPCL. Both AtHPCL and HsHPCL have a conserved thiamine pyrophosphate (TPP) binding domain. HsHPCL has a PTS1 type peroxisome target sequence at the C-terminus. AtHPCL does not have any known peroxisome target sequence, but the predicted subcellular localization of AtHPCL in the SUBA4 database is “peroxisome”. The data presented in this thesis show that AtHPCL is localized to the peroxisome, which suggests that AtHPCL may have a similar function as HsHPCL.

So far, two peroxisome targeting signal polypeptides were discovered, namely PTS1 and PTS2, respectively. PTS1 and PTS2 are quite different in terms of localizations with the protein sequence and import mechanisms.

The consensus sequence of PTS1 is [S/A][K/R][I/M/L] (Brocard & Hartig, 2006). PTS1 is localized at the extreme C-terminus and interacts with the soluble receptor protein Pex5 for targeting to peroxisomes (Dodt et al., 1995; Van der Leij et al., 1993).

The consensus sequence of PTS2 is [R/K][L/V/I/Q]XX[L/V/I/H/Q][L/S/G/A/K]-

X[H/Q][L/A/F] (X indicates any amino acid residues) (Petriv et al., 2004). PTS2 is mainly localized close to the N-terminus and interacts with the receptor Pex7 for targeting to peroxisomes (Braverman et al., 1997; Legakis & Terlecky, 2001; Motley et al., 1997).

Although most PTS2 are positioned near the N-terminus, internal PTS2 could also be found in some rare cases. For example, TLP is a bifunctional *Arabidopsis* protein with an N-terminal decarboxylase and a C-terminal hydrolase domain synthesized in three splice variants. The full-length TLP_{324} carries a PTS2 in the linker region between the two functional domains and is localized to peroxisomes. The His to Asp mutation in PTS2 of TLP_{324} led to localization to the cytosol and the nucleus (Reumann et al., 2007). Legakis et al expressed a recombinant protein, “the PTS2 reporter”, containing an internal PTS2 in CHO cells and human fibroblasts and found that the recombinant protein was localized to peroxisomes (Legakis & Terlecky, 2001).

Not all peroxisome proteins carry a PTS1 or PTS2. Therefore, alternative mechanisms of their import into peroxisomes must exist. To my knowledge, two possibilities exist, namely, piggy-back mechanism and the long-term sought, undefined PTS3.

Proteins without PTS could be imported into peroxisomes by binding to another protein containing PTS. This mechanism is referred to as piggy-back import (Glover et al., 1994). Piggy-back import of proteins into peroxisomes is found in plants (Kataya et al., 2015), mammals (Islinger et al., 2009) and yeasts (Effelsberg et al., 2015; Titorenko et al., 2002).

S.cerevisiae acyl-oxidase (AOx) is a peroxisomal protein and does not contain PTS1 or PTS targeting sequence. All the same, AOx is recognized by Pex5 and imported into peroxisomes, indicating that Pex5 is a bifunctional peroxisomal receptor (Skoneczny & Lazarow, 1998). These authors used random mutagenesis of the AOx-encoding gene to identify AOx amino acid residues that are essential for Pex5 recognition and peroxisomal import. Surprisingly, they found that the amino acid substitutions that affected AOx-Pex5 interaction and AOx import were scattered widely throughout in the AOx sequence. However, in the 3D model of the

AOx tertiary structure, they cluster together into two small regions., indicating that they form a signal patch that functions as novel peroxisomal targeting sequence, which provides some insights into the organization of PTS3. (Kempiński et al., 2020).

4.2 AtHPCL Has 2-Hydroxy-Acyl-CoA Lyase Activity

The presence of the conserved TPP binding sequence in AtHPCL indicates that TPP might be essential for AtHPCL activity. This scenario is also supported by the finding TPP is the necessary cofactor of HsHPCL. The AtHPCL protein was expressed in *E.coli*, Sf9 cells and wheat germ cell-free *in vitro* system and tested for the 2-hydroxy-acyl-CoA lyase activity via the substrate feeding experiment or *in vitro* enzyme assay. No significant activity difference could be found. However, the peroxisomal protein from *Arabidopsis* Col-0 wild type has very strong activity to convert 2-hydroxy-stearoyl-CoA (2-hydroxy-18:0-CoA) into heptadecanal (17:0 aldehyde). And this activity strongly depends on TPP. In contrast, the *hpcl-1* mutant completely lost this activity, while *hpcl-2* and *hpcl-3* still harbored residual activities. This result is in line with the expression analysis, indicating that *hpcl-1* is a null mutant, while *hpcl-2* and *hpcl-3* have residual expression.

4.3 Phytenal Is the Only Detectable Long Chain Aldehyde in Plants

Previous studies found that *Arabidopsis* could oxidize phytol released from chlorophyll in enzymatic and non-enzymatic reactions (P. Gutbrod et al., 2021), which is a powerful prove that plants have a phytol degradation pathway with phytenal as the intermediate. The attempt to identify two other aldehydes potentially involved in phytol degradation, namely phytanal and pristanal, failed. This indicates that phytanal is probably not an intermediate of phytol degradation, similar to the human pathway. To our knowledge, phytanal has never been found in humans and plants. But in ruminants, phytol is liberated from ingested plants and further oxidized to phytanic acid by the bacterial gut flora (Van Veldhoven, 2010). Pristanal, however, presumably is an intermediate of human and plant phytol degradation. However, it could also not be detected in our analysis.

Therefore, pristanal concentration may be very low, because it may be oxidized to pristanic acid quickly to avoid the detrimental effect on membranes.

4.4 AtHPCL and AtPAHX Are Involved in Phytol Degradation

Free phytol has detergent-like characteristics and is detrimental to the membrane stability. Plants have various ways to store or metabolize phytol. Free phytol can be esterified to form fatty acid phytyl esters (FAPE) (Wehler, 2017). Plants accumulate large amounts of FAPE under stress. But the increase of FAPE content is reversible, namely the FAPE content decreases when stress is removed. This indicates that FAPE is an intermediate sink for phytol storage. Phytol can also be incorporated into tocopherol and phylloquinol (L. Wang et al., 2017). Phytol kinase VTE5 (Valentin et al., 2006) and phytyl phosphate kinase VTE6 (vom Dorp et al., 2015) are essential for tocopherol synthesis. Tocopherol is a class of natural antioxidant, which humans must take up from the food (Rizvi et al., 2014). Finally, phytol can be degraded using a catabolic pathway which might be similar to the one found in humans. *Arabidopsis* was shown to have enzymatic and non-enzymatic activities to oxidize phytol (Gutbrod et al., 2021). The oxidation product, phytenal, was proven to be one intermediate product in phytol degradation. *Arabidopsis hpcl* and *pahx* mutants showed slower chlorosis compared with Col-0 under nitrogen deprivation and accumulated more phytol, phytenal, FAPE and tocopherol. Also, in the phytol supplementation assay, *hpcl* and *pahx* had higher phytenal, FAPE and tocopherol contents. Taken together, these results demonstrate that AtHPCL and AtPAHX are involved in phytol degradation.

4.5 Complementation of the *S.cerevisiae* Mutants Δ*pxp1* and Δ*mpo1* with AtHPCL

The homolog of AtHPCL in *S.cerevisiae* was designated ScPXP1. ScPXP1 has a C-terminal peroxisome target sequence and is localized to peroxisomes. The Δ*pxp1* mutant has a slightly impaired growth on oleate medium, confirming that ScPXP1 has a function in peroxisomal metabolism (Nötzel et al., 2016). In the growth assay, I found that the growth rate of Δ*pxp1* was impaired compared with

WT (wild type) on the synthetic medium lacking uracil. The finding that this severe growth impairment can be almost fully complemented by the introduction of AtHPCL into Δ*pxp1* shows that AtHPCL and ScPXP1 share very similar functions. Another *S.cerevisiae* gene, MPO1, was proven to contribute to most of 2-hydroxy-acyl-CoA/fatty acid decarboxylase activity (Kondo et al., 2014; Seki et al., 2019). However, the deletion of MPO1 in *S.cerevisiae* did not result in visible phenotypes. Therefore, AtHPCL was introduced into the *S.cerevisiae* mutant Δ*mpo1* and the expression of AtHPCL confirmed by SDS-PAGE. 2-Hydroxy-palmitic acid and thiamine pyrophosphate (TPP) were supplemented to *S.cerevisiae* cultures and pentadecanoic fatty acid and phosphatidylcholines with odd numbers of carbons in the acyl chains were quantified. The Δ*mpo1*: ev strain had lower levels of 15:0 acid and 31:x phosphatidylcholines. But the introduction of AtHPCL could rescue this impairment. Also, when TPP was omitted from the supplementation experiment, the levels of pentadecanoic acid in Δ*mpo1*:ev and Δ*mpo1*:AtHPCL were almost the same. Taken together, these results show that AtHPCL has 2-hydroxyl-acyl-CoA lyase activity *in vivo,* and this activity is strongly dependent on TPP.

4.6 MPO1 and PXP1 Expression

ScMPO1 is involved in the α-oxidation of 2-hydroxy-palmitic acid in phytosphingosine (PHS) metabolism (Kondo et al., 2014; Seki et al., 2019). Phytosphingosine (PHS) is the major long-chain base component of sphingolipids in *S.cerevisiae*.

Deletion of MPO1 in *S.cerevisiae* led to strong decrease of contents of 15:0 fatty acid and 31:x phosphatidylcholine. However, Δ*mpo1*:ev still harbors residue capacity to produce 15:0 fatty acid and 31:x phosphatidylcholine. This indicates that *S.cerevisiae* has a minor alternative α-oxidation pathway. PXP1 is a homolog of HPCL and presumably has the have capacity to convert 2-hydroxy-palmitic acid into pentadecanoic acid. The content of 31:0 phosphatidylcholine in Δ*pxp1*:ev is lower than in wt:ev in the 2-hydroxy-palmitic acid feeding experiment. Also, the contents of 15:0 fatty acid and 31:0 PC in Δ*pxp1*:AtHPCL were higher than

Δ*pxp1*:ev in the 2-hydroxy-palmitic acid feeding experiment. These results indicate that PXP1 has 2-hydroxy-fatty-acid decarboxylase activity. Further experiments are needed to prove the hypothesis that PXP1 can complement the function of MPO1 in PHS metabolism. Because PXP1 and MPO1 are localized to different organelles, namely, the former was proved to localize to peroxisomes (Nötzel et al., 2016), while the latter was at the ER (Mon et al., 2020). Therefore, the relationship of MPO1 and PXP1 still remains exclusive.

4.7 *Arabidopsis* α-Dioxygenases Are Not Involved in Phytol Degradation

Alternatively, *Arabidopsis* has another hypothetical phytol degradation pathway which does not involve AtPAHX and AtHPCL. AtαDOX1 and AtαDOX2 were proven to be able to convert long chain saturated or unsaturated fatty acids into 2-hydroperoxy-fatty acids. The 2-hydroperoxy-fatty acid can be converted to 2-hydroxy-fatty acid or (n-1) fatty aldehyde (Bannenberg et al., 2009; Sanz et al., 1998; Shimada et al., 2014). But it was unknown whether AtαDOXx1 and AtαDOX2 could metabolize phytanic acid and are involved in phytol degradation. The attempt to identify phytanic acid in the *Arabidopsis* mutants *αdox1*, *αdox2* and *αdox1αdox2* during nitrogen deprivation failed. Also, the lipid composition (phytol, phytenal, FAPE and tocopherol) of Col-0, *αdox1*, *αdox2* and *αdox1αdox2* were very similar during nitrogen deprivation and phytol supplementation. This indicates that AtαDOXx1 and AtαDOX2 are not involved in phytol degradation.

The expression of At*αdox1* and At*αdox2* is upregulated during senescence. The expression of Atα*DOX1* can be induced by microbial infection, while At*α*dox2 expression does not change upon infection (Bannenberg et al., 2009; Sanz et al., 1998; T. L. Shimada et al., 2014). It is noteworthy that AtαDOX1 is localized to leaf oil bodies and can produce a phytoalexin in response to microbial infection. But the deletion of AtαDOX2 cannot produce visible phenotype changes. Taken together, although the physiological function of AtαDOX2 remains still elusive, it may be concluded that *Arabidopsis* α-dioxygenases are not involved in phytol degradation.

4.8 WSD6 Has *in vivo* Long Chain Fatty Acid Phytyl Ester Synthase Activity.

The cuticular wax layer protects the plants against adverse water-deficit or other environmental stresses (Kunst & Samuels, 2009). Wax esters, one class of cuticular waxes, are the products of the acyl reduction pathway of cuticular wax biosynthesis and account for 1-5% of the total leaf and stem cuticular waxes in many plants. WSD6 belongs to the *Arabidopsis* wax ester synthase family. Heterologously expressed WSD6 in Sf9 cells could synthesize wax esters with 16:0 alcohol and long chain acyl-CoA (16:0, 18:0 and 20:0) (Patwari, 2019). But the *wsd6-1* and *wsd6-2* mutants showed no significant difference compared to Col-0 in terms of cuticular wax ester composition under control or drought condition (Patwari, 2019). Interestingly, in the *in vitro* assay, WSD6 could synthesize 16:0-phytyl ester from palmitoyl-CoA and phytol (Patwari, 2019). This indicates that WSD6 may have different functions other than wax ester synthase. Here, the author performed phytol supplementation experiment with *Arabidopsis* WT and mutants and measured FAPE contents. The results showed that *wsd6-1* and *wsd6-2* synthesize much less 20:0 and 22:0-phytyl esters compared to Col-0. This can be explained by the fact that 1) plants synthesize very long chain fatty acids (number of carbon atoms ≥20) at the ER; 2) the wax ester synthases, including WSD6, are localized to ER. Taken together, WSD6 has very long chain fatty acid phytyl ester synthase activity, which helps to store phytol under stress or senescence. FAPE was previous believed to be mainly stored in plastoglobules of chloroplasts (Gaude et al., 2007). Results presented here show that FAPE may be also synthesized in other organelles, such as ER. It is tempting to speculate that after synthesis, the FAPE with very long chain fatty acids might then be stored in the lipid droplets in the cytosol, similar to triacylglycerol and steryl esters.

4.9 Alternative Phytol Degradation Pathway(s)

4.9.1 ω-Oxidation

ω Oxidation widely exists in animals, yeast and plants (Miura, 2013). During ω oxidation, the methyl terminus of the fatty acid is hydroxylated, giving rise to an ω-1 hydroxy-fatty acid. Then the ω-1 hydroxy-fatty acid is oxidized to a dicarboxylic

acid. The dicarboxylic acid can be degraded via β oxidation from 2 directions, producing acetyl-CoA and succinyl-CoA. In plants, ω-1 hydroxy-fatty acids have many important functions, including wax ester synthesis and defense. It remains unclear whether phytol can be degraded via ω oxidation.

4.9.2 MPO1 Orthologues

Arabidopsis has two MPO1 orthologues. Both of them belong to the domain of unknown function (DUF) protein family. The mutant of one orthologue, *mhp1-1*, was hypersensitive to salt/osmotic stress and ABA (Zheng et al., 2021). MHP1 is localized at the ER, similar to MPO1. But the specific function of MHP1 is unknown. It is possible that MHP1 could participate in phytol degradation.

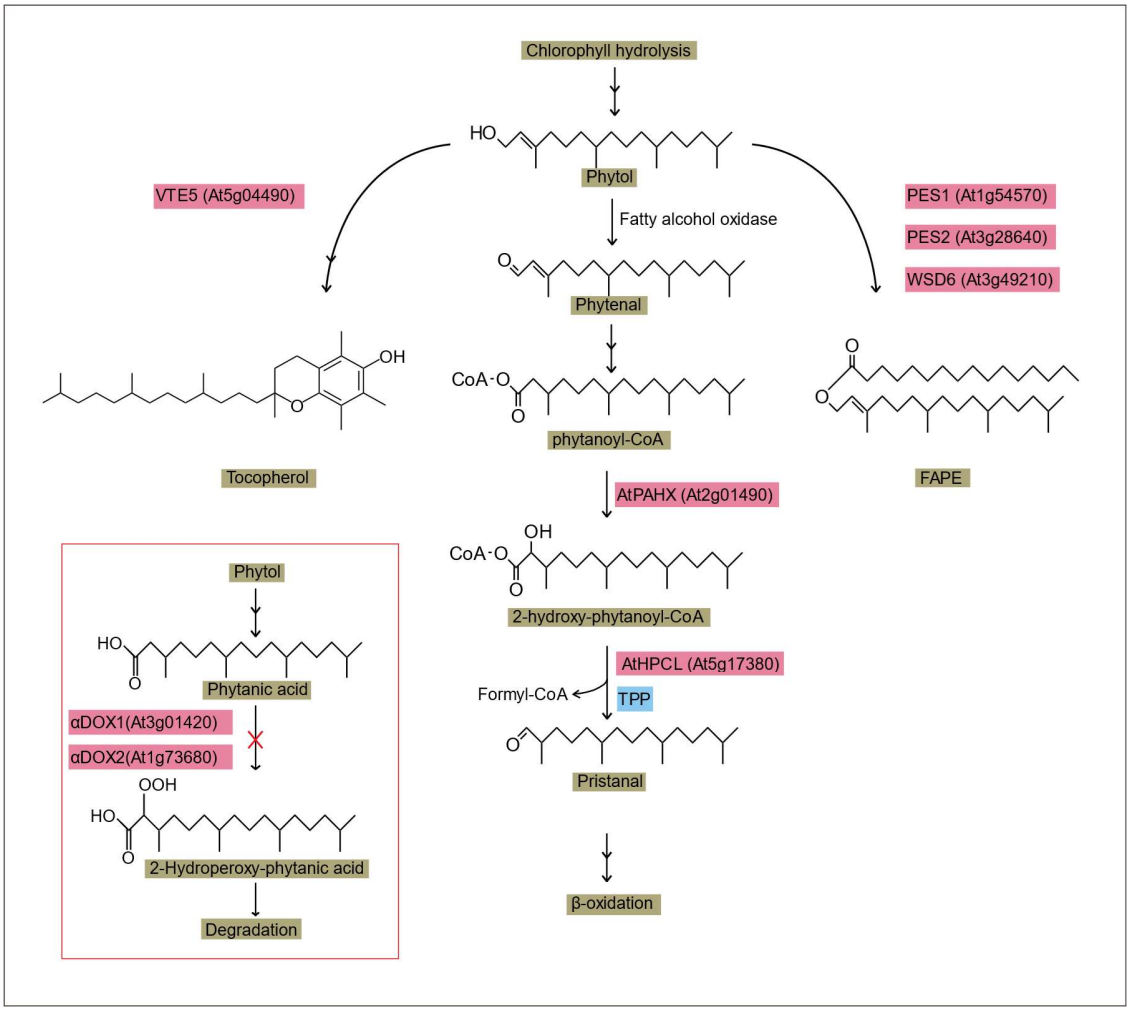

Figure. 4.1 Summarized phytol catabolism pathway in plants

Phytol released from chlorophyll during stress or senescence can enter three metabolism pathways: 1) the FAPE synthesis pathway, which involves phytyl ester synthase PES1, PES2 and WSD6; 2) the tocopherol synthesis pathway, which involves phytol kinase VTE5; 3) degradation pathway, which involves PAHX and HPCL.

5. SUMMARY

This research provides first insights into the pathway of phytol degradation in plants. Phytol belongs to the group of terpenoids (also known as isoprenoids or terpenes), which encompasses the largest class of natural products in plants. As the side chain of chlorophyll, phytol is considered to be the most abundant isoprenoid molecule in the biosphere. Although the phytol degradation pathway has been elucidated in humans, the degradation of phytol in plants still remains elusive.

Based on amino acid sequence similarities with human homologs, two proteins, namely AtHPCL (2-hydroxy-phytanoyl-CoA lyase) and AtPAHX (phytanoyl-CoA α-hydroxylase), were identified as candidate enzymes presumably involved in phytol degradation in the model plant *Arabidopsis thaliana*. Transient expression of AtHPCL in fusion with eGFP (enhanced green fluorescence protein) in *Nicotiana benthamiana* leaves revealed that AtHPCL was localized to peroxisomes. While the AtHPCL protein, heterologously expressed in *E.coli*, Sf9 insect cells or in the wheat germ cell-free *in vitro* system, did not show enzymatic activity, peroxisomal protein from *Arabidopsis* wild type (WT) leaves was shown to harbor 2-hydroxy-stearoyl-CoA lyase activity. This activity was lost in the *Arabidopsis* mutant lines *hpcl-1*, *hpcl-2* and *hpcl-3*. Introduction of AtHPCL into the *S.cerevisiae* mutant Δ*pxp1* deficient in hydroxy-acyl-CoA lyase activity, rescued the impaired growth. Moreover, expression of AtHPCL in the yeast Δ*mpo1* mutant deficient in hydroxy-fatty acid lyase activity, complemented the lower level of 15:0 fatty acid and 31:x phosphatidylcholines (number of carbons in the fatty acids : number of double bonds). Taken together, these results show that AtHPCL has 2-hydroxy-acyl-CoA lyase activity.

The *Arabidopsis* mutants *pahx* and *hpcl* showed delayed chlorosis compared to WT. Moreover, the contents of phytol-related lipids (chlorophyll, phytol, fatty acid phytyl esters and tocopherol) in *pahx* and *hpcl* were higher than in WT, indicating that AtPAHX and AtHPCL are involved in phytol degradation. The *pahx* and *hpcl* mutants have no visible phenotypes compared to WT, suggesting that under optimal growth conditions, only a small amount of phytol enters the

AtHPCL/AtPAHX-dependent degradation pathway. Plants have alternative pathway(s) to metabolize phytol. These pathways include the transient deposition of phytol in the form of fatty acid phytyl esters or the synthesis of tocopherol.

Alternatively, we tested the hypothesis whether *Arabidopsis* might have another, AtPAHX/AtHPCL-independent, phytol degradation pathway. The two α-dioxygenases αDOX1 and αDOX2 were previously shown to convert long chain fatty acids into 2-hydroperoxy-fatty acids. The 2-hydroperoxy-fatty acids can be converted to 2-hydroxy-fatty acids or (n-1) fatty aldehydes. But it was unknown whether αDOX1 and αDOX2 could also metabolize phytanic acid and thus be involved in phytol degradation. Phytanic acid was absent from the *Arabidopsis* mutants *αdox1*, *αdox2* and *αdox1 αdox2* pants grown under nitrogen deprivation or phytol supplementation. The progression of chlorosis of *αdox1*, *αdox2* and *αdox1 αdox2* was very similar to WT Col-0. Also, the lipid composition (phytol, phytenal, fatty acid phytyl esters, tocopherol) of Col-0, *αdox1*, *αdox2* and *αdox1-αdox2* were very similar. This indicates that αDOXx1 and αDOX2 are not involved in phytol degradation.

Taken together, these results demonstrate that phytol in *Arabidopsis* is degraded via the AtPAHX/AtHPCL pathway, similar to humans, but that αDOX1 and αDOX2 are not involved in phytol catabolism.

6. REFERENCE

Adam, P., Hecht, S., Eisenreich, W., Kaiser, J., Gra, T., Bacher, A., & Rohdich, F. (2002). *Biosynthesis of terpenes : Studies on 1-hydroxy-2-methyl-2- (E) - butenyl 4-diphosphate reductase*. *26*, 1–6.

Araújo, W. L., Ishizaki, K., Nunes-Nesi, A., Tohge, T., Larson, T. R., Krahnert, I., Balbo, I., Witt, S., Dörmann, P., Graham, I. A., Leaver, C. J., & Fernie, A. R. (2011). Analysis of a range of catabolic mutants provides evidence that phytanoyl-coenzyme a does not act as a substrate of the electron-transfer flavoprotein/ electron-transfer flavoprotein: Ubiquinone oxidoreductase complex in arabidopsis during dark-induced se. *Plant Physiology*, *157*(1), 55–69. https://doi.org/10.1104/pp.111.182188

Bannenberg, G., Martínez, M., Rodrígue, M. J., López, M. A., de León, I. P., Hamberg, M., & Castresana, C. (2009). Functional analysis of α-DOX2, an active α-dioxygenase critical for normal development in tomato plants. *Plant Physiology*, *151*(3), 1421–1432. https://doi.org/10.1104/pp.109.145094

Beisel, K. G., Jahnke, S., Hofmann, D., Köppchen, S., Schurr, U., & Matsubara, S. (2010). Continuous turnover of carotenes and chlorophyll a in mature leaves of Arabidopsis revealed by 14CO2 pulse-chase labeling. *Plant Physiology*, *152*(4), 2188–2199. https://doi.org/10.1104/pp.109.151647

Bergmüller, E., Porfirova, S., & Dörmann, P. (2003). Characterization of an Arabidopsis mutant deficient in γ-tocopherol methyltransferase. *Plant Molecular Biology*, *52*(6), 1181–1190. https://doi.org/10.1023/B:PLAN.0000004307.62398.91

Braverman, N., Steel, G., Obie, C., Moser, A., Moser, H., Gould, S. J., & Valle, D. (1997). Human PEX7 encodes the peroxisomal PTS2 receptor and is responsible for rhizomelic chondrodysplasia punctata. *Nature Genetics*, *15*(4), 369–376. https://doi.org/10.1038/ng0497-369

Brocard, C., & Hartig, A. (2006). Peroxisome targeting signal 1: Is it really a simple tripeptide? *Biochimica et Biophysica Acta*, *1763*(12), 1565–1573. https://doi.org/10.1016/j.bbamcr.2006.08.022

Cahoon, E. B., Hall, S. E., Ripp, K. G., Ganzke, T. S., Hitz, W. D., & Coughlan, S. J. (2003). Metabolic redesign of vitamin E biosynthesis in plants for tocotrienol production and increased antioxidant content. *Nature Biotechnology*, *21*(9), 1082–1087. https://doi.org/10.1038/nbt853

Carrie, C., Murcha, M. W., Millar, A. H., Smith, S. M., & Whelan, J. (2007). Nine 3-ketoacyl-CoA thiolases (KATs) and acetoacetyl-CoA thiolases (ACATs) encoded by five genes in Arabidopsis thaliana are targeted either to peroxisomes or cytosol but not to mitochondria. *Plant Molecular Biology*, *63*(1), 97–108. https://doi.org/10.1007/s11103-006-9075-1

Casteels, M., Sniekers, M., Fraccascia, P., Mannaerts, G. P., & Van Veldhoven, P. P. (2007). The role of 2-hydroxyacyl-CoA lyase, a thiamin pyrophosphate-dependent enzyme, in the peroxisomal metabolism of 3-methyl-branched fatty acids and 2-hydroxy straight-chain fatty acids. *Biochemical Society Transactions*, *35*(5), 876–880. https://doi.org/10.1042/BST0350876

Cheng, Z., Sattler, S., Maeda, H., Sakuragi, Y., Bryant, D. A., & DellaPenna, D. (2003). Highly divergent methyltransferases catalyze a conserved reaction in

tocopherol and plastoquinone synthesis in cyanobacteria and photosynthetic eukaryotes. *Plant Cell*, *15*(10), 2343–2356. https://doi.org/10.1105/tpc.013656

Chowdhary, G., Kataya, A. R. A., Lingner, T., & Reumann, S. (2012). Non-canonical peroxisome targeting signals: identification of novel PTS1 tripeptides and characterization of enhancer elements by computational permutation analysis. *BMC Plant Biology*, *12*, 1–14. https://doi.org/10.1186/1471-2229-12-142

Closa, M., Vranová, E., Bortolotti, C., Bigler, L., Arró, M., Ferrer, A., & Gruissem, W. (2010). The Arabidopsis thaliana FPP synthase isozymes have overlapping and specific functions in isoprenoid biosynthesis, and complete loss of FPP synthase activity causes early developmental arrest. *Plant Journal*, *63*(3), 512–525. https://doi.org/10.1111/j.1365-313X.2010.04253.x

Dodt, G., Braverman, N., Wong, C., Moser, A., Moser, H. W., Watkins, P., Valle, D., & Gould, S. J. (1995). Mutations in the PTS1 receptor gene, PXR1, define complementation group 2 of the peroxisome biogenesis disorders. *Nature Genetics*, *9*(2), 115–125. https://doi.org/10.1038/ng0295-115

Dörmann, P. (2007). Functional diversity of tocochromanols in plants. *Planta*, *225*(2), 269–276. https://doi.org/10.1007/s00425-006-0438-2

Effelsberg, D., Cruz-Zaragoza, L. D., Tonillo, J., Schliebs, W., & Erdmann, R. (2015). Role of Pex21p for piggyback import of Gpd1p and Pnc1p into peroxisomes of Saccharomyces cerevisiae. *Journal of Biological Chemistry*, *290*(42), 25333–25342. https://doi.org/10.1074/jbc.M115.653451

Endo, Y., & Sawasaki, T. (2003). High-throughput, genome-scale protein production method based on the wheat germ cell-free expression system. *Biotechnology Advances*, *21*(8), 695–713. https://doi.org/https://doi.org/10.1016/S0734-9750(03)00105-8

Estevez, J. M., Cantero, A., Romero, C., Kawaide, H., Jimenez, L. F., Kuzuyama, T., Seto, H., Kamiya, Y., & Leon, P. (2000). Analysis of the expression of CLA1, a gene that encodes the 1-deoxyxylulose 5-phosphate synthase of the 2-C-methyl-D-erythritol-4-phosphate pathway in arabidopsis. *Plant Physiology*, *124*(1), 95–103. https://doi.org/10.1104/pp.124.1.95

Falter, C., Thu, N. B. A., Pokhrel, S., & Reumann, S. (2019). New guidelines for fluorophore application in peroxisome targeting analyses in transient plant expression systems. *Journal of Integrative Plant Biology*, *61*(7), 884–899. https://doi.org/10.1111/jipb.12791

Fatihi, A., Latimer, S., Schmollinger, S., Block, A., Dussault, P. H., Vermaas, W. F. J., Merchant, S. S., & Basset, G. J. (2015). A dedicated type II NADPH dehydrogenase performs the penultimate step in the biosynthesis of vitamin K1 in Synechocystis and Arabidopsis. *Plant Cell*, *27*(6), 1730–1741. https://doi.org/10.1105/tpc.15.00103

Felsenstein, J. (1985). Confidence Limits on Phylogenies: an Approach Using the Bootstrap. *Evolution*, *39*(4), 783–791. https://doi.org/10.1111/j.1558-5646.1985.tb00420.x

Ferdinandusse, S., Denis, S., Ijlst, L., Dacremont, G., Waterham, H. R., & Wanders, R. J. A. (2000). Subcellular localization and physiological role of α-

methylacyl-CoA racemase. *Journal of Lipid Research*, *41*(11), 1890–1896. https://doi.org/10.1016/s0022-2275(20)31983-0

Foulon, V., Antonenkov, V. D., Croes, K., Waelkens, E., Mannaerts, G. P., Van Veldhoven, P. P., & Casteels, M. (1999). Purification, molecular cloning, and expression of 2-hydroxyphytanoyl-CoA lyase, a peroxisomal thiamine pyrophosphate-dependent enzyme that catalyzes the carbon-carbon bond cleavage during α-oxidation of 3-methyl-branched fatty acids. *Proceedings of the National Academy of Sciences of the United States of America*, *96*(18), 10039–10044. https://doi.org/10.1073/pnas.96.18.10039

Gasulla, F., Vom Dorp, K., Dombrink, I., Zähringer, U., Gisch, N., Dörmann, P., & Bartels, D. (2013). The role of lipid metabolism in the acquisition of desiccation tolerance in Craterostigma plantagineum: A comparative approach. *Plant Journal*, *75*(5), 726–741. https://doi.org/10.1111/tpj.12241

Gaude, N., Bréhélin, C., Tischendorf, G., Kessler, F., & Dörmann, P. (2007). Nitrogen deficiency in Arabidopsis affects galactolipid composition and gene expression and results in accumulation of fatty acid phytyl esters. *Plant Journal*, *49*(4), 729–739. https://doi.org/10.1111/j.1365-313X.2006.02992.x

Gil, G., Faust, J. R., Chin, D. J., Goldstein, J. L., & Brown, M. S. (1985). Membrane-bound domain of HMG CoA reductase is required for sterol-enhanced degradation of the enzyme. *Cell*, *41*(1), 249–258. https://doi.org/https://doi.org/10.1016/0092-8674(85)90078-9

Giorgi, M. De, Jarrett, K. E., Burton, J. C., Doerfler, A. M., Hurley, A., Li, A., Hsu, R. H., Furgurson, M., Patel, K. R., Han, J., Borchers, C. H., & Lagor, W. R. (2020). Depletion of essential isoprenoids and ER stress induction following acute liver-specific deletion of HMG-CoA reductase. *Journal Lipid Research*, *61*(12), 1675–1686. https://doi.org/10.1194/jlr.RA120001006

Gloerich, J., Ruiter, J. P. N., Van Den Brink, D. M., Ofman, R., Ferdinandusse, S., & Wanders, R. J. A. (2006). Peroxisomal trans-2-enoyl-CoA reductase is involved in phytol degradation. *FEBS Letters*, *580*(8), 2092–2096. https://doi.org/10.1016/j.febslet.2006.03.011

Glover, J. R., Andrews, D. W., & Rachubinski, R. A. (1994). Saccharomyces cerevisiae peroxisomal thiolase is imported as a dimer. *Proceedings of the National Academy of Sciences of the United States of America*, *91*(22), 10541–10545. https://doi.org/10.1073/pnas.91.22.10541

Grob, E. C., & Csupor, L. (1967). Zur Kenntnis der Blattlipide vonAcer platanoides L. während der herbstlichen Vergilbung. *Experientia*, *23*(12), 1004–1005. https://doi.org/10.1007/BF02136411

Gross, J., Won, K. C., Lezhneva, L., Falk, J., Krupinska, K., Shinozaki, K., Seki, M., Herrmann, R. G., & Meurer, J. (2006). A plant locus essential for phylloquinone (vitamin K1) biosynthesis originated from a fusion of four eubacterial genes. *Journal of Biological Chemistry*, *281*(25), 17189–17196. https://doi.org/10.1074/jbc.M601754200

Guo, Y., Cai, Z., & Gan, S. (2004). Transcriptome of Arabidopsis leaf senescence. *Plant, Cell and Environment*, *27*(5), 521–549. https://doi.org/10.1111/j.1365-3040.2003.01158.x

Gutbrod, K., Romer, J., & Dörmann, P. (2019). Phytol metabolism in plants.

Progress in Lipid Research, *74*, 1–17. https://doi.org/10.1016/j.plipres.2019.01.002

Gutbrod, P., Yang, W., Grujicic, G. V., Peisker, H., Gutbrod, K., Du, L. F., & Dörmann, P. (2021). Phytol derived from chlorophyll hydrolysis in plants is metabolized via phytenal. *Journal of Biological Chemistry*, *296*, 100530. https://doi.org/10.1016/j.jbc.2021.100530

Hamberg, M., Sanz, A., & Castresana, C. (1999). α-Oxidation of fatty acids in higher plants. Identification of a pathogen-inducible oxygenase (PIOX) as an α-dioxygenase and biosynthesis of 2-hydroperoxylinolenic acid. *Journal of Biological Chemistry*, *274*(35), 24503–24513. https://doi.org/10.1074/jbc.274.35.24503

Hooper, C. M., Castleden, I. R., Tanz, S. K., Aryamanesh, N., & Millar, A. H. (2017). SUBA4: The interactive data analysis centre for Arabidopsis subcellular protein locations. *Nucleic Acids Research*, *45*(D1), D1064–D1074. https://doi.org/10.1093/nar/gkw1041

Hooper, C. M., Tanz, S. K., Castleden, I. R., Vacher, M. A., Small, I. D., & Millar, A. H. (2014). SUBAcon: A consensus algorithm for unifying the subcellular localization data of the Arabidopsis proteome. *Bioinformatics*, *30*(23), 3356–3364. https://doi.org/10.1093/bioinformatics/btu550

Hsieh, M.-H., & Goodman, H. M. (2006). Functional evidence for the involvement of Arabidopsis IspF homolog in the nonmevalonate pathway of plastid isoprenoid biosynthesis. *Planta*, *223*(4), 779–784. https://doi.org/10.1007/s00425-005-0140-9

Islinger, M., Li, K. W., Seitz, J., Völkl, A., & Lüers, G. H. (2009). Hitchhiking of Cu/Zn superoxide dismutase to peroxisomes - Evidence for a natural piggyback import mechanism in mammals. *Traffic*, *10*(11), 1711–1721. https://doi.org/10.1111/j.1600-0854.2009.00966.x

Jansen, G. A., Verhoeven, N. M., Denis, S., Romeijn, G. J., Jakobs, C., Ten Brink, H. J., & Wanders, R. J. A. (1999). Phytanic acid α-oxidation: identification of 2-hydroxyphytanoyl-CoA lyase in rat liver and its localisation in peroxisomes. *Biochimica et Biophysica Acta*, *1440*(2–3), 176–182. https://doi.org/10.1016/S1388-1981(99)00126-2

Jenkins, B., De Schryver, E., Van Veldhoven, P. P., & Koulman, A. (2017). Peroxisomal 2-hydroxyacyl-coa lyase is involved in endogenous biosynthesis of heptadecanoic acid. *Molecules*, *22*(10), 10–15. https://doi.org/10.3390/molecules22101718

Kataya, A. R. A., Heidari, B., Hagen, L., Kommedal, R., Slupphaug, G., & Lillo, C. (2015). Protein phosphatase 2A holoenzyme is targeted to peroxisomes by piggybacking and positively affects peroxisomal beta-oxidation. *Plant Physiology*, *167*(2), 493–506. https://doi.org/10.1104/pp.114.254409

Keller, Y., Bouvier, F., D'Harlingue, A., & Camara, B. (1998). Metabolic compartmentation of plastid prenyllipid biosynthesis - Evidence for the involvement of a multifunctional geranylgeranyl reductase. *European Journal of Biochemistry*, *251*(1–2), 413–417. https://doi.org/10.1046/j.1432-1327.1998.2510413.x

Kempiński, B., Chełstowska, A., Poznański, J., Król, K., Rymer, Ł., Frydzińska,

Z., Girzalsky, W., Skoneczna, A., Erdmann, R., & Skoneczny, M. (2020). The Peroxisomal Targeting Signal 3 (PTS3) of the Budding Yeast Acyl-CoA Oxidase Is a Signal Patch. In *Frontiers in Cell and Developmental Biology* (Vol. 8). https://doi.org/10.3389/fcell.2020.00198

Kondo, N., Ohno, Y., Yamagata, M., Obara, T., Seki, N., Kitamura, T., Naganuma, T., & Kihara, A. (2014). Identification of the phytosphingosine metabolic pathway leading to odd-numbered fatty acids. *Nature Communications*, *5*. https://doi.org/10.1038/ncomms6338

Kunst, L., & Samuels, L. (2009). Plant cuticles shine: advances in wax biosynthesis and export. *Current Opinion in Plant Biology*, *12*(6), 721–727. https://doi.org/10.1016/j.pbi.2009.09.009

Kusaba, M., Ito, H., Morita, R., Iida, S., Sato, Y., Fujimoto, M., Kawasaki, S., Tanaka, R., Hirochika, H., Nishimura, M., & Tanaka, A. (2007). Rice non-yellow coloring1 is involved in light-harvesting complex II and grana degradation during leaf senescence. *Plant Cell*, *19*(4), 1362–1375. https://doi.org/10.1105/tpc.106.042911

Kutschera, U., & Niklas, K. J. (2005). Endosymbiosis, cell evolution, and speciation. *Theory in Biosciences*, *124*(1), 1–24. https://doi.org/10.1016/j.thbio.2005.04.001

Learned, R. M., & Fink, G. R. (1989). 3-Hydroxy-3-methylglutaryl-coenzyme A reductase from Arabidopsis thaliana is structurally distinct from the yeast and animal enzymes. *Proceedings of the National Academy of Sciences of the United States of America*, *86*(8), 2779–2783. https://doi.org/10.1073/pnas.86.8.2779

Legakis, J. E., & Terlecky, S. R. (2001). PTS2 protein import into mammalian peroxisomes. *Traffic*, *2*(4), 252–260. https://doi.org/10.1034/j.1600-0854.2001.90165.x

Lin, Y. P., Lee, T. Y., Tanaka, A., & Charng, Y. Y. (2014). Analysis of an Arabidopsis heat-sensitive mutant reveals that chlorophyll synthase is involved in reutilization of chlorophyllide during chlorophyll turnover. *Plant Journal*, *80*(1), 14–26. https://doi.org/10.1111/tpj.12611

Lin, Y. P., Wu, M. C., & Charng, Y. Y. (2016). Identification of a chlorophyll dephytylase involved in chlorophyll turnover in Arabidopsis. *Plant Cell*, *28*(12), 2974–2990. https://doi.org/10.1105/tpc.16.00478

Lippold, F., vom Dorp, K., Abraham, M., Hölzl, G., Wewer, V., Yilmaz, J. L., Lager, I., Montandon, C., Besagni, C., Kessler, F., Stymne, S., & Dörmann, P. (2012). Fatty acid phytyl ester synthesis in chloroplasts of Arabidopsis. *Plant Cell*, *24*(5), 2001–2014. https://doi.org/10.1105/tpc.112.095588

Lohmann, A., Schöttler, M. A., Bréhélin, C., Kessler, F., Bock, R., Cahoon, E. B., & Dörmann, P. (2006). Deficiency in phylloquinone (vitamin K1) methylation affects prenyl quinone distribution, photosystem I abundance, and anthocyanin accumulation in the Arabidopsis AtmenG mutant. *Journal of Biological Chemistry*, *281*(52), 40461–40472. https://doi.org/10.1074/jbc.M609412200

Manzano, D., Andrade, P., Caudepón, D., Altabella, T., Arró, M., & Ferrer, A. (2016). Suppressing Farnesyl Diphosphate Synthase Alters chloroplast

development and triggers sterol-dependent induction of jasmonate- and Fe-related responses. *Plant Physiology*, *172*(1), 93–117. https://doi.org/10.1104/pp.16.00431

Mène-Saffrané, L. (2018). Vitamin E biosynthesis and its regulation in plants. *Antioxidants*, *7*(1), 1–17. https://doi.org/10.3390/antiox7010002

Mezzar, S., De Schryver, E., Asselberghs, S., Meyhi, E., Morvay, P. L., Baes, M., & Van Veldhoven, P. P. (2017). Phytol-induced pathology in 2-hydroxyacyl-CoA lyase (HACL1) deficient mice. Evidence for a second non-HACL1-related lyase. *Biochimica et Biophysica Acta - Molecular and Cell Biology of Lipids*, *1862*(9), 972–990. https://doi.org/10.1016/j.bbalip.2017.06.004

Mihalik, S. J., Morrell, J. C., Kim, D., Sacksteder, K. A., Watkins, P. A., & Gould, S. J. (1997). Identification of PAHX, a Refsum disease gene. *Nature Genetics*, *17*(2), 185–189. https://doi.org/10.1038/ng1097-185

Miura, Y. (2013). The biological significance of ω-oxidation of fatty acids. *Proceedings of the Japan Academy Series B: Physical and Biological Sciences*, *89*(8), 370–382. https://doi.org/10.2183/pjab.89.370

Miziorko, H. M. (2011). Enzymes of the mevalonate pathway of isoprenoid biosynthesis. *Archives of Biochemistry and Biophysics*, *505*(2), 131–143. https://doi.org/https://doi.org/10.1016/j.abb.2010.09.028

Mon, K., Obara, T., Seki, N., Miyamoto, M., Naganuma, T., Kitamura, T., & Kihara, A. (2020). Catalytic residues, substrate specificity, and role in carbon starvation of the 2-hydroxy FA dioxygenase Mpol in yeast. *Journal of Lipid Research*, *61*(7), 1104–1114. https://doi.org/10.1194/JLR.RA120000803

Motley, A. M., Hettema, E. H., Hogenhout, E. M., Britesl, P., Asbroek, A. L. M. A., Wijburg, F. A., Baas, F., Heijmans, H. S., Tabak, H. F., Wanders, R. J. A., Distel, B., & Iirhiime, M. M. (1997). *Rhizomelic chondrodysplasia punctata is a peroxisomal protein targeting disease caused by a non-functional PTS2 receptor*. *15*(april), 377–380.

Murashige, T., & Skoog, F. (1962). A Revised Medium for Rapid Growth and Bio Assays with Tobacco Tissue Cultures. *Physiologia Plantarum*, *15*(3), 473–497. https://doi.org/10.1111/j.1399-3054.1962.tb08052.x

Nelson, N., Ben-shem, A., & Wise, T. G. S. (2004). *THE COMPLEX ARCHITECTURE OF OXYGENIC PHOTOSYNTHESIS*. *5*(December). https://doi.org/10.1038/nrm1525

Nötzel, C., Lingner, T., Klingenberg, H., & Thoms, S. (2016). Identification of New Fungal Peroxisomal Matrix Proteins and Revision of the PTS1 Consensus. *Traffic*, *17*(10), 1110–1124. https://doi.org/10.1111/tra.12426

Oster, U., Bauer, C. E., & Rüdiger, W. (1997). Characterization of chlorophyll a and bacteriochlorophyll a synthases by heterologous expression in *Escherichia coli*. *Journal of Biological Chemistry*, *272*(15), 9671–9676. https://doi.org/10.1074/jbc.272.15.9671

Patwari, P. (2019). Cuticular waxes contribute to drought tolerance in Arabidopsis and barley. *Dissertation*.

Petriv, O. I., Tang, L., Titorenko, V. I., & Rachubinski, R. A. (2004). A New Definition for the Consensus Sequence of the Peroxisome Targeting Signal Type 2. *Journal of Molecular Biology*, *341*(1), 119–134.

https://doi.org/https://doi.org/10.1016/j.jmb.2004.05.064
Phillips, M. A., D'Auria, J. C., Gershenzon, J., & Pichersky, E. (2008). The Arabidopsis thaliana type I isopentenyl diphosphate isomerases are targeted to multiple subcellular compartments and have overlapping functions in isoprenoid biosynthesis. *Plant Cell*, *20*(3), 677–696. https://doi.org/10.1105/tpc.107.053926
Piller, L. E., Besagni, C., Ksas, B., Rumeau, D., Bréhélin, C., Glauser, G., Kessler, F., & Havaux, M. (2011). Chloroplast lipid droplet type II NAD(P)H quinone oxidoreductase is essential for prenylquinone metabolism and vitamin K 1 accumulation. *Proceedings of the National Academy of Sciences of the United States of America*, *108*(34), 14354–14359. https://doi.org/10.1073/pnas.1104790108
Porra, R. J., Thompson, W. A., & Kriedemann, P. E. (1989). Determination of accurate extinction coefficients and simultaneous equations for assaying chlorophylls a and b extracted with four different solvents: verification of the concentration of chlorophyll standards by atomic absorption spectroscopy. *Bichimica et Biophysica Acta*, *975*(3), 384–394. https://doi.org/10.1016/S0005-2728(89)80347-0
Pružinská, A., Tanner, G., Anders, I., Roca, M., & Hörtensteiner, S. (2003). Chlorophyll breakdown: Pheophorbide a oxygenase is a Rieske-type iron-sulfur protein, encoded by the accelerated cell death 1 gene. *Proceedings of the National Academy of Sciences of the United States of America*, *100*(25), 15259–15264. https://doi.org/10.1073/pnas.2036571100
Querol, J., Campos, N., Imperial, S., Boronat, A., & Rodríguez-Concepción, M. (2002). Functional analysis of the Arabidopsis thaliana GCPE protein involved in plastid isoprenoid biosynthesis. *FEBS Letters*, *514*(2–3), 343–346. https://doi.org/10.1016/S0014-5793(02)02402-X
Rentsch, D., Laloi, M., Rouhara, I., Schmelzer, E., Delrot, S., & Frommer, W. B. (1995). NTR1 encodes a high affinity oligopeptide transporter in Arabidopsis. *FEBS Letters*, *370*(3), 264–268. https://doi.org/10.1016/0014-5793(95)00853-2
Reumann, S., Babujee, L., Changle, M., Wienkoop, S., Siemsen, T., Antonicelli, G. E., Rasche, N., Lüder, F., Weckwerth, W., & Jahnd, O. (2007). Proteome analysis of Arabidopsis leaf peroxisomes reveals novel targeting peptides, metabolic pathways, and defense mechanisms. *Plant Cell*, *19*(10), 3170–3193. https://doi.org/10.1105/tpc.107.050989
Reumann, S., & Singhal, R. (2014). Isolation of leaf peroxisomes from Arabidopsis for organelle proteome Chapter 36 Isolation of Leaf Peroxisomes from Arabidopsis for Organelle Proteome Analyses Sigrun Reumann and Rajneesh Singhal. June 2015. https://doi.org/10.1007/978-1-62703-631-3
Rizvi, S., Raza, S. T., Ahmed, F., Ahmad, A., Abbas, S., & Mahdi, F. (2014). The role of Vitamin E in human health and some diseases. *Sultan Qaboos University Medical Journal*, *14*(2), 157–165.
Rohdich, F., Wungsintaweekul, J., Lüttgen, H., Fischer, M., Eisenreich, W., Schuhr, C. A., Fellermeier, M., Schramek, N., Zenk, M. H., & Bacher, A.

(2000). Biosynthesis of terpenoids: 4-diphosphocytidyl-2-C-methyl-D-erythritol kinase from tomato. *Proceedings of the National Academy of Sciences of the United States of America*, *97*(15), 8251–8256. https://doi.org/10.1073/pnas.140209197

Rontani, J. F., Bonin, P. C., & Volkman, J. K. (1999). Production of wax esters during aerobic growth of marine bacteria on isoprenoid compounds. *Applied and Environmental Microbiology*, *65*(1), 221–230. https://doi.org/10.1128/aem.65.1.221-230.1999

Sadre, R., Gruber, J., & Frentzen, M. (2006). Characterization of homogentisate prenyltransferases involved in plastoquinone-9 and tocochromanol biosynthesis. *FEBS Letters*, *580*(22), 5357–5362. https://doi.org/10.1016/j.febslet.2006.09.002

Saitou, N., & Nei, M. (1987). The neighbor-joining method: a new method for reconstructing phylogenetic trees. *Molecular Biology and Evolution*, *4*(4), 406–425. https://doi.org/10.1093/oxfordjournals.molbev.a040454

Sanz, A., Moreno, J. I., & Castresana, C. (1998). PIOX, a new pathogen-induced oxygenase with homology to animal cyclooxygenase. *Plant Cell*, *10*(9), 1523–1537. https://doi.org/10.1105/tpc.10.9.1523

Sattler, S. E., Gilliland, L. U., Magallanes-Lundback, M., Pollard, M., & DellaPenna, D. (2004). Vitamin E is essential for seed longevity and for preventing lipid peroxidation during germination. *Plant Cell*, *16*(6), 1419–1432. https://doi.org/10.1105/tpc.021360

Schelbert, S., Aubry, S., Burla, B., Agne, B., Kessler, F., Krupinska, K., & Hörtensteiner, S. (2009). Pheophytin pheophorbide hydrolase (pheophytinase) is involved in chlorophyll breakdown during Leaf senescence in Arabidopsis. *Plant Cell*, *21*(3), 767–785. https://doi.org/10.1105/tpc.108.064089

Schenk, N., Schelbert, S., Kanwischer, M., Goldschmidt, E. E., Dörmann, P., & Hörtensteiner, S. (2007). The chlorophyllases AtCLH1 and AtCLH2 are not essential for senescence-related chlorophyll breakdown in Arabidopsis thaliana. *FEBS Letters*, *581*(28), 5517–5525. https://doi.org/10.1016/j.febslet.2007.10.060

Schumacher, M. M., Jun, D., Johnson, B. M., & Debose-boyd, R. A. (2018). UbiA prenyltransferase domain – containing protein-1 modulates HMG-CoA reductase degradation to coordinate synthesis of sterol and nonsterol isoprenoids. *Journal of Biological Chemistry*, *293*(1), 312–323. https://doi.org/10.1074/jbc.RA117.000423

Schwacke, R., Schneider, A., Van Der Graaff, E., Fischer, K., Catoni, E., Desimone, M., Frommer, W. B., Flügge, U. I., & Kunze, R. (2003). ARAMEMNON, a novel database for Arabidopsis integral membrane proteins. *Plant Physiology*, *131*(1), 16–26. https://doi.org/10.1104/pp.011577

Schwender, J., Müller, C., Zeidler, J., & Lichtenthaler, H. K. (1999). Cloning and heterologous expression of a cDNA encoding 1-deoxy-D-xylulose-5-phosphate reductoisomerase of Arabidopsis thaliana. *FEBS Letters*, *455*(1–2), 140–144. https://doi.org/10.1016/S0014-5793(99)00849-2

Seki, N., Mori, K., Kitamura, T., Miyamoto, M., & Kihara, A. (2019). *Yeast Mpo1*

Is a Novel Dioxygenase That Catalyzes the alpha-Oxidation of a 2-Hydroxy Fatty Acid in an Fe2+-Dependent Manner. *December 2018*, 1–16.

Shimada, H., Ohno, R., Shibata, M., Ikegami, I., Onai, K., Ohto, M. A., & Takamiya, K. I. (2005). Inactivation and deficiency of core proteins of photosystems I and II caused by genetical phylloquinone and plastoquinone deficiency but retained lamellar structure in a T-DNA mutant of Arabidopsis. *Plant Journal*, *41*(4), 627–637. https://doi.org/10.1111/j.1365-313X.2004.02326.x

Shimada, T. L., Takano, Y., Shimada, T., Fujiwara, M., Fukao, Y., Mori, M., Okazaki, Y., Saito, K., Sasaki, R., Aoki, K., & Hara-Nishimura, I. (2014). Leaf oil body functions as a subcellular factory for the production of a phytoalexin in Arabidopsis. *Plant Physiology*, *164*(1), 105–118. https://doi.org/10.1104/pp.113.230185

Shimoda, Y., Ito, H., & Tanaka, A. (2016). Arabidopsis STAY-GREEN, mendel's green cotyledon gene, encodes magnesium-dechelatase. *Plant Cell*, *28*(9), 2147–2160. https://doi.org/10.1105/tpc.16.00428

Simkin, A. J., Guirimand, G., Papon, N., Courdavault, V., Thabet, I., Ginis, O., Bouzid, S., Giglioli-Guivarc'h, N., & Clastre, M. (2011). Peroxisomal localisation of the final steps of the mevalonic acid pathway in planta. *Planta*, *234*(5), 903. https://doi.org/10.1007/s00425-011-1444-6

Skoneczny, M., & Lazarow, P. B. (1998). A novel, non-PTS1, peroxisomal import route dependent on the PTS1 receptor Pex5p. *MOLECULAR BIOLOGY OF THE CELL*, *9*, 348A-348A.

Steinberg, S. J., Wang, S. J., Kim, D. G., Mihalik, S. J., & Watkins, P. A. (1999). Human very-long-chain Acyl-CoA synthetase: Cloning, topography, and relevance to branched-chain fatty acid metabolism. *Biochemical and Biophysical Research Communications*, *257*(2), 615–621. https://doi.org/10.1006/bbrc.1999.0510

Tanaka, R., Kobayashi, K., & Masuda, T. (2011). *Tetrapyrrole Metabolism in Arabidopsis thaliana*. 1–40. https://doi.org/10.1199/tab.0145

Titorenko, V. I., Nicaud, J. M., Wang, H., Chan, H., & Rachubinski, R. A. (2002). Acyl-CoA oxidase is imported as a heteropentameric, cofactor-containing complex into peroxisomes of Yarrowia lipolytica. *Journal of Cell Biology*, *156*(3), 481–494. https://doi.org/10.1083/jcb.200111075

Tsuboi, T., Takeo, S., Iriko, H., Jin, L., Tsuchimochi, M., Matsuda, S., Han, E. T., Otsuki, H., Kaneko, O., Sattabongkot, J., Udomsangpetch, R., Sawasaki, T., Torii, M., & Endo, Y. (2008). Wheat germ cell-free system-based production of malaria proteins for discovery of novel vaccine candidates. *Infection and Immunity*, *76*(4), 1702–1708. https://doi.org/10.1128/IAI.01539-07

Tzin, V., & Galili, G. (2010). The Biosynthetic Pathways for Shikimate and Aromatic Amino Acids in Arabidopsis thaliana. *The Arabidopsis Book*, *8*(May), e0132. https://doi.org/10.1199/tab.0132

Valentin, H. E., Lincoln, K., Moshiri, F., Jensen, P. K., Qi, Q., Venkatesti, T. V., Karunanandaa, B., Baszis, S. R., Norris, S. R., Savidge, B., Grays, K. J., & Last, R. L. (2006). The Arabidopsis vitamin E pathway gene5-1 mutant reveals a critical role for phytol kinase in seed tocopherol biosynthesis. *Plant*

Cell, *18*(1), 212–224. https://doi.org/10.1105/tpc.105.037077
van den Brink, D. M., Van Miert, J. N. I., Dacremont, G., Rontani, J. F., Jansen, G. A., & Wanders, R. J. A. (2004). Identification of fatty aldehyde dehydrogenase in the breakdown of phytol to phytanic acid. *Molecular Genetics and Metabolism*, *82*(1), 33–37. https://doi.org/10.1016/j.ymgme.2004.01.019
van den Brink, D. M., Van Miert, J. N. I., Dacremont, G., Rontani, J. F., & Wanders, R. J. A. (2005). Characterization of the final step in the conversion of phytol into phytanic acid. *Journal of Biological Chemistry*, *280*(29), 26838–26844. https://doi.org/10.1074/jbc.M501861200
Van der Leij, I., Franse, M. M., Elgersma, Y., Distel, B., & Tabak, H. F. (1993). PAS10 is a tetratricopeptide-repeat protein that is essential for the import of most matrix proteins into peroxisomes of Saccharomyces cerevisiae. *Proceedings of the National Academy of Sciences of the United States of America*, *90*(24), 11782–11786. https://doi.org/10.1073/pnas.90.24.11782
Van Veldhoven, P. P. (2010). Biochemistry and genetics of inherited disorders of peroxisomal fatty acid metabolism. *Journal of Lipid Research*, *51*(10), 2863–2895. https://doi.org/10.1194/jlr.R005959
Vaughn, J. L., Goodwin, R. H., Tompkins, G. J., & McCawley, P. (1977). The establishment of two cell lines from the insectspodoptera frugiperda (lepidoptera; noctuidae). *In Vitro*, *13*(4), 213–217. https://doi.org/10.1007/BF02615077
Verhoeven, N. M., Schor, D. S. M., Ten Brink, H. J., Wanders, R. J. A., & Jakobs, C. (1997). Resolution of the phytanic acid α-oxidation pathway: Identification of pristanal as product of the decarboxylation of 2-hydroxyphytanoyl-CoA. *Biochemical and Biophysical Research Communications*, *237*(1), 33–36. https://doi.org/10.1006/bbrc.1997.7066
Verhoeven, Nanda M., Roe, D. S., Kok, R. M., Wanders, R. J. A., Jakobs, C., & Roe, C. R. (1998). Phytanic acid and pristanic acid are oxidized by sequential peroxisomal and mitochondrial reactions in cultured fibroblasts. *Journal of Lipid Research*, *39*(1), 66–74. https://doi.org/10.1016/s0022-2275(20)34204-8
Vidi, P. A., Kanwischer, M., Baginsky, S., Austin, J. R., Csucs, G., Dörmann, P., Kessler, F., & Bréhélin, C. (2006). Tocopherol cyclase (VTE1) localization and vitamin E accumulation in chloroplast plastoglobule lipoprotein particles. *Journal of Biological Chemistry*, *281*(16), 11225–11234. https://doi.org/10.1074/jbc.M511939200
vom Dorp, K. (2015). Phytol and Tocopherol Metabolism in Arabidopsis thaliana. *Dissertation*.
vom Dorp, K., Hölzl, G., Plohmann, C., Eisenhut, M., Abraham, M., Weber, A. P. M., Hanson, A. D., & Dörmann, P. (2015). Remobilization of phytol from chlorophyll degradation is essential for Tocopherol synthesis and growth of Arabidopsis. *Plant Cell*, *27*(10), 2846–2859. https://doi.org/10.1105/tpc.15.00395
Wach, A., Brachat, A., Pöhlmann, R., & Philippsen, P. (1994). New heterologous modules for classical or PCR‐based gene disruptions in Saccharomyces

cerevisiae. *Yeast*, *10*(13), 1793–1808. https://doi.org/10.1002/yea.320101310

Wang, G., & Dixon, R. A. (2009). Heterodimeric geranyl(geranyl)diphosphate synthase from hop (Humulus lupulus) and the evolution of monoterpene biosynthesis. *Proceedings of the National Academy of Sciences of the United States of America*, *106*(24), 9914–9919. https://doi.org/10.1073/pnas.0904069106

Wang, L., Li, Q., Zhang, A., Zhou, W., Jiang, R., Yang, Z., Yang, H., Qin, X., Ding, S., Lu, Q., Wen, X., & Lu, C. (2017). The Phytol Phosphorylation Pathway Is Essential for the Biosynthesis of Phylloquinone, which Is Required for Photosystem I Stability in Arabidopsis. *Molecular Plant*, *10*(1), 183–196. https://doi.org/10.1016/j.molp.2016.12.006

Wehler, R. (2017). Phytyl ester synthases from Arabidopsis thaliana and Solanum lycopersicum. *Dissertation*.

Wildermuth, M. C., Dewdney, J., Wu, G., & Ausubel, F. M. (2002). Isochorismate synthase is required to synthesize salicylic acid for plant defence. *Nature*, *417*(6888), 562–565. https://doi.org/10.1038/417571a

Yang, W., Cahoon, R. E., Hunter, S. C., Zhang, C., Han, J., Borgschulte, T., & Cahoon, E. B. (2011). Vitamin E biosynthesis: Functional characterization of the monocot homogentisate geranylgeranyl transferase. *Plant Journal*, *65*(2), 206–217. https://doi.org/10.1111/j.1365-313X.2010.04417.x

Zbierzak, A. M., Kanwischer, M., Wille, C., Vidi, P. A., Giavalisco, P., Lohmann, A., Briesen, I., Porfirova, S., Bréhélin, C., Kessler, F., & Dörmann, P. (2010). Intersection of the tocopherol and plastoquinol metabolic pathways at the plastoglobule. *Biochemical Journal*, *425*(2), 389–399. https://doi.org/10.1042/BJ20090704

Zheng, M., Peng, T., Yang, T., Yan, J., Yang, K., Meng, D., & Hsu, Y.-F. (2021). Arabidopsis MHP1, a homologue of yeast Mpo1, is involved in ABA signaling. *Plant Science*, *304*, 110732. https://doi.org/https://doi.org/10.1016/j.plantsci.2020.110732

7. APPENDIX

7.1 Targeted List for Q-TOF MS/MS Analysis of FAPE

FAPE was positively charged as ammonium adduct ($NH4^+$) and measured with Q-TOF MS/MS direct infusion in the positive mode. The neutral loss of the phytol-H_2O moiety (m=278.2974) was scanned for the FAPE quantification.

FAPE	Mass of Molecule	Parental ion $[M+NH_4]^+$
10:0-phytyl ester	450.44368	468.478054
12:0-phytyl ester	478.47498	496.509354
14:0-phytyl ester	506.50628	524.540654
16:0-phytyl ester	534.53758	552.571954
16:1-phytyl ester	532.52193	550.556304
16:2-phytyl ester	530.50628	548.540654
16:3-phytyl ester	528.49063	546.525004
16:4-phytyl ester	526.47498	544.509354
17:0-phytyl ester[a]	548.55323	566.587604
18:0-phytyl ester	562.56888	580.603254
18:1-phytyl ester	560.55323	578.587604
18:2-phytyl ester	558.53758	576.571954
18:3-phytyl ester	556.52193	574.556304
18:4-phytyl ester	554.50628	572.540654

a Internal standard

7.2 Targeted List for Q-TOF MS/MS Analysis of Phosphatidylcholine (PC)

Phosphatidylcholine was protonated and quantified on Q-TOF direct infusion mode by scanning the product ion with a m/z=184.0739.

Fatty acid moieties of PC	Mass of parental ion (m/z) $[M+H]^+$
24:0[a]	622.4448
31:2	716.523
31:1	718.5387
31:0	720.5543
32:2	730.5387
32:1	732.5543
32:0	734.57
33:2	744.5543
33:1	746.57
33:0	748.5856
34:2	758.57
34:1	760.5856
34:0	762.6013
35:2	772.5856
35:1	774.6013
35:0	776.6169
36:2	786.6013
36:1	788.6169
36:0	790.6326

a Internal standard

7.3 Parameters for Detection of Aldehyde-methoximes by Multiple Reaction Monitoring Using LC-MS/MS Measurements with the Q-Trap Instrument.

Abbreviation	Aldehyde	Q1 Mass (m/z)	Q3 Mass (m/z)	Dwell Time (ms)
10:0al		186.19	60.04	100
11:0al		200.20	60.04	100
12:0al		214.22	60.04	100
13:0al		228.23	60.04	100
14:0al		242.25	60.04	100
15:0al		256.26	60.04	100
15:3al	Farnesal	250.22	60.04	100
16:0al	Hexadecanal	270.28	60.04	100
17:0al		284.30	60.04	100
18:0al		298.31	60.04	100
19:0al	Nonadecanal/ Pristanal	312.33	60.04	100
20:0al	Eicosanal/ Phytanal	326.34	60.04	100
20:1al	Phytenal	324.33	96.08	100
20:4al	Geranylgeranal	318.28	60.04	100

7.4 Synthetic Oligonucleotides

Oligo-nucleotides	Comment	Sequence 5'-3'
bn2895	Genotype *hpcl-1* forward primer	ATCGAACCAATGTCTGCAATC
bn2896	Genotype *hpcl-1* reverse primer	GAAGATATCGGAATCGGAAGC
bn2889	Genotype *hpcl-2* forward primer	ACATTGCCATTTAACTCTCGG
bn2890	Genotype *hpcl-2* reverse primer	GTTGTCGCTGTTGAAGGAGAC
bn2897	Genotype *hpcl-3* forward primer	AACCAGAGATCATCACCATCG
bn2898	Genotype *hpcl-3* reverse primer	TGGAATTCACTACCGTTGGAG
bn2880	Genotype SALK lines insertion primer	TCAAACAGGATTTTCGCCTGCT
bn2882	Genotype SAIL lines insertion primer	TAGCATCTGAATTTCATAACCAATCTC GATACAC
bn2924	Construct pET-HPCL forward primer	TTTGGATCCCATGGCGGATAAATCAG AAACC
bn2925	Construct pET-HPCL reverse primer	TTTCTGCAGGTTCTTGTGCTGTAATCT CCC
bn3586	Sequence pETb43-HPCL forward primer	GGAATTGTGAGCGGATAA
bn3587	Sequence pETb43-HPCL reverse primer	CCACTAGTCGCTTCGTCA
bn3149	Construct pIVEX-HPCL forward primer	TTTCATATGGCGGATAAATCAGAAACC
bn3150	Construct pIVEX-HPCL reverse primer	TTTCCCGGGGTTCTTGTGCTGTAATC TCCC
bn3175	Sequence pIVEX-HPCL forward primer1	AATACGACTCACTATAGGC
bn3176	Sequence pIVEX-HPCL reverse primer1	TATGCATCTTGACTACCTC
bn3220	Sequence pIVEX-HPCL forward primer2	AGATGTTCGTGAAATCC
bn3221	Sequence pIVEX-HPCL forward primer3	CAAGCTCATTGAAGCC
bn3222	RT-PCR forward primer	TTGAAGGAGACTCTGGTTT
bn3223	RT-PCR reverse primer	GTGTTTCCACAATATAACCT
bn3346	Sequence pFastBac1-HPCL forward primer	TCCGGATTATTCATACCGTC
bn3347	Sequence pFastBac1-HPCL reverse primer	TGGTATGGCTGATTATGATCC
bn3387	Construct pFastBac1-His-HPCL forward	TTTACTAGTATGAGAGGATCGCATCAC

	primer	CA
bn3388	Construct pFastBac1-His-HPCL reverse primer	TTTCTGCAGTTAGTTCTTGTGCTGTAA TCTCCC
bn3390	Construct pLH9000-35s-eGFP forward primer	TTTGGATCCATGGCGGATAAATCAGAA AC
bn3391	Construct pLH9000-35s-eGFP reverse primer	TTTCTCGAGTTAGTTCTTGTGCTGTAA TCTCC
bn3487	Sequence pL9000-35s-GFP-HPCL forward primer1	ATGGTGAGCAAGGGCGAGG
bn3488	Sequence pL9000-35s-GFP-HPCL reverse primer1	ATTAGAATGAACCGAAAC
bn3508	Sequence pL9000-35s-GFP-HPCL reverse primer2	GTTTCTGATTTATCCGCCATGGATCC
bn3991	Genotype *S.cerevisiae mpo1* forward primer	ATGGGCGAAGGTTTGCTGGA
bn3992	Genotype *S.cerevisiae mpo1* reverse primer	TTATTGTCTTTGCATCCGCA
bn3993	Genotype *S.cerevisiae pxp1* forward primer	ATGACCACGACCGCTACCCA
bn3994	Genotype *S.cerevisiae pxp1* reverse primer	CTATAAACGCGGTTTATTCT

7.5 Constructs for Expression of AtHPCL in *E.coli*, *S.cerevisiae*, Wheat Germ *in vitro* System, Sf9 Cells and *N.benthamiana*

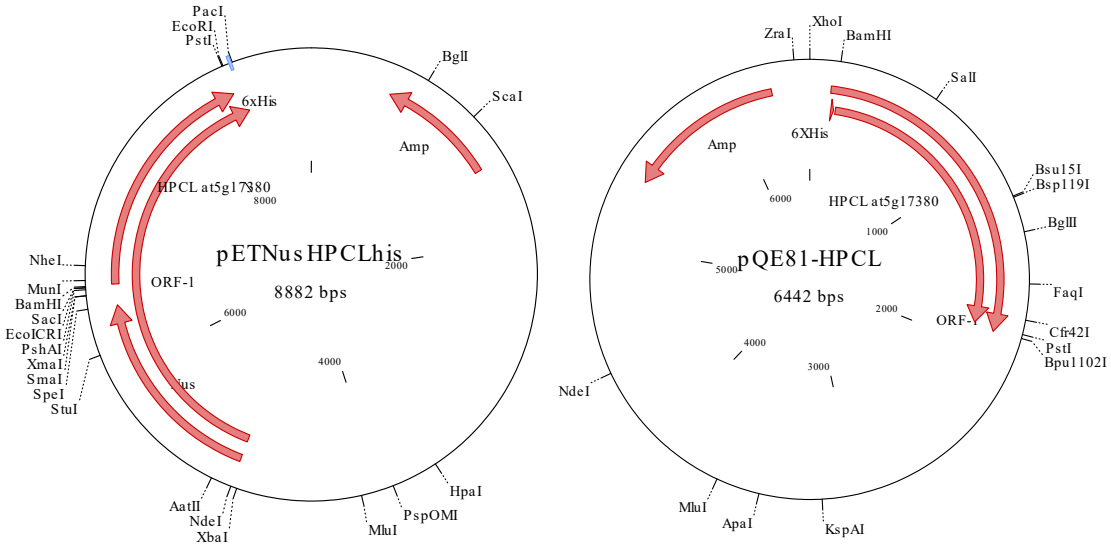

Figure. 7.1 Vectors which were used for protein expression in *E.coli*

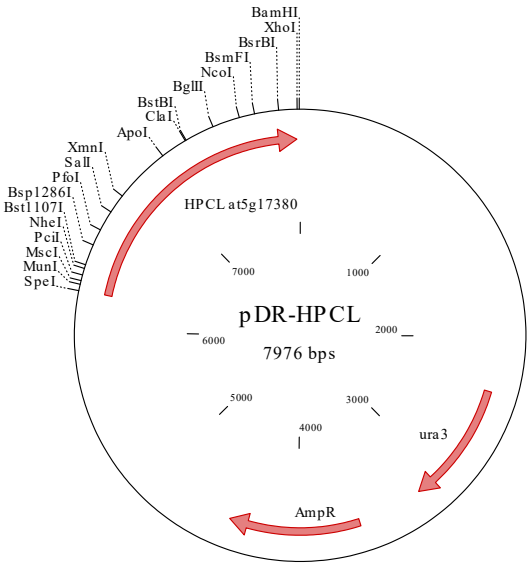

Figure. 7.2 The vector which was used for protein expression in *S.cerevisiae*

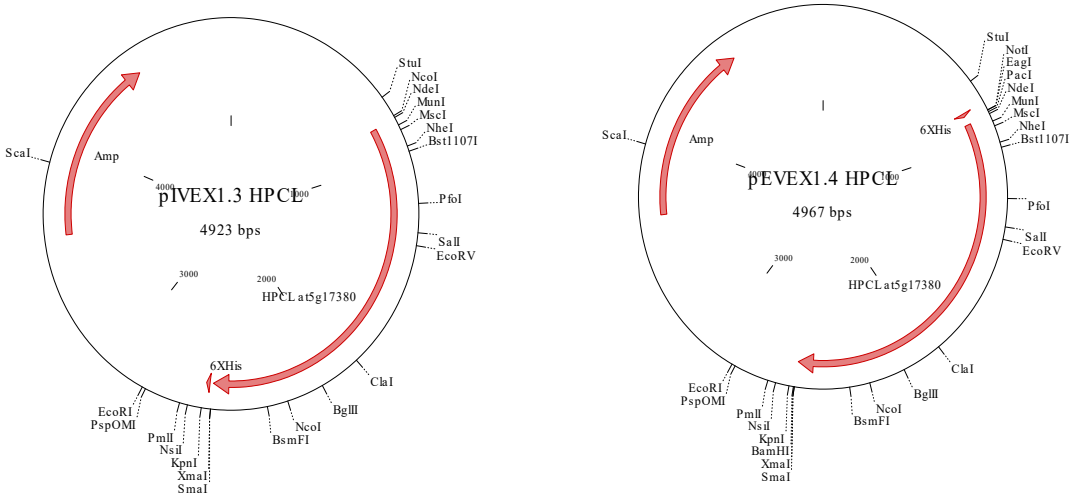

Figure. 7.3 Vectors which were used for protein expression in wheat germ cell-free *in vitro* expression system

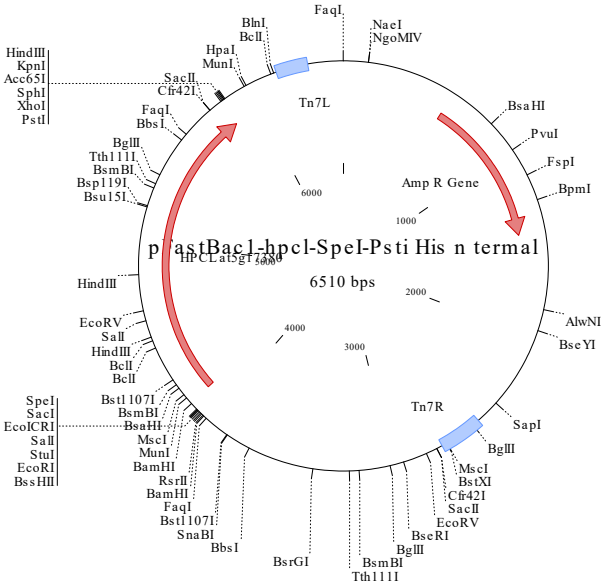

Figure. 7.4 The vector which was used for protein expression in Sf9 cells

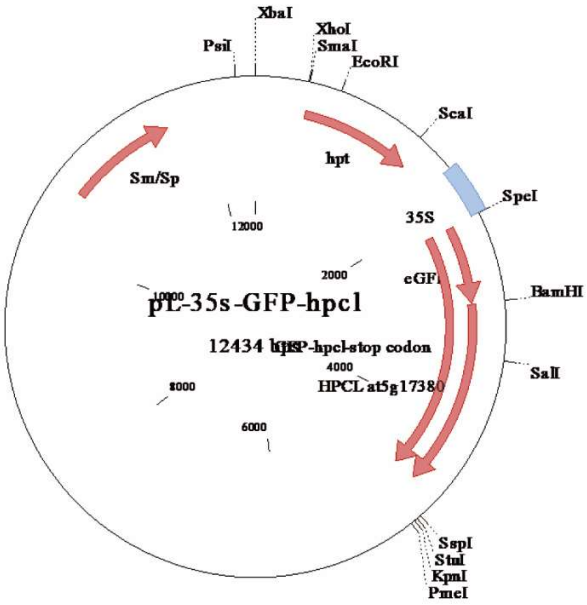

Figure. 7.5 The vector which was used for protein expression in *N. benthamiana*

8. PUBLICATION

Parts of this thesis were published in:

Philipp Gutbrod ‡; Wentao Yang ‡, Goran Vuk Grujicic, Helga Peisker, Katharina Gutbrod, Lin Fang Du, Peter Dörmann* (2021). Phytol derived from chlorophyll hydrolysis in plants is metabolized *via* phytenal. Journal of Biological Chemistry, Vol 296, 100530. DOI: https://doi.org/10.1016/j.jbc.2021.100530.

‡ equal contributions

* corresponding author

9. ACKNOWLEDGEMENTS

众里寻他千百度，蓦然回首，那人却在，灯火阑珊处

辛弃疾

But in the crowd once and again
I look for her in vain.
When all at once I turn my head,
I find her there where lantern light is dimly shed.
Qiji Xin

Firstly, most thanks to my supervisor, Prof. Dr. Peter Dörmann, for providing me this precious opportunity to make my thesis in his lab. His continuous supports and advices are very important for this dissertation. I'd like to thank China Scholarship Council (CSC) for the funding. I would like to thank members of my PhD defense committee, Prof Peter Dörmann, Prof Dorothea Bartels, Prof Lukas Schreiber and Prof Barbara Reichert, for their timing and comments.

My colleagues in IMBIO, **THANK YOU SO MUCH!-非常感谢！**

Philipp and Katharina, thank you so much for your driving when we first come to Bonn. Philipp, thank you for your help in initializing my project and your generous assistance. I want to thank Katharina, Helga and Jill for your help in mass spectrometry. Special thanks to Helga, for your patience and tireless answers to mu questions. I want to thank Biggi for your help in insect cells, which makes it really convenient and easy for me. I want to thank Payal for your help in Western blot and *A.tumefaciens*. Thank you, George, for your help in cloning and microorganisms. Thank you, Mathias and Regina, my benchmates. I hope everything is fine with you in your new labs. Thank you, Vici, for your help in HPLC. Thank you Marlies, for your warm encouragements. I want to thank Anna-Lena Falz and Stefanie Müller-Schüssele from Prof. Dr. Andreas Meyer's group in your help in CLSM. Of course, I want to thank Prof. Dr. Andreas Meyer for your agreement to use the CLSM.

Nina, Julia, Vadim and Yannic, good luck with your next experiments. Jiaxin, I hope

everything is smoothy with your project. Andreas, thank you for your help. Ellen and Christine, thanks for your efforts. Thank you, Duan, I hope everything is fine. Thank you, everyone, for the precious days spent with you in Bonn. I will keep them in mind.

Finally, to my family. Thank you, Xiaoning, my wife, for your warm hug and continuous encouragement when I was driven crazy. Mom, dad, you are the light in my darkest time. Grandpa, I will always remember your smile and voice. Thank you, Qiusheng, I believe sunshine is waiting for you in the future. Just hold on, things will get better. Thank you, Nic and Yining, for your correction and comments.

Stay healthy, everyone!